12-4-2015

Converted Measurement Trackers for Systems with Nonlinear Measurement Functions

Steven V. Bordonaro
University of Connecticut - Storrs, steveb@theonlinepeople.com

Converted Measurement Trackers for Systems with Nonlinear Measurement Functions

Steven V. Bordonaro, Ph.D.

University of Connecticut, 2015

Converted measurement tracking is a technique that filters in the coordinate system where the underlying process of interest is linear and Gaussian, and requires the measurements to be nonlinearly transformed to fit. The goal of the transformation is to allow for tracking in the coordinate system that is most natural for describing system dynamics. There are two potential issues that arise when performing converted measurement tracking. The first is conversion bias that occurs when the measurement transformation introduces a bias in the expected value of the converted measurement. The second is estimation bias that occurs because the estimate of the converted measurement error covariance is correlated with the measurement noise, leading to a biased Kalman gain. The goal of this research is to develop a new approach to converted measurement tracking that eliminates the conversion bias and mitigates the estimation bias. This new decorrelated unbiased converted measurement (DUCM) approach is developed and applied to numerous

tracking problems applicable to sonar and radar systems. The resulting methods are compared to the current state of the art based on their mean square error (MSE) performance, consistency and performance with respect to the posterior Cramer-Rao lower bound.

Converted Measurement Trackers for Systems with Nonlinear Measurement Functions

Steven V. Bordonaro

B.S. Electrical Engineering, Boston University, Boston, MA 1991

M.S. Electrical Engineering, University of Massachusetts, Dartmouth, MA 1996

A Dissertation

Submitted in Partial Fulfillment of the

Requirements for the Degree of

Doctor of Philosophy

at the

University of Connecticut

2015

APPROVAL PAGE

Doctor of Philosophy Dissertation

Converted Measurement Trackers for Systems with Nonlinear Measurement Functions

Presented by

Steven V. Bordonaro, B.S.E.E, M.S.E.E

Major Advisor

Prof. Peter Willett

Co-Major Advisor

Prof. Yaakov Bar-Shalom

Associate Advisor

Dr. Tod Luginbuhl

University of Connecticut

2015

To Mom.

ACKNOWLEDGEMENTS

I would like to thank my advisors, Dr. Peter Willett, Dr. Yaakov Bar-Shalom, and Dr. Tod Luginbuhl. Peter has been a wonderful resource while I was conducting my research and often had more faith in my abilities than I had in myself. Yaakov set high standards for thoroughness and attention to detail. Tod has been an excellent mentor both in my academic and professional endeavours. It has been a privilege to work with such a talented team. I would also like to thank the Naval Undersea Warfare Center for their financial support. Without the generous fellowship program, training resources and support for scientific research, this degree would not have been possible. Finally, I would like to thank my family. To my late father, Vincent, who instilled the importance of education and who, I'm sure, is very proud. To my mother, Lorraine, who showed me you are never too old to learn by earning a doctorate in education at age fifty-three. To my wife Susan, the love of my life, who showed tremendous support and took on more than her fair share of the family workload while I was off studying. To my children, Matthew and Samantha, who I love and cherish.

TABLE OF CONTENTS

Chapter 1

Introduction

1.1 Purpose

Nonlinear state estimation has important commercial and military application. Novel contributions to the field have the potential to improve the performance of existing radar and sonar systems. There is also the potential to reduce the cost of new systems by achieving required estimation performance with less measurement accuracy, hence reducing the requirements on the hardware.

1.2 Background

In tracking problems, it is common for the state prediction function to be linear while the measurements are a nonlinear function of the state. Perhaps the most common example of this is target tracking with a Cartesian state for estimation using a nearly constant velocity (or acceleration) dynamic model with measurements of range and bearing. Other important examples are (1) measurement of range, bearing and range rate and (2) measurements from a bi-static sonar or

radar system. There are many approaches to deal with the nonlinear measurements that can be put into two broad categories: the converted measurement approach and the converted prediction approach.

In the converted measurement approach the measurement is transformed from the measurement coordinate system into the estimation coordinate system (e.g. Cartesian) using a nonlinear transformation. The converted measurement, now a linear function of the state, can be used in a standard (linear) Kalman filter. The challenges of this approach are accounting for biases in the conversion and calculating an approximation to the converted measurement error covariance. Approximation is required since the bias introduced by the conversion (for bi-static cases) and the converted measurement error covariance (for both bi-static and mono-static cases with and without range rate) are a function of the true state, that is not available in practice.

The Extended Kalman Filter (EKF) and other numerical approximation approaches such as the Unscented Kalman Filter (UKF) and Cubature Kalman Filter (CKF) [1] are converted prediction approaches (or mixed coordinate approaches [3]). In these approaches the state prediction is converted into the measurement coordinate system using the nonlinear observation function. The innovation is also calculated in the measurement coordinate system and the innovation covariance and cross-covariance are approximated using a first or second order series expansion (EKF and second order EKF) or by using approximate numerical integration

(UKF and CKF).

The premise of this work is that for certain problems, the converted measurement approach is superior in terms of mean square error and consistency. The converted measurement approach, if employed naively, can, however, lead to errors [3]. The first of these errors is conversion bias [39,45,4]. Conversion bias occurs when the conversion process introduces a bias in the expected value of the converted measurement. Use of a biased converted measurement violates an assumption of the Kalman filter, leading to degraded performance. The second source of bias is estimation bias [43,26,11]. Estimation bias comes about due to the practical issue that the calculation of the converted measurement error covariance requires the true target position, that is unavailable in practice. A previously proposed practical resolution to this problem is to evaluate the covariance at the measurement. This results in correlation between the measurement error covariance estimate and the measurement error itself, leading to an estimation bias when the converted measurement is used in tracking.

The research conducted in this thesis is the development of a new measurement conversion that addresses the issues of conversion bias and estimation bias. An ideal measurement conversion would be unbiased, consistent, provide minimum mean square error estimates and would not suffer from estimation bias. In many problems, no single conversion can achieve all these goals, so compromises must be made. The primary trade-off is the MSE performance versus bias. Since

a fundamental assumption in the Kalman filter is that the measurement errors are unbiased, an unbiased conversion is preferred. An adjustment to the output of the filter can be made to achieve improved MSE performance. The measurement error covariance must also be uncorrelated with the measurement error to overcome estimation bias.

The goal of this research is to develop such a measurement conversion technique and employ the resulting filters for numerous tracking problems. The first problem addressed, in Chapter 2, is one of the most studied examples of converted measurement tracking — tracking in Cartesian coordinates with polar (or spherical) measurements. In Chapter 3 the technique is examined for the problem of range rate measurements from a moving platform which is shown to need de-biasing. In these two cases the use of a converted measurement is natural and the bias and converted measurement error covariance can be derived. In Chapter 4 the method is used to address the problem of tracking with polar (or spherical) measurements with the addition of a range rate measurement. In this case the conversion is less obvious and requires the inclusion of a non-informative measurement. In Chapter 5 the method is extended to tracking with bi-static measurements. In this case the calculation of the conversion requires numerical integration. The result is the development of a new converted measurement sigma point Kalman filter. Chapter 6 provides the final extension of the method for the case of extended target tracking. This chapter explores the case where

the measurement conversion process requires an iterative approach. The iterative approach used is the expectation-maximization (EM) algorithm using the probabilistic multi-hypothesis tracker (PMHT) association model (assignment is 1–to–1; association can be several–to–1).

1.2.1 Converted Measurement Tracker for Range and Bearing Measurements

One of the most studied examples of the converted measurement Kalman filter (CMKF) uses polar measurements and performs tracking in Cartesian coordinates. If the conversion from polar to Cartesian is unbiased, the performance of a CMKF is superior to a mixed coordinate EKF (i.e. target motion in Cartesian coordinates and measurements in polar coordinates) [39]. Existing approaches for the conversion include the conventional conversion [3], the unbiased converted measurement (UCM) [45], the modified unbiased converted measurement (MUCM) [44,20], and the unscented transform (UT) [34].

In this research a decorrelated version of the UCM technique (DUCM) is proposed to address both conversion and estimation bias. The polar to Cartesian conversion is used to analyze and evaluate the conversion bias and estimation bias for each existing conversion technique as well as the proposed technique. The MSE performance and consistency of a CMKF utilizing each technique is examined. The technique is then extended from polar to spherical measurements.

1.2.2 Unbiased Range Rate Estimation from a Moving Platform

Estimation of range rate using active sonar or radar by taking advantage of the Doppler effect can be advantageous for improved target state estimation, track association and for discriminating targets from stationary clutter. When estimating range rate from a moving platform it is necessary to nullify the effect of the platform speed. This nullification process suffers from a similar bias problem as the position measurement conversion.

The decorrelated, unbiased converted measurement approach can be used to address this issue. First an evaluation of the conversion bias and its significance is conducted. This is followed by the development of an unbiased range rate estimator.

1.2.3 Converted Measurement Tracker for Range, Bearing and Range Rate Measurements

In addition to range and bearing, in many active sonar and radar applications measurements also include range rate. The extension of the CMKF to use range rate as a linear measurement is possible [4], but previous implementations have been limited to cases with small bearing errors. The use of range rate as a nonlinear measurement requires the use of a nonlinear tracker such as the EKF or UKF. Due to their poor performance in some situations, various modifications have been proposed, including use of a pseudo measurement [23,21,27,32], an alter-

native linearization of the measurement prediction function [8], and sequentially processing the converted position and range rate measurements (applied to the EKF [21,27,32] and the UKF [22,38]).

Based on the success of the CMKF for tracking with range and bearing measurements, many existing approaches for tracking with range, bearing and range rate use a converted measurement approach for the position portion of the measurements. However, by leaving the range rate measurement as a nonlinear function of the state, the resulting filters have the potential for inconsistent performance. The question that is asked in the research is whether the converted measurement approach can be extended to include the range rate measurement, resulting in a converted measurement that is fully linear with respect to the Cartesian state, thus allowing for the use of a linear Kalman filter.

The goal is the development of a converted measurement approach that converts range, bearing and range rate to Cartesian position and velocity. This converted measurement, now linear with respect to the state, can be used in a linear Kalman filter. The resulting filter has advantages over the current state of the art for cases with poor angle accuracy (high nonlinearity).

This part of the research examines existing techniques, develops a new converted measurement approach for polar and spherical measurements with range rate, employs the conversion in a Kalman filter, and evaluates the resulting filter against the state of the art.

1.2.4 Converted Measurement Sigma Point Kalman Filter for Bi-Static Sonar and Radar Tracking

Tracking with bi-static sonar or radar measurements is challenging due to the fact that the measurements are a nonlinear function of the Cartesian state. The performance of existing approaches, including the EKF and sigma point Kalman filters such as the UKF, may not be acceptable in terms of mean square error or tracker consistency (i.e. the trackers estimate of the predicted state estimation error covariance is not statistically consistent with the underlying estimation errors). This research reformulates the general sigma point Kalman filter (SPKF) [52] as a converted measurement SPKF. The resulting filter is compared to the existing multistatic approaches [17,18,41] when employed in a bi-static tracking scenario.

Consistent with the underlying premise of this thesis, the expectation was that a converted measurement approach will be superior in terms of mean square error and consistency. The converted measurement sigma point Kalman filter (CMSPKF) is developed for cases, such as the bi-static case, in which it is not possible to derive an unbiased measurement conversion and converted measurement error covariance. Of particular interest is the case when the bi-static system has good range accuracy, but relatively poor angle accuracy. This is relevant for small sensors, as the range accuracy is primarily a function of waveform used, while the angle accuracy is a function of aperture (size of the sensor).

The CMSPKF does not simply employ the UT (or Cubature Transform) to convert the measurement from measurement coordinates to Cartesian coordinates. The reasons for this are two-fold. The first is that the UT does not provide an unbiased estimate of the truth [33,15]. The second is that employing the UT to approximate the converted measurement error covariance results in a dependency between the measurement error covariance estimate and the measurement error itself, leading to an estimation bias when the converted measurement is used in tracking [15]. To resolve these issues, the proposed CMSPKF estimates conversion bias and the converted measurement error covariance with a sigma point transform using a combination of the tracker's predicted estimate and the raw measurement error covariance.

The research is organized as follows. First the bi-static tracking problem is introduced and existing approaches based on sigma point transformations are described. Then the CMSPKF is derived, the implementation of the filter defined and the approximations used in its development discussed. A Monte-Carlo evaluation of the CMSPKF with respect to existing methods is conducted to demonstrate the advantage of the technique for specific bi-static tracking cases.

1.2.5 Extended Object Tracking with Exploitation of Range Rate Measurements

The final extension to the converted measurement approach is for the challenging case of extended object tracking. In most cases there is an underlying assumption in the tracking algorithm that the target is a point target (i.e. the target has no physical extent). A related assumption is that, at most, one measurement per scan originates from the target. There is, however, a growing body of literature [30,29,36,6,54,5,55,37] that relaxes the point target assumption, often referred to as extended object tracking. In extended object tracking, the problem involves estimating the target state (e.g. position and dynamics) and the target's spatial characteristics. The target can be represented as a set of point sources. Since there is uncertainty in the measurement to source assignment, a direct converted measurement approach is not feasible and an iterative maximization approach must be employed.

The problem addressed in this research can be stated as follows. Given over-resolved measurements of range, bearing and range rate, of a rigid target whose spatial characteristics are fixed with respect to the line of motion, provide unbiased, minimized mean square error estimates for the target state and spatial characteristics, with associated mean square errors (covariances) that are consistent with the underlying errors.

The end result of the development of this tracking system is an advance-

ment in the state of the art in extended object tracking. Raw measurements of range, bearing and range rate are converted into the tracking coordinate system of position, velocity and turn rate (as opposed to the traditional approach of position only). The dynamic estimation problem is then solved with a converted measurement Kalman filter, whose only nonlinearities are in the calculation of the state prediction covariance. The filter also provides spatial extent estimates using a model of the target spatial characteristics. The conversion is performed using the EM algorithm based on the PMHT [48] association model.

1.3 Summary

The result of the research conducted in this thesis is an advancement in the state-of-the-art in nonlinear tracking by providing significant contributions in tracking using converted measurements. By developing and evaluating new converted measurement techniques for a wide range of tracking problems, the resulting research has the potential to provide a benefit to many commercial and military systems. By developing conversion techniques for cases where (1) the bias and converted measurement error covariance can be derived; (2) the bias and converted measurement error covariance can be derived with the addition of a non-informative measurement; (3) the bias and converted measurement error covariance must be evaluated using numerical integration and (4) the bias and converted measurement error covariance must be evaluated using iterative maximization, the flexibility and

utility of the new converted measurement approach has been demonstrated.

1.3.1 Publications to Date

The following is a list of journal papers and conference papers that will be submitted for publication as a result of this research.

Journal Publications

S. Bordonaro, P. Willett, and Y. Bar-Shalom, "Decorrelated, Unbiased Converted Measurement Kalman Filter" *IEEE Trans. on Aerospace and Electronic Systems.* on 50.2 (2014): 1431-1444.

S. Bordonaro, P. Willett, and Y. Bar-Shalom, "Consistent Linear Tracker with Converted Range, Bearing and Range Rate Measurements" accepted for publication (26 August 2014) in *IEEE Trans. on Aerospace and Electronic Systems; to appear in 2016.*

S. Bordonaro, P. Willett, Y. Bar-Shalom, and Tod Luginbuhl, "Converted Measurement Sigma Point Kalman Filter for Bi-Static Sonar and Radar Tracking" submitted (29 September 2014) in *IEEE Trans. on Aerospace and Electronic Systems.*

S. Bordonaro, P. Willett, Y. Bar-Shalom, Tod Luginbuhl, and Marcus Baum, "Extended Object Tracking with Exploitation of Range Rate Measurements" submitted (November 2015) in the *Journal of Advances in Information Fusion (JAIF).*

Conference Publications

S. Bordonaro, P. Willett, and Y. Bar-Shalom, "Tracking with converted position and Doppler measurements," in *Proceedings of SPIE Conference on Signal and Data Processing of Small Targets*, ser. Proc. SPIE, O. E. Drummond, Ed., vol. 8137, 2011, paper 8137-12.

S. Bordonaro, P. Willett, and Y. Bar-Shalom, "Bias elimination in tracking with converted position and Doppler measurements," in *IEEE Conference on Decision and Control*, ser. Proc. IEEE, Dec. 2012.

S. Bordonaro, P. Willett, and Y. Bar-Shalom, "Unbiased tracking with converted measurements," in *IEEE Radar Conference Proceedings*, ser. Proc. IEEE, May 2012, p. 4197.

S. Bordonaro, P. Willett, and Y. Bar-Shalom, "Consistent linear tracker with position and range rate measurements" in *2012 Conference Record of the Forty Sixth Asilomar Conference on Signals, Systems and Computers (ASILOMAR)*, 2012, pp. 880-884.

S. Bordonaro, P. Willett, and Y. Bar-Shalom, "Performance analysis of the converted range rate and position linear Kalman filter" in *2013 Conference Record of the Forty Sixth Asilomar Conference on Signals, Systems and Computers (ASILOMAR)*, 2013, pp. 1751–1755.

S. Bordonaro, P. Willett, Y. Bar Shalom, M. Baum, and T. Luginbuhl, "Extracting Speed, Heading and Turn-Rate Measurements from Extended Objects Using

the EM Algorithm." in Proc. IEEE Aerospace Conference, Big Sky, Montana, USA, March 2015.

Chapter 2

Converted Measurement Tracker for Range and Bearing Measurements

2.1 Abstract

Converted measurement tracking is a technique that filters in the coordinate system where the underlying process of interest is linear and Gaussian, and requires the measurements to be nonlinearly transformed to fit. The goal of the transformation is to allow for tracking in the coordinate system that is most natural for describing system dynamics. There are two potential issues that arise when performing converted measurement tracking. The first is conversion bias that occurs when the measurement transformation introduces a bias in the expected value of the converted measurement. The second is estimation bias that occurs because the estimate of the converted measurement error covariance is correlated with the measurement noise, leading to a biased Kalman gain. First, previously proposed unbiased conversions are examined. Following this, the "Decorrelated Unbiased Converted Measurement" (DUCM) approach is presented. Results show

that to overcome conversion bias and estimation bias, an unbiased measurement conversion should be employed that calculates the converted measurement error covariance using the predicted measurement. The conversion approaches are evaluated in tracking scenarios relevant to radar and sonar measurements.

2.2 Introduction

The Converted Measurement Kalman Filter (CMKF) is commonly employed to address the problem of target tracking when the measurements are in polar or spherical coordinates [4]. The technique involves conversion of the raw measurement into Cartesian coordinates prior to tracking, allowing for the use of a linear Kalman filter. The avoids the pitfalls of the Extended Kalman Filter (EKF), that include the EKF's potential for divergence and inconsistency between the filter calculated estimation error covariance and the true estimation error.

When utilizing a CMKF, two sources of bias must be examined and, if significant, eliminated. The first source of bias is conversion bias [39,45,4]. Conversion bias occurs when the conversion process introduces a bias in the expected value of the converted measurement. Use of a biased converted measurement violates an assumption of the Kalman filter, leading to degraded performance.

The second source of bias is estimation bias [43,26,11]. Estimation bias comes about due to the practical issue that the calculation of the converted measurement error covariance requires the true target position, unavailable in prac-

tice. A previously proposed practical resolution to this problem is to evaluate the covariance at the measurement. This results in correlation between the measurement error covariance estimate and the measurement error itself, leading to an estimation bias when the converted measurement is used in tracking.

One of the most studied examples of the CMKF uses polar measurements and performs tracking in Cartesian coordinates. If the conversion from polar to Cartesian is unbiased, the performance of a CMKF is superior to a mixed coordinate EKF (i.e. target motion in Cartesian coordinates and measurements in polar coordinates) [39]. Proposed approaches for conversion include the conventional conversion, the Unbiased Converted Measurement (UCM), the Modified Unbiased Converted Measurement (MUCM), and the Unscented Transform (UT). Recently, a decorrelated version of the UCM technique (DUCM) has been proposed to address both conversion and estimation bias [11]. Although DUCM was developed as an extension to the UCM conversion, it is closely related to the approximate Best Linear Unbiased Estimator (BLUE) developed in [60]. Section 2.3 uses the polar to Cartesian conversion to analyze and evaluate the conversion bias and estimation bias for each conversion technique. The Decorrelated Unbiased Converted Measurement (DUCM) is presented in Section 2.4 and compared to BLUE filter. Section 2.5 evaluates the mean square error (MSE) performance and consistency of a CMKF utilizing each technique. Section 2.6 extends the evaluation from polar to spherical coordinates.

Table 2.1: Methods Evaluated

Acronym	**Method**
CONV	Conventional
UCM	Unbiased Converted Measurement [45]
MUCM	Modified Unbiased Converted Measurement [44,20]
UT	Unscented Transform [34]
BLUE	Best Linear Unbiased Estimator [60]
DUCM	Decorrelated Unbiased Converted Measurement [11]

2.3 Evaluation of Existing Conversion Techniques

The conversion process required to employ a CMKF involves transforming the raw measurement into a converted measurement and estimating the converted measurement error covariance. The primary measures of performance include bias, mean square error and consistency. For a conversion to be unbiased, the expected value of the converted measurement (or the result of an estimator using the converted measurement) should equal the truth. For a conversion to be consistent, the estimate of the converted measurement error covariance should be statistically compatible with the converted measurement errors relative to the truth.

2.3.1 Review of Existing Measurement Conversion Techniques

The four conversion processes analyzed include the conventional conversion, UCM, MUCM and UT.

Conventional Conversion

The conventional measurement conversion from polar to Cartesian coordinates is

$$\begin{bmatrix} x_m \\ y_m \end{bmatrix} = \begin{bmatrix} r_m \cos \alpha_m \\ r_m \sin \alpha_m \end{bmatrix} \tag{2.1}$$

with the associated estimate of the converted measurement error covariance based on linearization [3]

$$R^{11}_{\text{CONV}} = r_m^2\sigma_\alpha^2 \sin^2\alpha_m + \sigma_r^2 \cos^2\alpha_m$$

$$R^{22}_{\text{CONV}} = r_m^2\sigma_\alpha^2 \cos^2\alpha_m + \sigma_r^2 \sin^2\alpha_m$$

$$R^{12}_{\text{CONV}} = \left(\sigma_r^2 - r_m^2\sigma_\alpha^2\right) \sin\alpha_m \cos\alpha_m \tag{2.2}$$

Analysis of the expected value of the conventional conversion (2.1) shows that the conversion has a bias in the mean of the converted measurement [3]. The bias can be found by taking the expectation of the converted range and bearing measurements, x_m and y_m. If the range measurement noise, w_r, and bearing measurement noise, w_α, are uncorrelated, zero mean, and Gaussian with standard deviations of σ_r and σ_α, respectively, the expected converted measurement is

$$E\begin{bmatrix} (r+w_r)\cos(\alpha+w_\alpha) \\ (r+w_r)\sin(\alpha+w_\alpha) \end{bmatrix} = e^{-\sigma_\alpha^2/2}\begin{bmatrix} r\cos\alpha \\ r\sin\alpha \end{bmatrix} \tag{2.3}$$

Evident in (2.3) is that there is bias along the true bearing to the target.

Unbiased Measurement Conversion (UCM)

Given σ_α the bias can be calculated and eliminated. Although the original proposal for bias removal used an additive correction term [39], the exact compensation is multiplicative [45]. The unbiased conversion with multiplicative compensation is

$$\begin{bmatrix} x_m^{\text{UCM}} \\ y_m^{\text{UCM}} \end{bmatrix} = e^{\sigma_\alpha^2/2} \begin{bmatrix} r_m \cos\alpha_m \\ r_m \sin\alpha_m \end{bmatrix} \tag{2.4}$$

Calculation of the true measurement error covariance of the UCM requires the true range and bearing, and therefore cannot be calculated in practice. This practical concern is at the crux of the variation in performance of the various conversion techniques. The practical implementation of the UCM approach evaluates the covariance at the measurements [45], namely,

$$\begin{aligned} R_{\text{UCM}}^{11} &= \frac{1}{2}\left(r_m^2 + \sigma_r^2\right)\left[1 + \cos(2\alpha_m)e^{-2\sigma_\alpha^2}\right] + \left(e^{\sigma_\alpha^2} - 2\right) r_m^2 \cos^2\alpha_m \\ R_{\text{UCM}}^{22} &= \frac{1}{2}\left(r_m^2 + \sigma_r^2\right)\left[1 - \cos(2\alpha_m)e^{-2\sigma_\alpha^2}\right] + \left(e^{\sigma_\alpha^2} - 2\right) r_m^2 \sin^2\alpha_m \\ R_{\text{UCM}}^{12} &= \frac{1}{2}\left(r_m^2 + \sigma_r^2\right)\sin(2\alpha_m)e^{-2\sigma_\alpha^2} + \left(e^{\sigma_\alpha^2} - 2\right) r_m^2 \cos(\alpha_m)\sin(\alpha_m) \end{aligned} \tag{2.5}$$

Modified Unbiased Measurement Conversion (MUCM)

It can be seen that the UCM measurement conversion (2.4) is derived by conditioning on the true range and bearing, while the error covariance (2.5) is derived by conditioning on the measurements. This incompatibility was pointed out by previous authors along with a Modified Unbiased Converted Measurement (MUCM) [44,20], shown below,

$$\begin{bmatrix} x_m^{\text{MUCM}} \\ y_m^{\text{MUCM}} \end{bmatrix} = e^{-\sigma_\alpha^2/2} \begin{bmatrix} r_m \cos\alpha_m \\ r_m \sin\alpha_m \end{bmatrix} \tag{2.6}$$

$$R^{11}_{\text{MUCM}} = \frac{1}{2}\left(r_m^2 + \sigma_r^2\right)\left[1 + \cos(2\alpha_m)e^{-2\sigma_\alpha^2}\right] - e^{\sigma_\alpha^2} r_m^2 \cos^2\alpha_m$$
$$R^{22}_{\text{MUCM}} = \frac{1}{2}\left(r_m^2 + \sigma_r^2\right)\left[1 - \cos(2\alpha_m)e^{-2\sigma_\alpha^2}\right] - e^{\sigma_\alpha^2} r_m^2 \sin^2\alpha_m$$
$$R^{12}_{\text{MUCM}} = \frac{1}{2}\left(r_m^2 + \sigma_r^2\right)\sin(2\alpha_m)e^{-2\sigma_\alpha^2} - e^{\sigma_\alpha^2} r_m^2 \cos(\alpha_m)\sin(\alpha_m) \tag{2.7}$$

Unscented Transform (UT)

The Unscented Transform (UT) approximates the mean and covariance of the converted measurement by passing five (2nd order UT) or nine (4th order UT) sigma points through the non-linear function (2.1) and calculating a weighted mean and covariance [34]. For the assumption that the range and bearing measurement errors are uncorrelated, the sigma points for the second order UT are given by

$$\begin{bmatrix} \underline{r} \\ \underline{\alpha} \end{bmatrix} = \begin{bmatrix} r_m & r_m & r_m & r_m^+ & r_m^- \\ \alpha_m & \alpha_m^+ & \alpha_m^- & \alpha_m & \alpha_m \end{bmatrix} \tag{2.8}$$

where:

$$r_m^+ = r_m + \sqrt{3}\sigma_r \qquad r_m^- = r_m - \sqrt{3}\sigma_r \tag{2.9}$$
$$\alpha_m^+ = \alpha_m + \sqrt{3}\sigma_\alpha \qquad \alpha_m^- = \alpha_m - \sqrt{3}\sigma_\alpha \tag{2.10}$$

and the weights, W, are

$$[W] = \begin{bmatrix} \frac{1}{3} & \frac{1}{6} & \frac{1}{6} & \frac{1}{6} & \frac{1}{6} \end{bmatrix} \tag{2.11}$$

2.3.2 Evaluation of Conversion Bias

Conversion bias is defined as the difference between the expected value of the converted measurement and the truth. Table 2.2 shows the conversion bias for each technique, and indicates that UCM is the only unbiased conversion.

Monte-Carlo simulation verifies that the UCM is unbiased for all bearing angles. Fig. 2.1 shows the results of Monte-Carlo simulation for various bearing angles. An important observation is that the distribution of the converted position is very close to Gaussian along the cross-range axis, but is non-Gaussian along the down-range axis. For this distribution, the unbiased estimate is not necessarily the minimum mean square error estimate or the maximum likelihood estimate.

For each of the biased conversions, the bias is along the true bearing to the target and is proportional to the range. The absolute bias increases for long ranges and poor angle accuracies. The relative bias (i.e. the bias divided by the true range) is a function of angle accuracy. The significance of the bias is the absolute bias divided by the standard deviation of the range measurement noise, σ_r. Therefore angle accuracy, σ_α, range accuracy, σ_r, and range, r, all play a role in how the bias impacts estimation performance.

The claim that the UT is a biased conversion may seem at odds with the claims of Julier [34], but it is not. The UT provides an unbiased estimate of the *mean of the conversion*, not an unbiased estimate of the ground truth. The UT, in essence, properly captures the bias, but does not eliminate it [33]. It is also

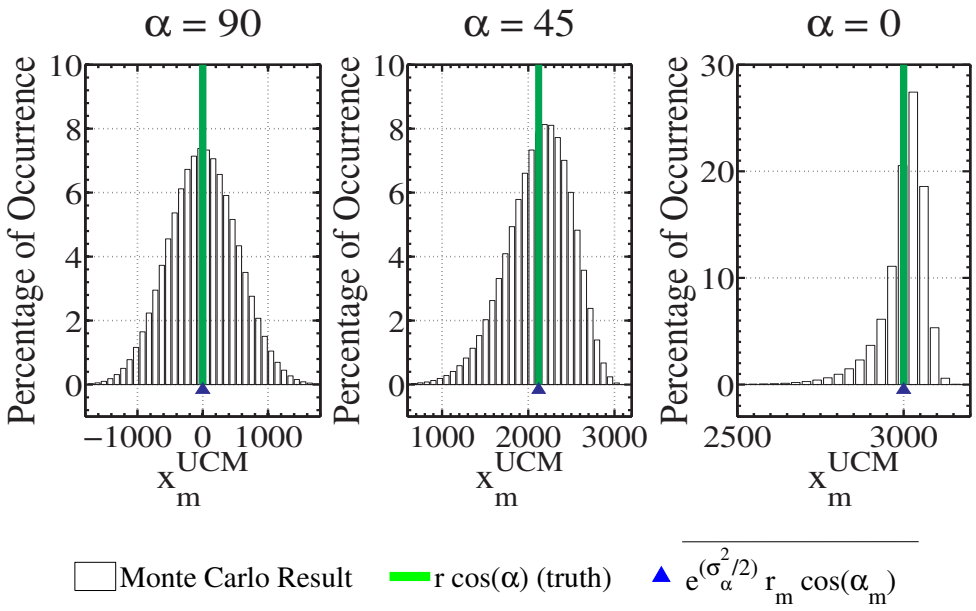

Fig. 2.1: Histogram of 10^6 Monte-Carlo runs using a range of 3,000m and bearing of 0° to 90°. The range and bearing measurement noises used were uncorrelated Gaussian with $\sigma_r = 30$ and $\sigma_\alpha = 10°$ respectively. The mean value of the Monte-Carlo result and the ground truth are plotted for comparison. In all cases, the UCM was unbiased.

Table 2.2: Conversion Bias

Method	**Bias**
Conventional	$r\left(e^{-\sigma_\alpha^2/2}-1\right)$
UCM	0
MUCM	$r\left(e^{-\sigma_\alpha^2}-1\right)$
UT	$r\left[e^{-\sigma_\alpha^2/2}\left(\frac{2}{3}+\frac{1}{3}\cos\left(\sqrt{3}\sigma_\alpha\right)\right)-1\right]$

interesting to note that the series expansion of the MUCM and UT bias at $\sigma_\alpha = 0$ are equal up to, but not including, the sixth order. In this light, the polar to Cartesian UT can be considered an approximation to the MUCM approach [12].

Fig. 2.2 provides a comparison of the expected value and expected covariances of the conventional, UCM and MUCM/UT techniques in polar and Cartesian coordinates. The expected value of the conventional conversion is straddled by the expected values of the UCM and MUCM/UT techniques.

The advantage of the UCM conversion is that it is unbiased, an essential attribute in state estimation, while the MUCM conversion has a lower mean squared error [11]. Both conversion techniques use a multiplicative term. The multiplicative term that results in the smallest expected square error can be derived using a factor η as follows:

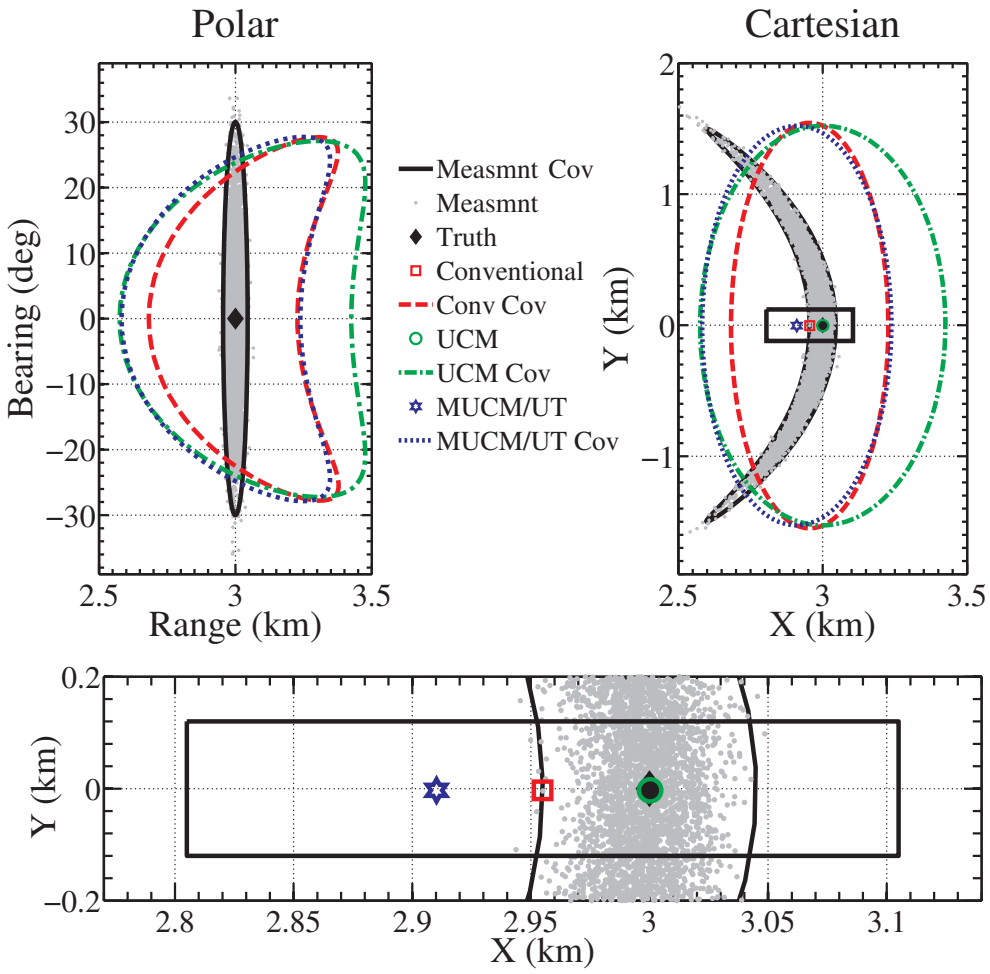

Fig. 2.2: Conversion bias for the Conventional, UCM and MUCM/UT conversion methods for 10,000 measurements with a true range of 3,000m and true bearing of $0\,^\circ$ with $\sigma_\alpha = 10\,^\circ$ and $\sigma_r = 15$m. Covariance estimates are displayed for a Mahalanobis distance of 3.

$$\begin{bmatrix} x_m^{\text{MMSE}} \\ y_m^{\text{MMSE}} \end{bmatrix} = \eta \begin{bmatrix} r_m \cos \alpha_m \\ r_m \sin \alpha_m \end{bmatrix} \tag{2.12}$$

The expected squared error,

$$\begin{aligned} &E\left[\left(\eta\left(r+w_r\right)\cos\left(\alpha+w_\alpha\right)-r\cos\alpha\right)^2\right] \\ &+E\left[\left(\eta\left(r+w_r\right)\sin\left(\alpha+w_\alpha\right)-r\sin\alpha\right)^2\right] \end{aligned} \tag{2.13}$$

can be found to be

$$\eta^2(r+\sigma_r^2) - 2\eta r^2 e^{-\sigma_\alpha^2/2} + r^2 \tag{2.14}$$

The minimizing η, given by

$$\eta = \frac{r^2}{r^2+\sigma_r^2} e^{-\sigma_\alpha^2/2} \tag{2.15}$$

is bounded by the MUCM scaling term. Therefore, the mean square error of the MUCM conversion is always less than that of the UCM conversion [40]. This is confirmed by Fig. 2.3, that shows UCM is unbiased, MUCM has the minimum mean square error, and the conventional conversion is a compromise of the two.

2.3.3 Evaluation of Consistency

In addition to bias and mean square error performance of the conversion, consistency is an important metric. For a conversion to be consistent, the mean square error of the converted measurement relative to the truth must be consistent with the estimated converted measurement error covariance. A common measure of consistency is the the Normalized Error Squared (NES) [3],

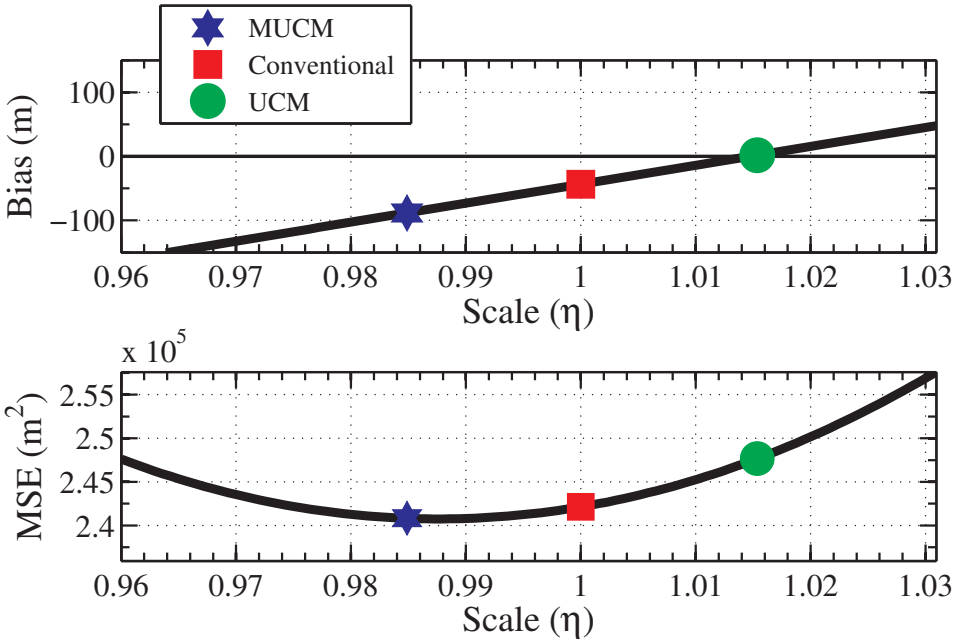

Fig. 2.3: Bias and MSE versus scale factor η for a range of 3000m, $\sigma_\alpha = 10\,^\circ$ and $\sigma_r = 30$m

$$\text{NES} = \frac{1}{N}\sum_{i=1}^{N} \tilde{\mathbf{z}}_i' R_i^{-1} \tilde{\mathbf{z}}_i \tag{2.16}$$

where $\tilde{\mathbf{z}}_i$ is the converted measurement error, R_i is the converted measurement error covariance estimate for trial i, and N is the number of trials. The NES of a consistent estimator should be close to the state dimension, which in this case is 2, and (if $\tilde{\mathbf{z}}_i$ is zero-mean Gaussian with covariance R_i) be chi-square distributed with nN degrees of freedom.

Both UCM and MUCM approaches are statistically consistent based on their NES, while the conventional conversion is not. The individual components of the UCM and MUCM converted measurements, however, are inconsistent in certain geometries. In particular, the covariance estimate along the true bearing is overestimated, resulting in an NES less than one. Fig. 2.4 shows the total NES and the individual components' NES. The overestimation of the covariance is exhibited for small angles in the x component and near 90° in the y component. The UT results, not shown, are very similar to the MUCM results, with the fourth order UT performance being nearly identically to the MUCM approach.

2.3.4 Evaluation of Estimation Bias

To allow for practical implementation, each of the conversion methods described in Section 2.3 use the measurement to calculate the converted measurement error covariance. As a result, *the estimate of the covariance becomes correlated with*

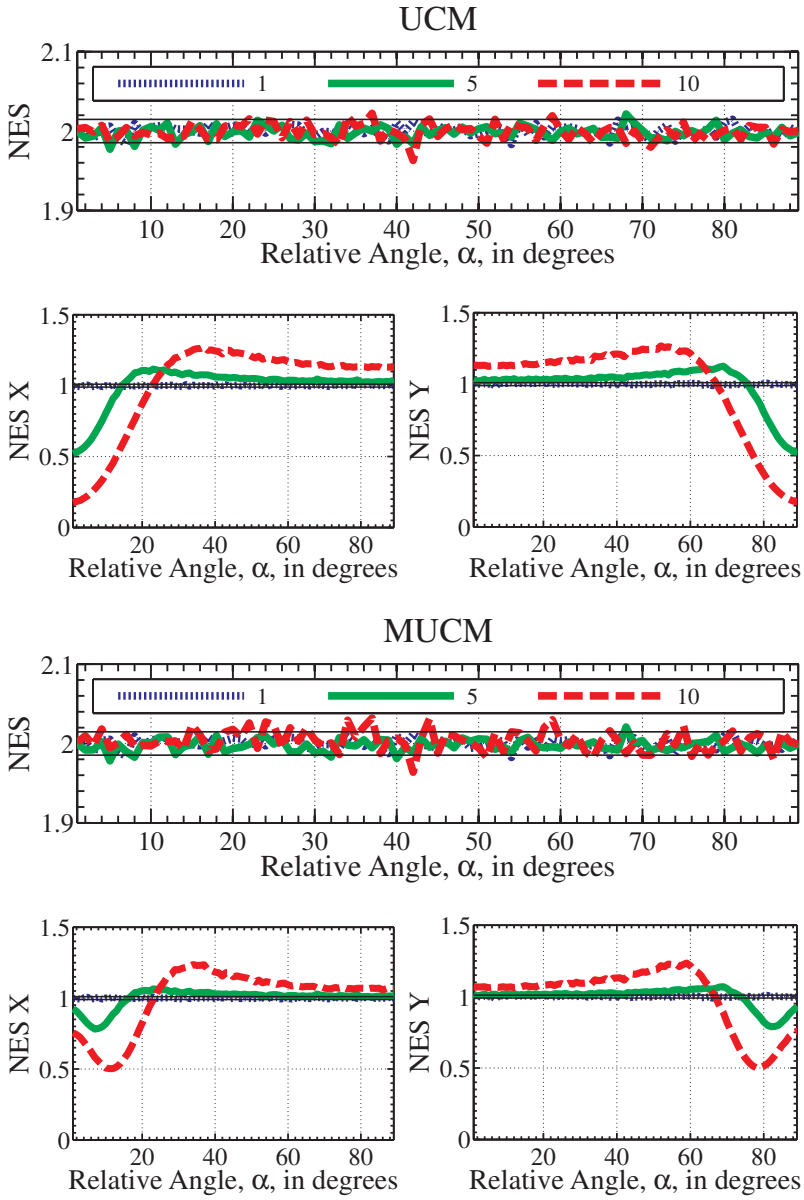

Fig. 2.4: Normalized Error Squared (NES) for the UCM and MUCM conversions based on 10^4 Monte-Carlo runs using a range of 3,000m and bearing of 0° to 90°. The range and bearing measurement noises used were uncorrelated Gaussian with $\sigma_r = 30$m and $\sigma_\alpha = 1°$, 5° and 10°. Plots include chi-square 0.99 probability bounds.

the measurement noise, leading to a *biased estimator* [43,26,11]. This estimation bias can be illustrated using a linear least squares estimator (LLSE) for a static target. The LLSE, $\hat{x}$, is an average of the converted measurements, weighted by the inverse of the converted measurement noise covariance. A true bearing of 0° is used in the evaluation to place the bias conveniently along the x-axis. The estimation bias, b_{est}, and overall bias, b_{tot} are defined as:

$$b_{est,\mathrm{UCM}} = E\left[\hat{x}\right] - E\left[e^{\sigma_\alpha^2/2} r_m \cos\alpha_m\right] \tag{2.17}$$

$$b_{est,\mathrm{MUCM}} = E\left[\hat{x}\right] - E\left[e^{-\sigma_\alpha^2/2} r_m \cos\alpha_m\right] \tag{2.18}$$

$$b_{tot} = E\left[\hat{x}\right] - x_{true} \tag{2.19}$$

In the example geometry the bias is along the x-axis, while in general it is along the true line of sight to the target. The bias can have a negative impact on performance for sonar [11] and radar [13] applications. An implementation of a LLSE using 10,000 measurements was used to evaluate estimation bias. Fig. 2.5 evaluates the estimation bias for two cases, one applicable to sonar with σ_r = 50m, and the second applicable to radar with σ_r = 0.5m. As the figure shows, estimation bias is a problem for all conversion methods. It is interesting to note that while the estimation bias for each method is nearly identical (Fig. 2.5), the total bias (Fig. 2.6) is smaller for the MUCM and UT techniques. This is due to the fact that the MUCM and UT conversion bias and estimation bias are in opposite directions and have approximately the same magnitude. While

the conversion bias and estimation bias fortuitously nearly cancel, using a biased conversion is not ideal for recursive estimation. For trackers using low process noise, the MUCM conversion will eventually converge to a solution with little bias. For higher process noise situations, where the tracker relies more on the converted measurement, the biased measurement conversion will degrade performance.

Also disconcerting for all the methods is that a static target will, on average, initially appear to be moving away from the sensor as the estimator transitions from the initial conversion bias to the total bias. Fig. 2.7 shows the apparent motion for the static case using the UCM conversion.

2.4 Decorrelated Unbiased Converted Measurement

An ideal measurement conversion would be unbiased, consistent, provide minimum mean square error estimates and would not suffer from estimation bias. Since no single conversion can achieve all these goals, compromises must be made. The primary trade-off is the MSE performance of the MUCM and the UT conversions against the unbiased characteristic of the UCM conversion. Since a fundamental assumption in the Kalman filter is that the measurement errors are unbiased, the unbiased UCM conversion is preferred, and an adjustment to the output of the filter can be made to achieve the MSE performance of MUCM and the UT. The measurement error covariance must also be uncorrelated with the measurement error to overcome estimation bias. DUCM is proposed [11] to achive these goals.

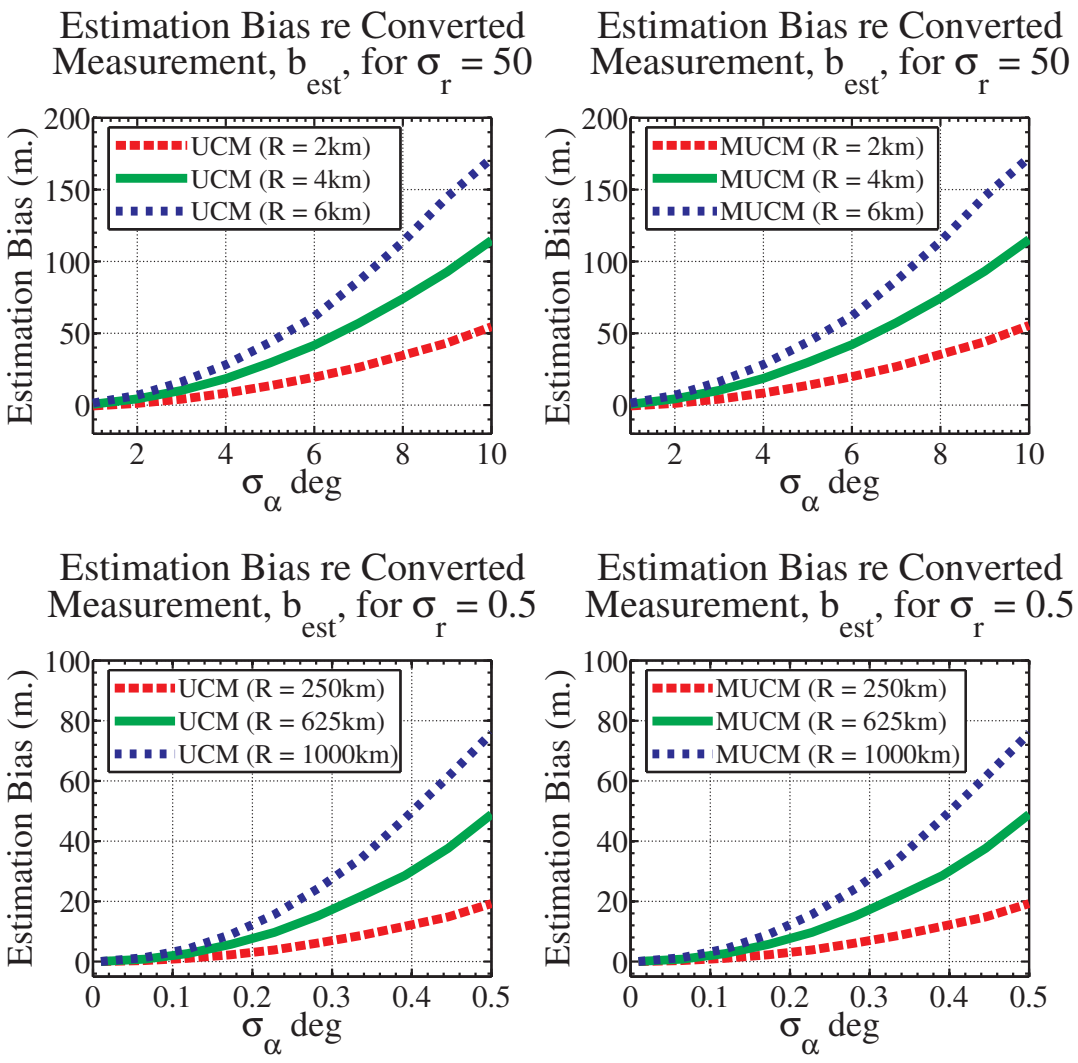

Fig. 2.5: Estimation bias versus σ_α for a 10,000 sample LLSE using the UCM and MUCM/UT conversion methods for various ranges and $\sigma_r = 50$m and 0.5m.

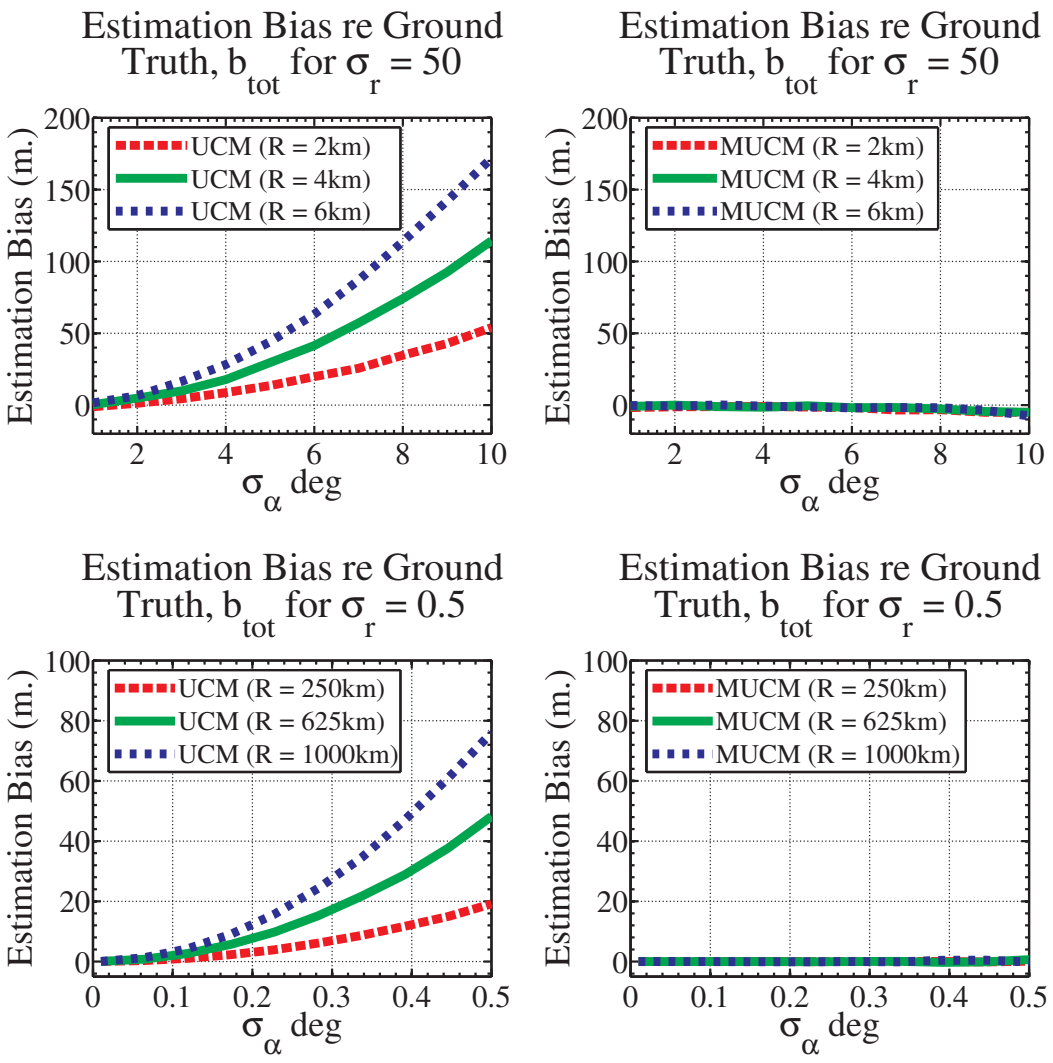

Fig. 2.6: Total bias versus σ_α for a 10,000 sample LLSE using the UCM and MUCM/UT conversion methods for various ranges and $\sigma_r = 50$m and 0.5m..

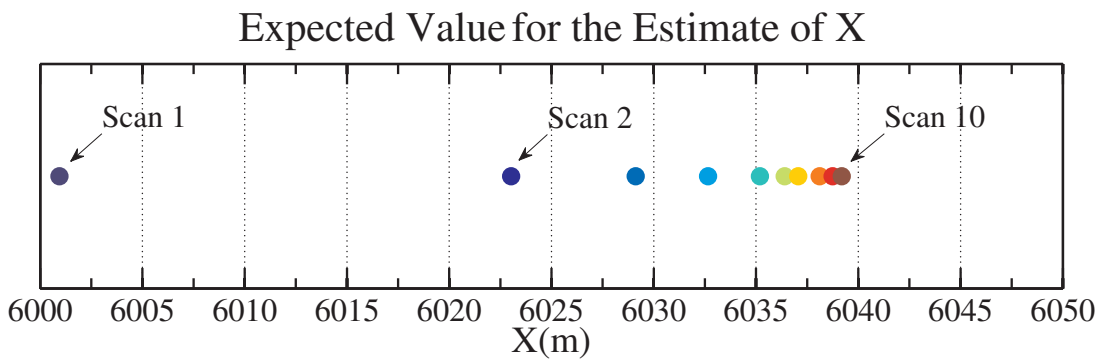

Fig. 2.7: Expected values of the first 10 scans of the LLSE for a range of 6000m and $\alpha = 0$. $\sigma_\alpha = 5^\circ$ and $\sigma_r = 50$m.

The DUCM conversion utilizes the UCM measurement conversion to eliminate conversion bias and avoids correlation of the converted measurement error covariance estimate and the measurement noise to preclude estimation bias. To decorrelate the measurement error covariance from the measurement noise, the measurement error covariance can be conditioned on the previous measurement [43] or on the predicted estimate (i.e., use one-step predictions). Conditioning on the predicted estimate leads to improved performance [47]. The use of the estimate versus the previous measurement provides for improvement in two ways. First, the estimate is, in general, more accurate than the measurement and second, the estimate can be propagated to the time of the new measurement, while the previous measurement lags the current target position.

Two approaches have been proposed that evaluate the measurement error covariance at the prediction. The implementation of [47] evaluates at either the

measurement or the prediction, depending on which estimate is viewed as more accurate. This implementation, however, utilizes the biased MUCM conversion (2.6). The BLUE filter [60] was originally developed by disregarding the Kalman filter framework in favor of a recursive linear minimum mean square error estimator. The resulting filter however can be reformulated as a converted measurement Kalman filter [25] that uses the UCM conversion (2.4) and a converted measurement error covariance calculated with the predicted estimate. Defining the predicted position as x_t and y_t and its associated covariance at scan $k+1$ given observations up to and including scan k as P_{p}, the equivalent BLUE error covariance for the Kalman filter framework is

$$\begin{aligned}
S^{11}_{\mathrm{BLUE}} &= \frac{1}{2}\left(1+e^{-2\sigma_\alpha^2}\right)\left(P^{11}_{\mathrm{p}}+x_t^2\right) - e^{-\sigma_\alpha^2}x_t^2 \\
&\quad + \frac{1}{2}\left(1-e^{-2\sigma_\alpha^2}\right)\left(P^{22}_{\mathrm{p}}+y_t^2\right) \\
&\quad + \frac{1}{2}\sigma_r^2\left(1+e^{-2\sigma_\alpha^2}\frac{x_t^2-y_t^2}{x_t^2+y_t^2}\right) \\
S^{22}_{\mathrm{BLUE}} &= \frac{1}{2}\left(1+e^{-2\sigma_\alpha^2}\right)\left(P^{22}_{\mathrm{p}}+y_t^2\right) - e^{-\sigma_\alpha^2}y_t^2 \\
&\quad + \frac{1}{2}\left(1-e^{-2\sigma_\alpha^2}\right)\left(P^{11}_{\mathrm{p}}+x_t^2\right) \\
&\quad + \frac{1}{2}\sigma_r^2\left(1+e^{-2\sigma_\alpha^2}\frac{y_t^2-x_t^2}{x_t^2+y_t^2}\right) \\
S^{12}_{\mathrm{BLUE}} &= e^{-2\sigma_\alpha^2}P^{12}_{\mathrm{p}} + \sigma_r^2 e^{-2\sigma_\alpha^2}\frac{x_t y_t}{x_t^2+y_t^2} \\
&\quad + \left(e^{-2\sigma_\alpha^2}-e^{-\sigma_\alpha^2}\right)x_t y_t
\end{aligned} \tag{2.20}$$

$$R_{\text{BLUE}} = e^{\sigma_\alpha^2} S_{\text{BLUE}} - P_{\text{p}} \tag{2.21}$$

The approach proposed for the DUCM technique also conditions the UCM error covariance on the predicted estimate but the derivation is in the measurements' coordinate system, namely,

$$\begin{aligned}
R_{\text{DUCM}}^{11} &= \frac{1}{2}\left(r_t^2 + \sigma_r^2 + \sigma_{r_t}^2\right) \\
&\quad \cdot \left[1 + \cos(2\alpha_t) e^{-2\sigma_\alpha^2} e^{-2\sigma_{\alpha_t}^2}\right] e^{\sigma_\alpha^2} \\
&\quad - \frac{1}{2}\left(r_t^2 + \sigma_{r_t}^2\right)\left[1 + \cos(2\alpha_t) e^{-2\sigma_{\alpha_t}^2}\right] \\
R_{\text{DUCM}}^{22} &= \frac{1}{2}\left(r_t^2 + \sigma_r^2 + \sigma_{r_t}^2\right) \\
&\quad \cdot \left[1 - \cos(2\alpha_t) e^{-2\sigma_\alpha^2} e^{-2\sigma_{\alpha_t}^2}\right] e^{\sigma_\alpha^2} \\
&\quad - \frac{1}{2}\left(r_t^2 + \sigma_{r_t}^2\right)\left[1 - \cos(2\alpha_t) e^{-2\sigma_{\alpha_t}^2}\right] \\
R_{\text{DUCM}}^{12} &= \frac{1}{2}\left(r_t^2 + \sigma_r^2 + \sigma_{r_t}^2\right) \\
&\quad \cdot \left[\sin(2\alpha_t) e^{-2\sigma_\alpha^2} e^{-2\sigma_{\alpha_t}^2}\right] e^{\sigma_\alpha^2} \\
&\quad - \frac{1}{2}\left(r_t^2 + \sigma_{r_t}^2\right)\left[\sin(2\alpha_t) e^{-2\sigma_{\alpha_t}^2}\right]
\end{aligned} \tag{2.22}$$

where r_t and α_t are the track's predicted estimate's range and bearing and $\sigma_{\alpha_t}^2$ and $\sigma_{r_t}^2$ are their associated variances (see appendix A). These quantities are approximated using a linearization of the track's covariance, ignoring correlation between range and bearing errors. The track's predicted range and approximated range variance are as follows

$$r_t = \sqrt{{x_t}^2 + {y_t}^2} \tag{2.23}$$

$$\sigma^2_{r_t} = \begin{bmatrix} \frac{\partial r_t}{\partial x_t} & \frac{\partial r_t}{\partial y_t} \end{bmatrix} P_{\mathrm{p}} \begin{bmatrix} \frac{\partial r_t}{\partial x_t} \\ \\ \frac{\partial r_t}{\partial y_t} \end{bmatrix} \tag{2.24}$$

which simplifies to

$$\sigma^2_{r_t} = \frac{1}{r_t^2} \begin{bmatrix} x_t & y_t \end{bmatrix} P_{\mathrm{p}} \begin{bmatrix} x_t \\ \\ y_t \end{bmatrix} \tag{2.25}$$

Similarly, the predicted bearing and approximated bearing variance are

$$\alpha_t = \tan^{-1}\left(\frac{y_t}{x_t}\right) \tag{2.26}$$

$$\sigma^2_{\alpha_t} = \begin{bmatrix} \frac{\partial \alpha_t}{\partial x_t} & \frac{\partial \alpha_t}{\partial y_t} \end{bmatrix} P_{\mathrm{p}} \begin{bmatrix} \frac{\partial \alpha_t}{\partial x_t} \\ \\ \frac{\partial \alpha_t}{\partial y_t} \end{bmatrix} \tag{2.27}$$

which simplifies to:

$$\sigma^2_{\alpha_t} = \frac{1}{r_t^4} \begin{bmatrix} -y_t & x_t \end{bmatrix} P_{\mathrm{p}} \begin{bmatrix} -y_t \\ \\ x_t \end{bmatrix} \tag{2.28}$$

The difference in the BLUE and DUCM techniques is in the assumptions and approximations for the error statistics of the predicted estimate. The BLUE filter approximation is based on an assumption that the error statistics are Gaussian in Cartesian coordinates, while the DUCM approach assumes that the error statistics are Gaussian in polar coordinates. The DUCM approximation is more valid for the initial scans of the tracker, while over time, the BLUE approximation has more validity.

2.4.1 Evaluation of Conversion Bias and Consistency

Since the DUCM conversion is exactly the UCM conversion, it is unbiased. For the calculation of R_{DUCM}, a predicted estimate x_t and y_t is required. To simulate this in an evaluation of the NES, the predicted estimates x_t and y_t were set to the ground truth state corrupted by normally distributed noise with σ_x and σ_y at 30m with a correlation of 0.1. P_{p} was set appropriately based on this noise. Under the condition that the underlying error distribution of the predicted estimate is normally distributed in Cartesian coordinates, the DUCM conversion is consistent overall, as well as consistent in the individual components of the conversion. If, however, the underlying error distribution of the predicted estimate is normally distributed in polar coordinates, DUCM remains consistent overall, but the individual components exhibit inconsistencies similar to the UCM, MUCM and UT conversions. Fig. 2.8 shows the NES of the DUCM conversion. The NES of the BLUE conversion, not shown, is nearly identical to the DUCM conversion.

2.4.2 Evaluation of Estimation Bias

By evaluating the converted measurement error covariance at the predicted estimate, the covariance is no longer correlated with the measurement noise, thus precluding estimation bias. Evaluation of the BLUE and DUCM techniques indicates that neither the estimation bias nor the overall bias are significant. Fig. 2.9 and 2.10 show the estimation and total bias for DUCM in the sonar and radar

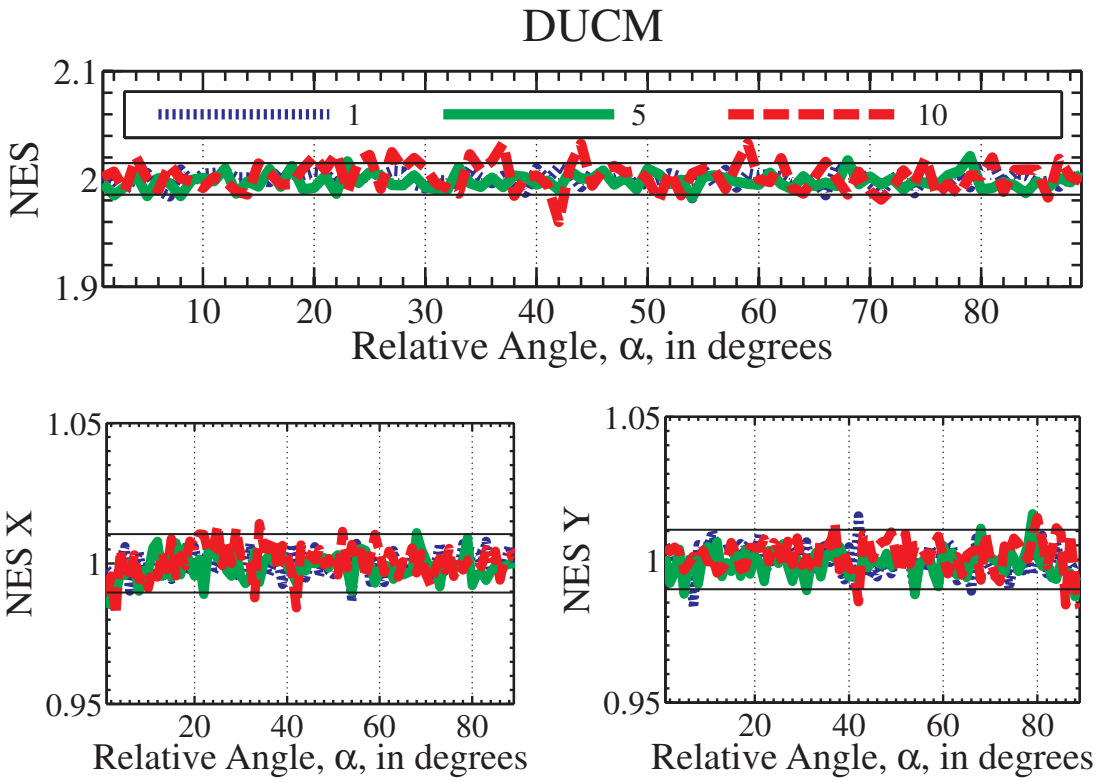

Fig. 2.8: Normalized Error Squared (NES) for the DUCM conversions based on 10^4 Monte-Carlo runs using a range of 3,000m and bearing of 0° to 90°. The range and bearing measurement noises used were uncorrelated Gaussian with $\sigma_r = 30$m and $\sigma_\alpha = 1°$, 5° and 10°. Plots include chi-square 0.99 probability bounds.

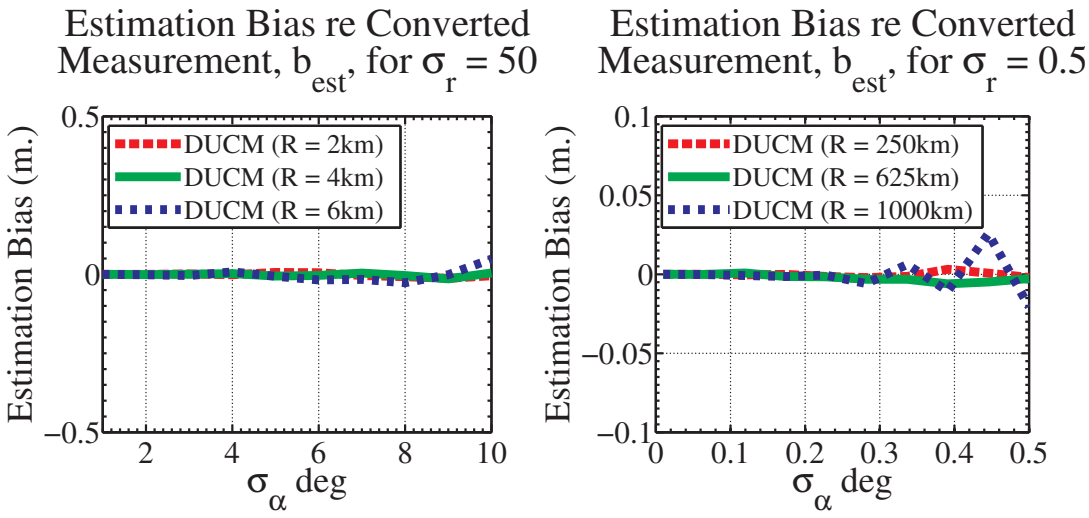

Fig. 2.9: Estimation bias versus σ_α for a 10,000 sample LLSE using the DUCM conversion methods for various ranges and σ_r = 50m and 0.5m..

test cases.

2.4.3 Improvement of MSE Performance

While the DUCM conversion is unbiased, the MSE of the conversion is larger than that of the MUCM conversion as shown in Fig. 2.3. This figure shows the relationship of an unbiased estimate, with a scale factor of $e^{\sigma_\alpha^2/2}$, and a MMSE estimate, with a scale factor of $e^{-\sigma_\alpha^2/2}$ (i.e. different by $e^{-\sigma_\alpha^2}$). Based on this relationship, the following scale factor (2.29) converts the unbiased estimate into an approximate MMSE estimate[1].

[1] Some researchers prefer the name 'Federated Unbiased Converted Measurements (FedUCM)', alluding to the union of decorrelating, debiasing and MMSE scaling. Subsequent plots referencing DUCM performance include the MMSE scaling.

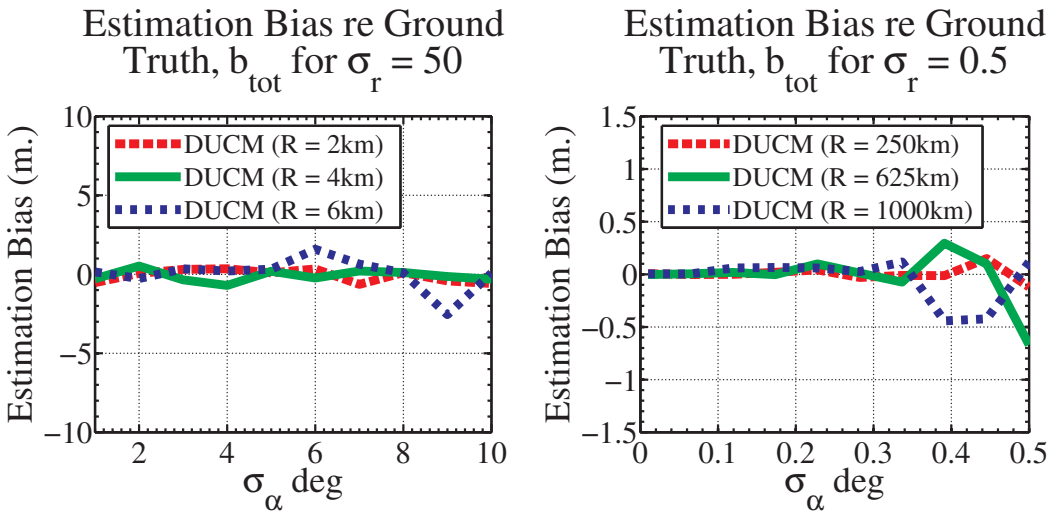

Fig. 2.10: Total bias versus σ_α for a 10,000 sample LLSE using the DUCM conversion methods for various ranges and $\sigma_r = 50$m and 0.5m.

$$\eta_{\text{DUCM}} = e^{-\sigma^2_{\alpha_t}} \tag{2.29}$$

To improve the MSE performance of DUCM, this scale factor is applied to the output of the filter. Unlike the MUCM approach, that supplies a MMSE and biased converted measurement to the filter, the DUCM application of the scaling factor only to the output allows for the Kalman filter assumption of unbiased measurements to be maintained while achieving MMSE performance.

2.5 Application to Converted Measurement Kalman Filter

The DUCM technique can be applied to the Converted Measurement Kalman Filter (CMKF) for improved state estimation. The DUCM CMKF is identical to

the standard KF [3], with the use of the converted measurement (2.4) and the DUCM estimate for the measurement error covariance using (2.22)–(2.28).

The CMKF state estimate, $\hat{\mathbf{x}} = \begin{bmatrix} x_t & y_t & \dot{x}_t & \dot{y}_t \end{bmatrix}'$, and associated error covariance, P, can be scaled as follows for improved MSE performance.

$$\hat{\mathbf{x}}_{\mathrm{o}}\left(k+1|k+1\right) = e^{-\sigma^2_{\alpha_t}}\hat{\mathbf{x}}\left(k+1|k+1\right) \tag{2.30}$$

$$P_{\mathrm{o}}\left(k+1|k+1\right) = e^{-2\sigma^2_{\alpha_t}}P\left(k+1|k+1\right) \tag{2.31}$$

The scaled estimates are for output only, and are not used as the prior for time $k+2$. As such, the use of this scaling is optional and application dependent. Since the bias is along the line of sight to the target, the scaled output is closer to the sensor than the unscaled estimate and should be employed when minimum mean square error estimates are desirable. If, however, an unbiased estimate is preferred, the unscaled estimate should be used. Regardless of the implementation chosen, the unbiased estimate is used as the prior for the next filter iteration.

To evaluate tracking performance, two scenarios are examined, in which the

1. True initial target range, r, normally distributed,
2. True initial target bearing uniformly distributed ($-\pi$ to π),
3. True target heading uniformly distributed ($-\pi$ to π), and
4. True target speed χ_{2DOF} distributed, scaled by σ_s

Table 2.3: CMKF Test Cases

Parameter	**Test Case I**	**Test Case II**
Initial Target Range ($\mu \pm \sigma$)	$4,000 \pm 30m$	$500 \pm 10km$
Target Speed σ_s	$10m/s$	$50m/s$
Sensor σ_r	$20m$	$0.5m$
Sensor σ_α	5°	$\frac{3}{15}^\circ$
Tracker Process Noise $\tilde{q}$	$0.44m^2/s^3$	$2.18m^2/s^3$

The target follows a nearly constant velocity track and is estimated using a CMKF with a discretized continuous white noise acceleration model [3]. One-point initialization of the tracker is used with an initial velocity estimate of 0 m/s and standard deviation of σ_s m/s in each component. The parameters for each test case are listed in Table 2.3.

Evaluation of tracking performance indicates that CMKFs using decorrelated techniques (i.e. DUCM and BLUE) outperform the CMKF using the conventional, UCM, MUCM or UT in position and velocity MSE. As expected, the performances of the MUCM and UT conversions are nearly identical. Fig. 2.11 shows the MSE comparison of the techniques for each test case. The posterior Cramer-Rao lower bound (PCRLB), as defined in [50], is shown for reference.

Both decorrelated techniques nearly achieve the bound. The conventional performance in Test Case II was very poor, and removed from the plot to allow for better comparison of the other techniques.

An inspection of the DUCM and BLUE filters show that performance is very similar. The DUCM filter, with the scaling of (2.31), exhibits improved MSE performance for initialization. After the initial updates performance is nearly identical to the BLUE filter, with the BLUE filter having an insignificant advantage.

To ensure credibility of the methods, the ANEES performance is examined. The ANEES scaled by the state dimension, n, is [3]

$$\text{ANEES} = \frac{1}{Nn} \sum_{i=1}^{N} \tilde{\mathbf{x}}_i^T P_i^{-1} \tilde{\mathbf{x}}_i \tag{2.32}$$

where $\tilde{\mathbf{x}}_i$ is the estimation error and P_i is the error covariance for trial i. Ideally, the ANEES of a consistent estimator is 1. Fig. 2.11 shows that the decorrelated approaches are the most consistent, with an ANEES that is approximately 1.

2.6 Extension to Spherical Coordinates

The results of the previous two sections can be extended from polar to spherical coordinates for cases in which the measurements include elevation, θ. Details on the extension of the UCM, MUCM, UT and BLUE conversions to spherical can be found in [45], [20], [34] and [59] respectively. The conventional conversion is

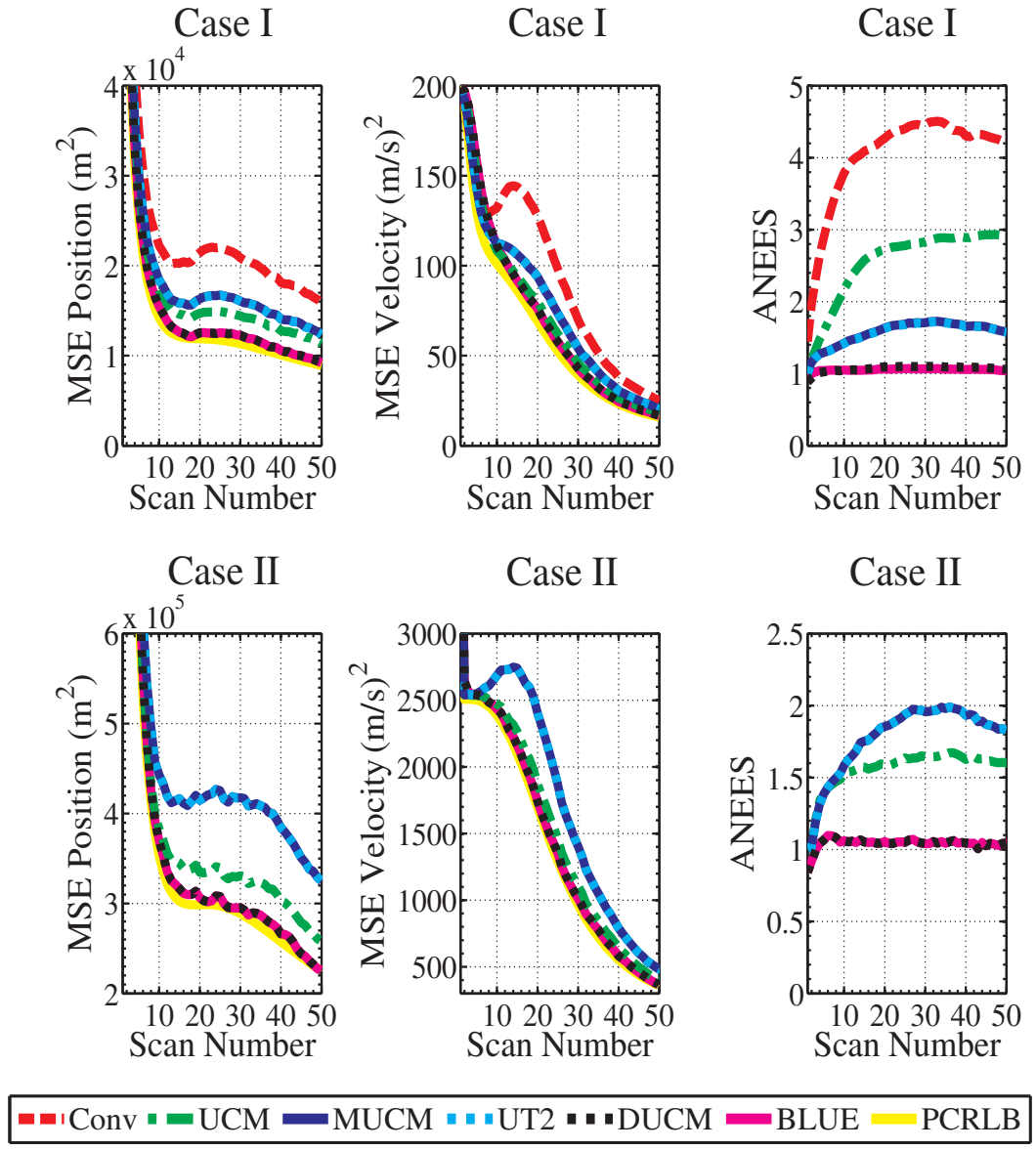

Fig. 2.11: CMKF position MSE, velocity MSE, and ANEES for the Conventional, UCM, MUCM, UT, DUCM and BLUE conversion methods from 5000 Monte-Carlo runs of two target tracking scenarios.

$$\begin{bmatrix} x_m^{\text{CONV}} \\ y_m^{\text{CONV}} \\ z_m^{\text{CONV}} \end{bmatrix} = \begin{bmatrix} r_m \cos\alpha_m \cos\theta_m \\ r_m \sin\alpha_m \cos\theta_m \\ r_m \sin\theta_m \end{bmatrix} \tag{2.33}$$

which has an expected value of

$$E\begin{bmatrix} x_m^{\text{CONV}} \\ y_m^{\text{CONV}} \\ z_m^{\text{CONV}} \end{bmatrix} = \begin{bmatrix} e^{-\sigma_\alpha^2/2} e^{-\sigma_\theta^2/2} r_m \cos\alpha_m \cos\theta_m \\ e^{-\sigma_\alpha^2/2} e^{-\sigma_\theta^2/2} r_m \sin\alpha_m \cos\theta_m \\ e^{-\sigma_\theta^2/2} r_m \sin\theta_m \end{bmatrix} \tag{2.34}$$

To apply a decorrelated and unbiased technique, the conversion of [45] is employed

$$\begin{bmatrix} x_m^{\text{UCM3D}} \\ y_m^{\text{UCM3D}} \\ z_m^{\text{UCM3D}} \end{bmatrix} = \begin{bmatrix} e^{\sigma_\alpha^2/2} e^{\sigma_\theta^2/2} r_m \cos\alpha_m \cos\theta_m \\ e^{\sigma_\alpha^2/2} e^{\sigma_\theta^2/2} r_m \sin\alpha_m \cos\theta_m \\ e^{\sigma_\theta^2/2} r_m \sin\theta_m \end{bmatrix} \tag{2.35}$$

As in the 2D case, the converted measurement error covariance should be calculated at the predicted measurement to avoid estimation bias. Extending the methodology in [25] to 3D, the BLUE filter for spherical measurements [59] can be put into a CMKF form. Defining the predicted position as x_t, y_t and z_t and its associated covariance at scan $k+1$ given observations up to and including scan k as P_{p}, the BLUE equivalent converted measurement error covariance for the CMKF is

$$R_{\text{BLUE3D}} = \Gamma S \Gamma' - P_{\text{p}} \tag{2.36}$$

where S is defined in [59] and

$$\Gamma = \begin{bmatrix} e^{\sigma_{\alpha_t}^2/2} e^{\sigma_{\theta_t}^2/2} & 0 & 0 \\ 0 & e^{\sigma_{\alpha_t}^2/2} e^{\sigma_{\theta_t}^2/2} & 0 \\ 0 & 0 & e^{\sigma_{\theta_t}^2/2} \end{bmatrix} \tag{2.37}$$

The extention of the DUCM technique for spherical measurement has the form

$$
\begin{aligned}
R^{11}_{\text{DUCM3D}} &= \frac{1}{4}\left(r_t^2+\sigma_r^2+\sigma_{r_t}^2\right)\left[1+\cos(2\alpha_t)e^{-2\sigma_\alpha^2}e^{-2\sigma_{\alpha_t}^2}\right]e^{\sigma_\alpha^2} \\
&\quad\cdot\left[1+\cos(2\theta_t)e^{-2\sigma_\theta^2}e^{-2\sigma_{\theta_t}^2}\right]e^{\sigma_\theta^2} \\
&\quad-\frac{1}{4}\left(r_t^2+\sigma_{r_t}^2\right)\left[1+\cos(2\alpha_t)e^{-2\sigma_{\alpha_t}^2}\right]\left[1+\cos(2\theta_t)e^{-2\sigma_{\theta_t}^2}\right] \\
R^{22}_{\text{DUCM3D}} &= \frac{1}{4}\left(r_t^2+\sigma_r^2+\sigma_{r_t}^2\right)\left[1-\cos(2\alpha_t)e^{-2\sigma_\alpha^2}e^{-2\sigma_{\alpha_t}^2}\right]e^{\sigma_\alpha^2} \\
&\quad\cdot\left[1+\cos(2\theta_t)e^{-2\sigma_\theta^2}e^{-2\sigma_{\theta_t}^2}\right]e^{\sigma_\theta^2} \\
&\quad-\frac{1}{4}\left(r_t^2+\sigma_{r_t}^2\right)\left[1-\cos(2\alpha_t)e^{-2\sigma_{\alpha_t}^2}\right]\left[1+\cos(2\theta_t)e^{-2\sigma_{\theta_t}^2}\right] \\
R^{33}_{\text{DUCM3D}} &= \frac{1}{2}\left(r_t^2+\sigma_r^2+\sigma_{r_t}^2\right)\left[1-\cos(2\theta_t)e^{-2\sigma_\theta^2}e^{-2\sigma_{\theta_t}^2}\right]e^{\sigma_\theta^2} \\
&\quad-\frac{1}{2}\left(r_t^2+\sigma_{r_t}^2\right)\left[1-\cos(2\theta_t)e^{-2\sigma_{\theta_t}^2}\right] \\
R^{12}_{\text{DUCM3D}} &= \frac{1}{4}\left(r_t^2+\sigma_r^2+\sigma_{r_t}^2\right)\left[\sin(2\alpha_t)e^{-2\sigma_\alpha^2}e^{-2\sigma_{\alpha_t}^2}\right]e^{\sigma_\alpha^2} \\
&\quad\cdot\left[1+\cos(2\theta_t)e^{-2\sigma_\theta^2}e^{-2\sigma_{\theta_t}^2}\right]e^{\sigma_\theta^2} \\
&\quad-\frac{1}{4}\left(r_t^2+\sigma_{r_t}^2\right)\left[\sin(2\alpha_t)e^{-2\sigma_{\alpha_t}^2}\right]\left[1+\cos(2\theta_t)e^{-2\sigma_{\theta_t}^2}\right] \\
R^{13}_{\text{DUCM3D}} &= \frac{1}{2}\left(r_t^2+\sigma_r^2+\sigma_{r_t}^2\right)\cos\alpha_t e^{-\sigma_\alpha^2/2}\left[\sin(2\theta_t)e^{-2\sigma_\theta^2}e^{-2\sigma_{\theta_t}^2}\right]e^{\sigma_\theta^2} \\
&\quad-\frac{1}{2}\left(r_t^2+\sigma_{r_t}^2\right)\cos\alpha_t e^{-\sigma_\alpha^2/2}\left[\sin(2\theta_t)e^{-2\sigma_{\theta_t}^2}\right] \\
R^{23}_{\text{DUCM3D}} &= \frac{1}{2}\left(r_t^2+\sigma_r^2+\sigma_{r_t}^2\right)\sin\alpha_t e^{-\sigma_\alpha^2/2}\left[\sin(2\theta_t)e^{-2\sigma_\theta^2}e^{-2\sigma_{\theta_t}^2}\right]e^{\sigma_\theta^2} \\
&\quad-\frac{1}{2}\left(r_t^2+\sigma_{r_t}^2\right)\sin\alpha_t e^{-\sigma_\alpha^2/2}\left[\sin(2\theta_t)e^{-2\sigma_{\theta_t}^2}\right] \qquad (2.38)
\end{aligned}
$$

where r_t, α_t and θ_t are the predicted estimate's range, bearing and elevation. Their associated variances are $\sigma_{r_t}^2$, $\sigma_{\alpha_t}^2$ and $\sigma_{\theta_t}^2$. As in the 2D case, these quantities are approximated using a linearization of tracked covariance, ignoring correlation be-

tween range, bearing and elevation errors. The predicted range and approximated range variance are as follows:

$$r_t = \sqrt{{x_t}^2 + {y_t}^2 + {z_t}^2} \tag{2.39}$$

$$\sigma^2_{r_t} = \frac{1}{r_t^2} \begin{bmatrix} x_t & y_t & z_t \end{bmatrix} P_{\mathrm{p}} \begin{bmatrix} x_t \\ y_t \\ z_t \end{bmatrix} \tag{2.40}$$

The predicted elevation an approximated elevation variance is

$$\theta_t = \tan^{-1}\left(\frac{z_t}{s_t}\right) \tag{2.41}$$

$$\sigma^2_{\theta_t} = \frac{1}{s_t^2 r_t^4} \begin{bmatrix} -x_t z_t & -y_t z_t & s_t^2 \end{bmatrix} P_{\mathrm{p}} \begin{bmatrix} -x_t z_t \\ -y_t z_t \\ s_t^2 \end{bmatrix} \tag{2.42}$$

where

$$s_t = \sqrt{{x_t}^2 + {y_t}^2} \tag{2.43}$$

The predicted bearing, α_t, and bearing variance, $\sigma^2_{\alpha_t}$, remain unchanged from the 2D case (2.27)–(2.28).

2.6.1 Evaluation of Conversion Bias

As in the 2D case, there is a multiplicative bias that occurs as a byproduct of the conventional conversion. The UCM technique eliminates this bias, while the

MUCM and UT conversions magnify the bias. The bias multiplier is different for the z component then it is for the z and y components. Table 2.4 shows the bias multiplier for each technique. Again, the UT bias is an approximation of the MUCM bias, however the approximation is equal up to, but not including, the fourth order for the 3D case.

2.6.2 Evaluation of Consistency

In the 2D case, the consistency of the conversion, based on the NES, was a function of the true bearing to the target. In the extension to 3D, consistency is a function of the true bearing and elevation to the target. In order to visualize the NES performance, the NES is plotted as the radius of a surface at each bearing and elevation. A consistent conversion would be a sphere with the radius of the state dimension at all angles. Fig. 2.12 show the consistency plots for the UCM conversion, including the overall consistency and the consistency of each component. Similar to the 2D results, the x component of the covariance is overestimated for bearings near 0° and 180°, and the y component is overestimated for bearings 90° and 270°. The z component is also overestimated for elevations near 90° and -90°. In the 2D case, despite the inconsistencies in the individual components, the overall NES is consistent. This is not true for the 3D case. The conversion is consistent for most angles, however, the overall covariance is overestimated for large elevation angles near $\pm 90^\circ$. This, however, is not a problem for the many

Table 2.4: 3D Conversion Bias Multiplier

Method	**Bias Multiplier (X and Y)**
Conventional	$e^{-\sigma_\alpha^2/2}e^{-\sigma_\theta^2/2}$
UCM	1 (Unbiased)
MUCM	$e^{-\sigma_\alpha^2}e^{-\sigma_\theta^2}$
UT	$\frac{1}{3}e^{-\sigma_\alpha^2/2}e^{-\sigma_\theta^2/2}\left[1+\cos\left(\sqrt{3}\sigma_\alpha\right)+\cos\left(\sqrt{3}\sigma_\alpha\right)\right]$
Method	**Bias Multiplier (Z)**
Conventional	$e^{-\sigma_\theta^2/2}$
UCM	1 (Unbiased)
MUCM	$e^{-\sigma_\theta^2}$
UT	$e^{-\sigma_\theta^2/2}\left[\frac{2}{3}+\frac{1}{3}\cos\left(\sqrt{3}\sigma_\alpha\right)\right]$

systems that deal with shallow elevation angles. Fig. 2.13 shows the NES for the MUCM conversion. MUCM exibits inconsistencies at the same bearings and elevations as UCM, with different characteristics.

Fig. 2.14 shows the NES for the DUCM conversion. This conversion is consistent overall and in each of the individual components at all angles except for elevations of $\pm 90^\circ$ under the assumption that the previous estimate is Gaussian distributed in Cartesian coordinates. To simulate the predicted estimate in the evaluation of the NES, x_t, y_t and z_t were set to the ground truth state corrupted by normally distributed noise with σ_x, σ_y and σ_z at 30m with a correlation of 0.1. P_{p} was set appropriately based on this noise.

2.6.3 DUCM CMKF with Spherical Measurements

The DUCM CMKF from Section 2.5 can be expanded to spherical measurements with the use of the 3D measurement conversion (2.35) and associated error covariance, R_{DUCM3D}, using (2.38)–(2.43).

To scale the state estimate, $\hat{\mathbf{x}}$ and associated covariance for improved MSE performance (for output only), the scaling matrix Λ is defined as

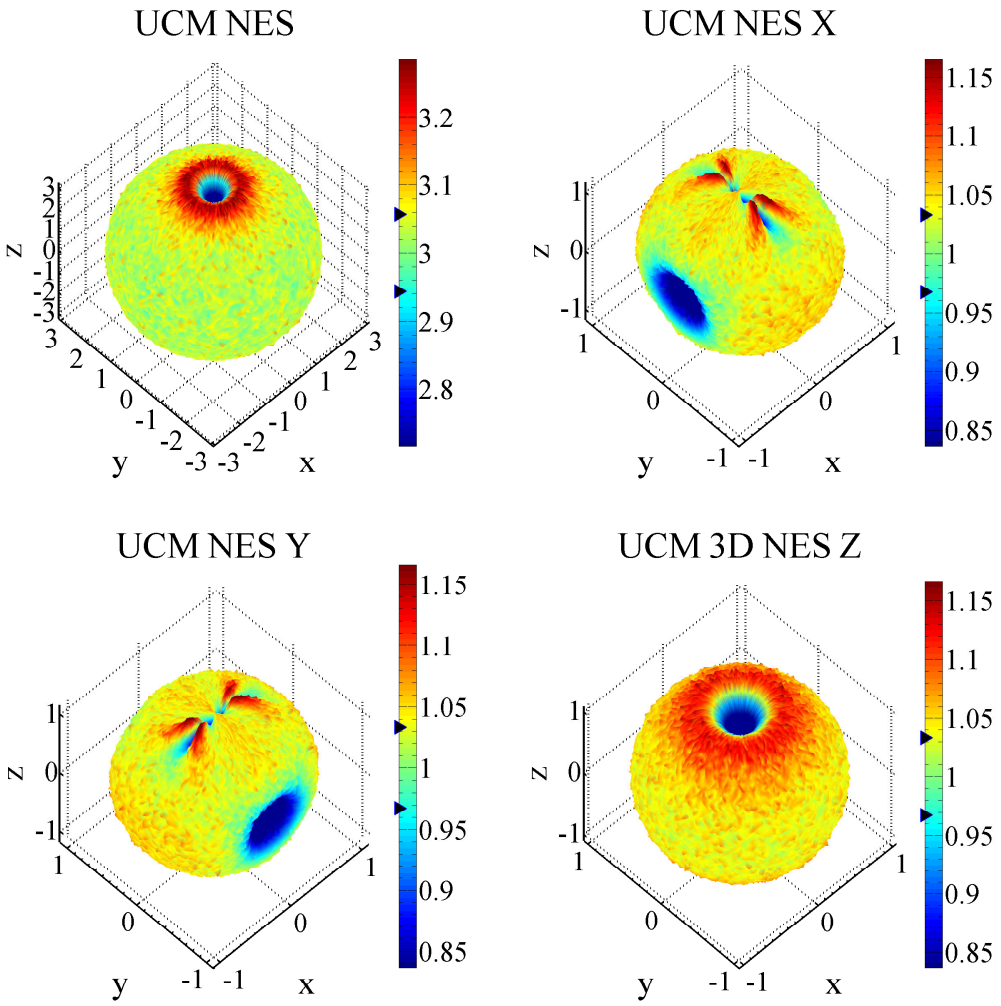

Fig. 2.12: Normalized Error Squared for the total, x component, y component and z component of UCM conversion at all target bearings and elevations. The range and bearing measurement noises used were uncorrelated Gaussian with $\sigma_r = 30$m and $\sigma_\alpha = 5°$. Chi-square upper (0.99) and lower (0.01) probability bounds are indicated on the colorbar as arrowheads.

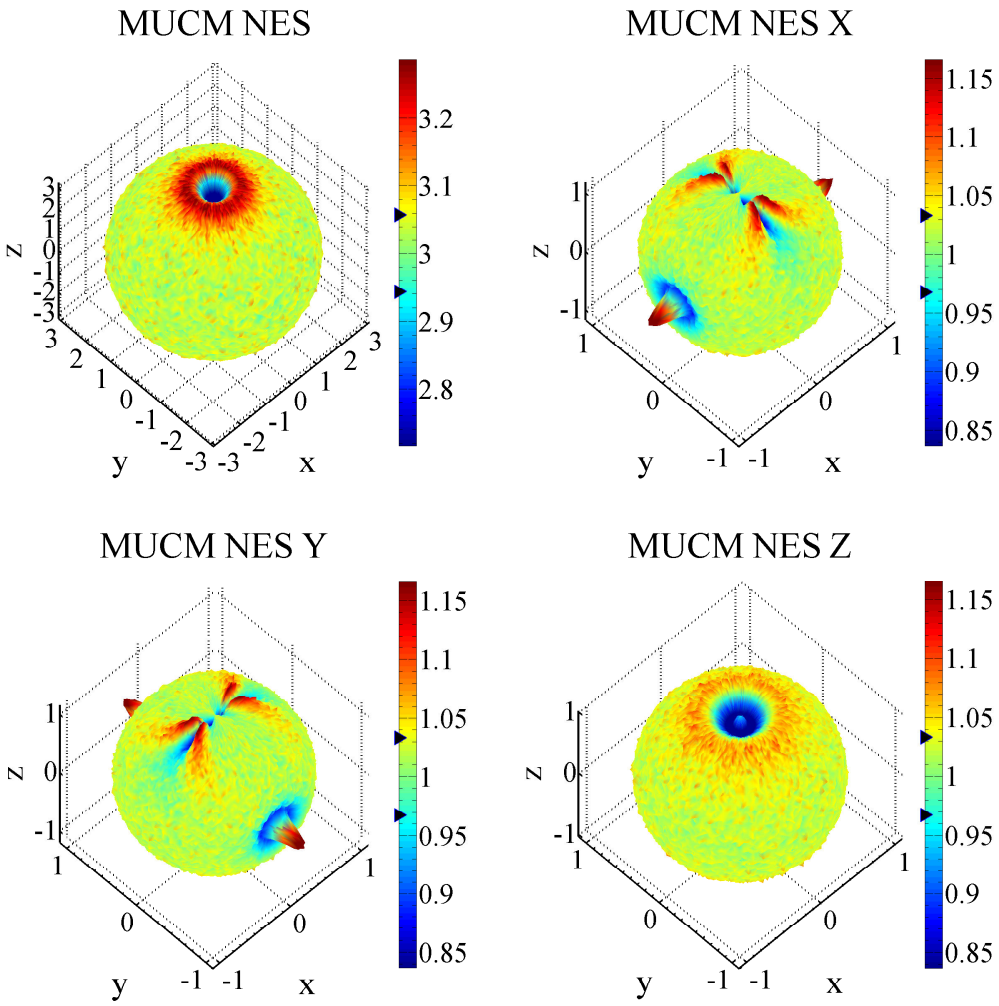

Fig. 2.13: Normalized Error Squared for the total, x component, y component and z component of MUCM conversion at all target bearings and elevations. The range and bearing measurement noises used were uncorrelated Gaussian with $\sigma_r = 30$m and $\sigma_\alpha = 5°$. Chi-square upper (0.99) and lower (0.01) probability bounds are indicated on the colorbar as arrowheads.

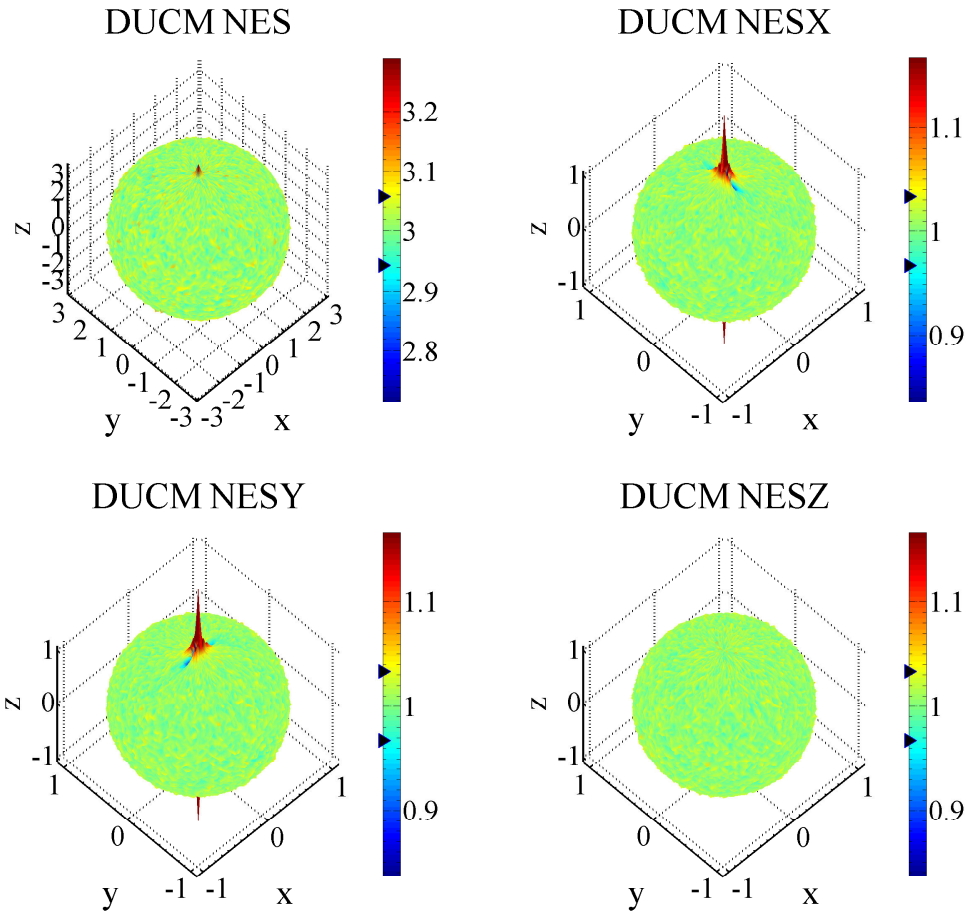

Fig. 2.14: Normalized Error Squared for the total, x component, y component and z component of DUCM conversion at all target bearings and elevations. The range and bearing measurement noises used were uncorrelated Gaussian with $\sigma_r = 30$m and $\sigma_\alpha = 5°$. Chi-square upper (0.99) and lower (0.01) probability bounds are indicated on the colorbar as arrowheads.

$$\lambda_1 = e^{-\sigma_{\alpha_t}^2} e^{-\sigma_{\theta_t}^2} \tag{2.44}$$

$$\lambda_2 = e^{-\sigma_{\theta_t}^2} \tag{2.45}$$

$$\Lambda = \begin{bmatrix} \lambda_1 & 0 & 0 & 0 & 0 & 0 \\ 0 & \lambda_1 & 0 & 0 & 0 & 0 \\ 0 & 0 & \lambda_2 & 0 & 0 & 0 \\ 0 & 0 & 0 & \lambda_1 & 0 & 0 \\ 0 & 0 & 0 & 0 & \lambda_1 & 0 \\ 0 & 0 & 0 & 0 & 0 & \lambda_2 \end{bmatrix} \tag{2.46}$$

and applied as follows

$$\hat{\mathbf{x}}_{\mathrm{o}}(k+1|k+1) = \Lambda \hat{\mathbf{x}}(k+1|k+1) \tag{2.47}$$

$$P_{\mathrm{o}}(k+1|k+1) = \Lambda P(k+1|k+1) \Lambda' \tag{2.48}$$

where $\hat{\mathbf{x}} = \begin{bmatrix} x_t & y_t & z_t & \dot{x}_t & \dot{y}_t & \dot{z}_t \end{bmatrix}'$. The CMKF performance evaluation for the two scenarios in Section 2.5 was repeated for the 3D case with the following modifications

1. True initial target elevation uniformly distributed from $-\frac{\pi}{3}$ to $\frac{\pi}{3}$,

2. True target pitch uniformly distributed from $-\pi$ to π,

3. True target speed χ_{3DOF} distributed, scaled by σ_s, and

4. Sensor elevation measurement standard deviation, $\sigma_\theta = \sigma_\alpha$

Evaluation of tracking performance indicates that the CMKF using the DUCM or BLUE technique outperforms the CMKF using UCM or MUCM in position MSE. Velocity MSE was also the best for the CMKF using the decorrelated techniques for all but the initial scans of Test Case I. Based on the ANEES, the decorrelated CMKFs maintained consistency, with an ANEES approximately equal to 1.

2.7 Conclusion

An ideal tracker provides state estimates that are unbiased, have minimum mean square error and are consistent. For a converted measurement tracker to achieved idealized results, two sources of bias need to be evaluated and eliminated. The first is measurement conversion bias that occurs when the conversion process introduces a bias in the mean of the converted measurement. The second is estimation bias that occurs when the estimate of the measurement error covariance is correlated with the measurement noise, leading to a biased Kalman gain. It has been shown for converted measurement tracking problems that a decorrelated version of the Unbiased Converted Measurement (DUCM) exhibits improved performance over many previously proposed techniques, and equivalent performance to the BLUE approach. The results show that decorrelation of the measurement error covariance from the measurement noise is key to the improved performance. Tracker performance has been demonstrated for estimation of position and velocity for

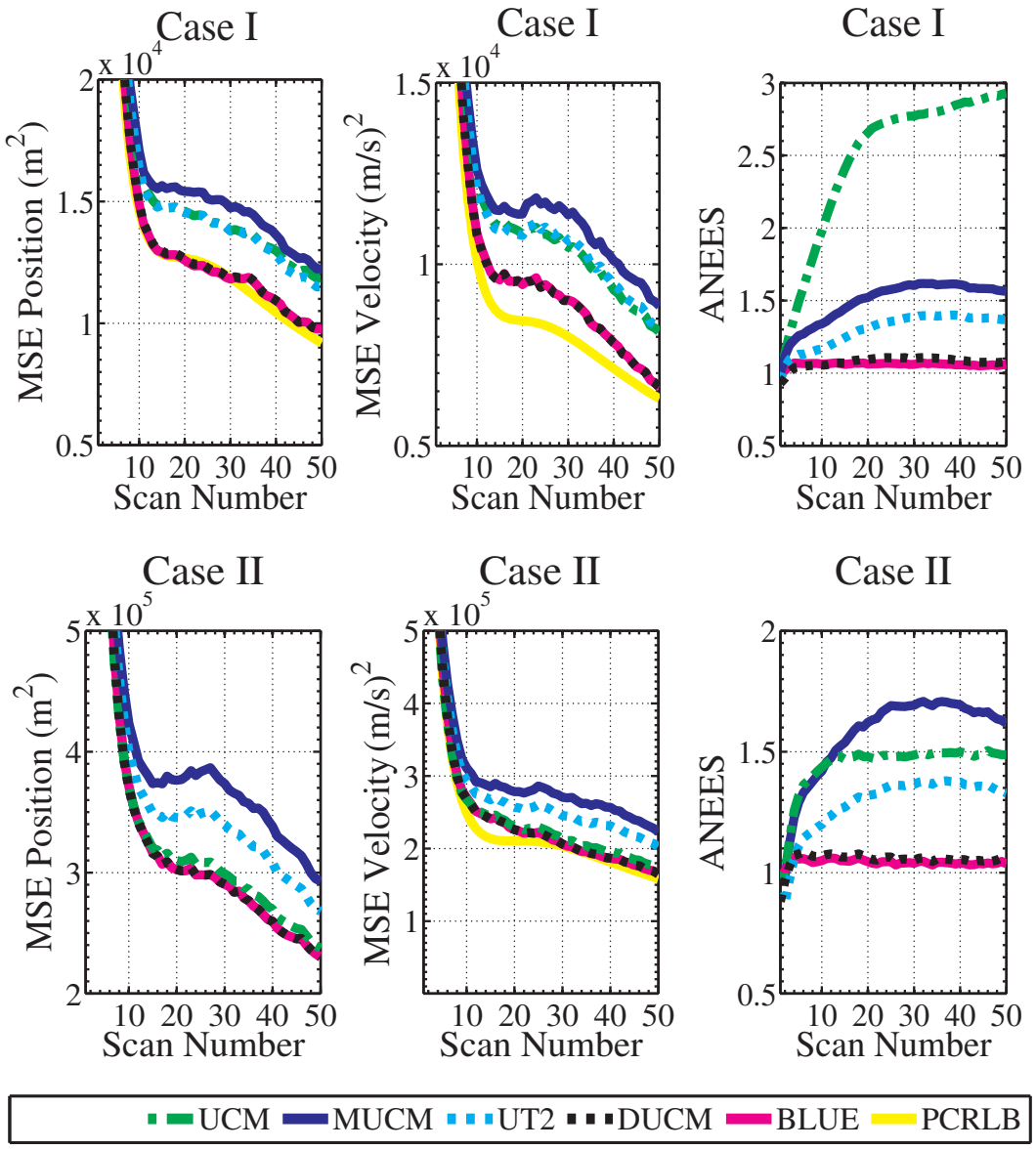

Fig. 2.15: CMKF position MSE, velocity MSE, and ANEES for the UCM, MUCM, UT, DUCM and BLUE conversion methods from 5000 Monte-Carlo runs of two target tracking scenarios.

sonar and radar applications with polar and spherical measurements.

Chapter 3

Unbiased Range Rate Estimation from a Moving Platform

3.1 Abstract

In many active sonar and radar applications, the sensor also provides a Doppler, or equivalently range rate, measurement. Use of Doppler in the estimation process has also been proposed by various authors. Here, the "decorrelated unbiased converted measurement" approach is derived for Doppler measurements from a moving platform. The goals are two-fold. The first goal is to show that a bias, similar to the bias shown by previous authors for conversion of position measurements, exists when measuring Doppler from a moving platform. The second is to examine the effects of biased measurements on estimation performance and the effectiveness of proposed compensation approaches.

3.2 Introduction

Estimation of range rate using active sonar or radar by taking advantage of the Doppler effect can be advantageous for improved target state estimation, track

association and for discriminating targets from stationary clutter. When estimating range rate from a moving platform it is necessary to nullify the effect of the platform speed. This nullification process suffers from a similar bias problem as the position measurement conversion.

Figure 1 provides an illustration of estimation from a moving platform. Measurements of relative range, r, and bearing, α, are related to the relative Cartesian coordinates as in (2.1). The relative position is translated into a reference coordinate system for tracking using the seeker position and heading, ψ, both of which are assumed known.

$$\begin{bmatrix} x_{ref} \\ y_{ref} \end{bmatrix} = \begin{bmatrix} \cos\psi & -\sin\psi \\ \sin\psi & \cos\psi \end{bmatrix} \begin{bmatrix} x \\ y \end{bmatrix} + \begin{bmatrix} \Delta x \\ \Delta y \end{bmatrix} \tag{3.1}$$

Also available is the additional measurement of range rate through the Doppler effect using the known transmit frequency, f_t, speed of the transmitted signal, c, and receive frequency, f_r. The Doppler imparted by the velocity of the own ship must be nullified based its known speed, V, and estimated bearing α.

$$d = \frac{(f_r - f_t)\, c}{2 f_t} - V \cos\alpha \tag{3.2}$$

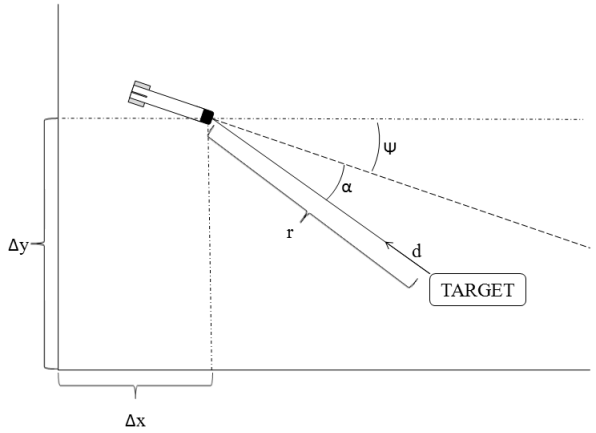

Fig. 3.1: Illustration of target tracking from a moving platform. The seeker has a known position and heading in the Cartesian tracking coordinate system. Relative range, r, and bearing, α, to the target are measured using active sonar or radar, converted to relative position, and translated to the tracking coordinate system using the seeker position, Δx and Δy, and heading, ψ.

3.3 Application to range rate estimation from a moving platform

The results of Chapter 2 can be applied to the problem of own Doppler nullification. The conventional technique used to estimate range rate is to nullify the effect of own-ship motion using (3.2). This conversion results in a biased measurement through the same mechanism as the polar to Cartesian conversion process. This bias can be avoided using a form of the decorrelated unbiased measurement conversion.

3.3.1 Evaluation of the Doppler conversion bias

The bias of the conventional technique can be found by taking the expected value of the converted frequency and bearing measurements, $f_{r,m}$ and α_m. Assuming the received frequency measurement noise, w_f, and bearing measurement noise, w_α, are uncorrelated, zero mean, and Gaussian with standard deviations of σ_f and σ_α respectively; the expected value is

$$\begin{aligned} E\left[\frac{(f_{r,m}-f_t)\,c}{2f_t} - V\cos\left(\alpha_m\right)\right] &= E\left[\frac{(f_r+w_f-f_t)\,c}{2f_t} - V\cos\left(\alpha+w_\alpha\right)\right] \\ &= \frac{(f_r-f_t)\,c}{2f_t} - V\cos\left(\alpha\right)e^{-\sigma_\alpha^2/2} \end{aligned} \tag{3.3}$$

resulting in the following bias

$$V\cos\left(\alpha\right)\left(1-e^{-\sigma_\alpha^2/2}\right). \tag{3.4}$$

The corresponding mean squared error is

$$R = \frac{\sigma_f^2 c^2}{4f_t^2} + V^2\left[\frac{1}{2}\left(1+\cos(2\alpha)e^{-2\sigma_\alpha^2}\right) + \cos^2\left(\alpha\right)\left(1-2e^{-\sigma_\alpha^2/2}\right)\right] \tag{3.5}$$

3.3.2 Bias significance

The significance of the bias depends on the characteristics of the radar or sonar system being employed. Key features include the velocity of the platform and the operating frequency relative to the speed of the sound (i.e. the wavelength). The ability of the system to estimate frequency and bearing is also important. Examining the Cramer-Rao Lower Bound (CRLB) for bearing and frequency estimation is useful for understanding the types of systems in which the bearing estimation error is more significant than the frequency estimation error. For the geometry of Figure 1, the CRLB definition for bearing estimation shows that bearing error is a function of signal to noise ratio, wavelength, array length and true bearing, α [35]. The ability to estimate bearing degrades as bearing increases. The CRLB definition for frequency estimation shows that the ability to estimate frequency is a function of data record length and signal to noise ratio [35]. For a realization of a signal with a given signal to noise ratio, the size of the array is a determining factor in the bias significance. Overall, the bias is most significant for high speed platforms with small arrays. Figure 13 shows the bias significance, defined as the bias divided by the square of the variance, for a conceptual sonar system operating at 50 kHz.

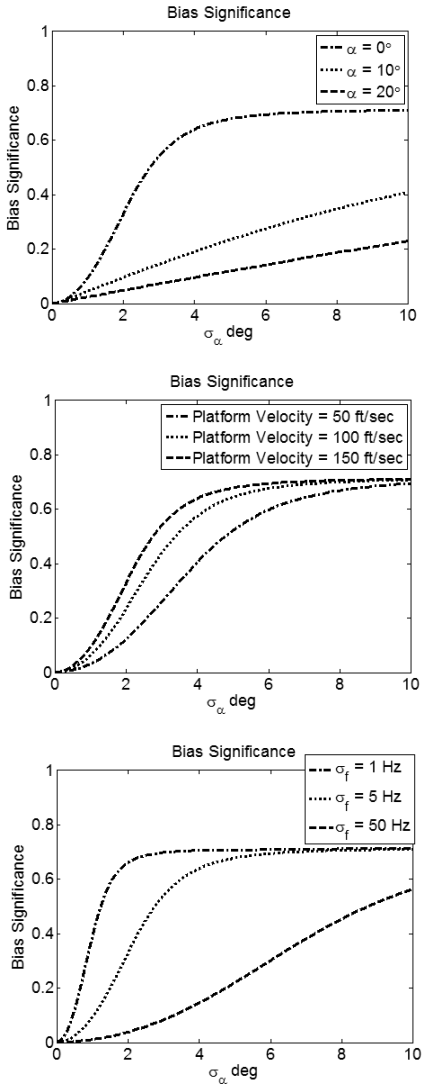

Fig. 3.2: Bias significance vs. σ_α of a 50 kHz sonar for various bearing angles, platform velocities and frequency measurement accuracies. Unless specified otherwise, platform velocity = 150 ft/s, $\sigma_f = 5$Hz and $\alpha = 0°$

.

3.3.3 Unbiased range rate estimation

Using the approach for polar to Cartesian coordinate conversion, the standard and unbiased range rate conversion is shown in the following equations

$$d_m^{\text{STANDARD}} = \frac{(f_{r,m} - f_t)\, c}{2 f_t} - V \cos \alpha_m \tag{3.6}$$

$$d_m^{\text{DUCM}} = \frac{(f_{r,m} - f_t)\, c}{2 f_t} - V \cos\left(\alpha_m\right) e^{\sigma_\alpha^2/2} \tag{3.7}$$

The MSE approximation from the standard conversion is

$$R_{\text{STANDARD}} = \frac{\sigma_f^2 c^2}{4 f_t^2} + V^2 \sin^2 \alpha_m \tag{3.8}$$

The true MSE of the unbiased conversion is

$$R = \frac{\sigma_f^2 c^2}{4 f_t^2} + V^2 \left[\frac{1}{2} \left(1 + \cos(2\alpha) e^{-2\sigma_\alpha^2} \right) e^{\sigma_\alpha^2} - \cos^2 \alpha \right] \tag{3.9}$$

As in the CMKF case, the measurement covariance requires knowledge of the true range. When using the converted measurements in a Kalman filter range rate estimator, or in an extended Kalman filter that uses range rate in the estimation process, the measurement covariance must be approximated. To avoid estimation bias, the DUCM approach of conditioning on the previous value or measurement is chosen.

$$R_{\text{DUCM}} = \frac{\sigma_f^2 c^2}{4 f_t^2} + \frac{1}{2} V^2 \left[\left(1 + \cos(2\alpha_{trk}) e^{-2\sigma_\alpha^2} e^{-2\sigma_{\alpha,trk}^2} \right) e^{\sigma_\alpha^2} - \left(1 + \cos(2\alpha_{trk}) e^{-2\sigma_{\alpha,trk}^2} \right) \right] \tag{3.10}$$

To evaluate the performance of the conversion techniques, a simple range rate recursive estimator is used. For the case where the seeker and the target are on a collision course, both following constant velocity motion, the bearing rate is zero and the range rate is constant. Using these assumptions, a seeker using a 50 kHz sonar system with a velocity of 150 ft/s, $\sigma_\alpha = 2.5^\circ$ and $\sigma_f = 5$ Hz approaches a target with a true Doppler of 20 ft/s. The true bearing angle, α, is uniformly distributed from -45 to 45 degrees. The estimation bias, MSE performance and consistency, based on the ANEES, of the DUCM approach are superior to the standard conversion for this evaluation, as shown in Figure 14.

The bias of the DUCM approach was consistently less than that of the conventional approach. However, the MSE performance and consistency of the DUCM approach was degraded for very small bearings and large σ_α.

3.4 Conclusion

When using converted measurements in tracking, two sources of bias need to be evaluated and eliminated. The first is measurement conversion bias, which occurs when the conversion process introduces a bias in the mean of the converted measurement. The second source of bias is estimation bias, which occurs when the estimate of the measurement covariance is correlated with the converted measurement noise, leading to a biased Kalman gain. Estimation of range rate from a moving platform exhibits these biases. It has been shown that a decorrelated

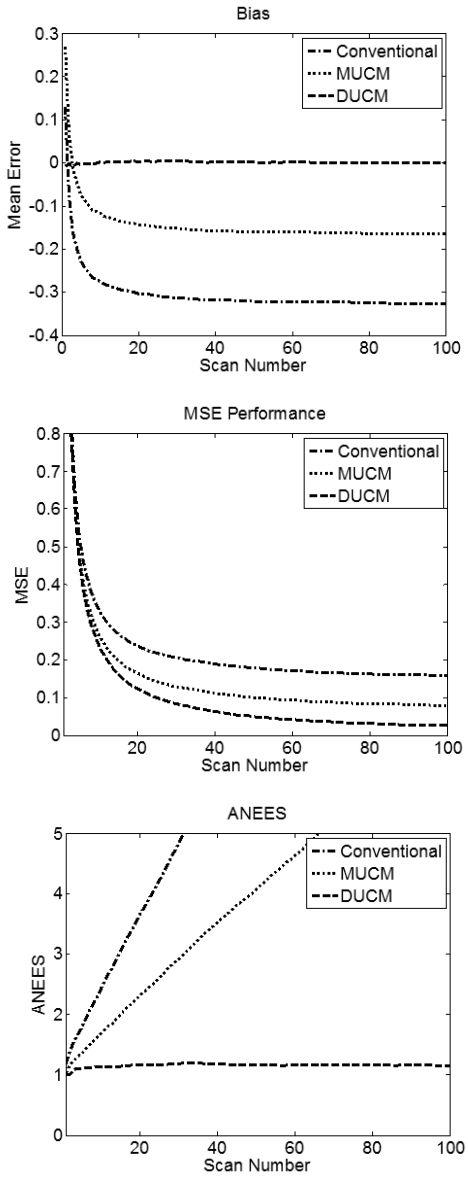

Fig. 3.3: Performance of the conventional, MUCM and DUCM conversion techniques utilized in a range rate tracker.

version of the Unbiased Measurement Conversion (DUCM) exhibits improved performance over the traditional method.

Chapter 4

Converted Measurement Tracker for Range, Bearing and Range Rate Measurement

4.1 Abstract

Active sonar and radar systems often include a measurement of range rate in addition to the position-based measurements of range and bearing. Due to the nonlinearity of the range rate measurement with respect to a target state in the Cartesian coordinate system, this measurement is not always fully exploited. The state of the art methods to utilize range rate include the Extended Kalman Filter (EKF) and the Unscented Kalman Filter (UKF) with sequential processing of the position based measurements and the range rate measurement. Common to these approaches is that the measurement prediction function remains nonlinear. The goal of this work is to develop a measurement conversion from range, bearing and range rate to Cartesian position and velocity that is unbiased and consistent, with appropriate elimination of estimation bias. The converted measurement is then used with a linear Kalman filter. Performance of this new method is compared

to state of the art techniques and shown to match or exceed that of existing techniques over a wide range of scenarios.

4.2 Introduction

When tracking using measurements consisting of range and bearing, a common approach is to first convert the measurements to Cartesian coordinates. Since target dynamics are linear in the Cartesian coordinate system, tracking can be performed with a linear Kalman filter. Performance of this approach, referred to as the Converted Measurement Kalman Filter (CMFK), exceeds that of a mixed coordinate EKF if an unbiased conversion from polar to Cartesian coordinates is used [39]. Performance is further enhanced if estimation bias is eliminated by evaluating the converted measurement error covariance using the state prediction [15].

In addition to range and bearing, in many active sonar and radar applications measurements also include range rate. The extension of the CMKF to use range rate as a linear measurement is possible [4], but previous implementations have been limited to cases with small bearing errors. The use of range rate as a nonlinear measurement requires the use of a nonlinear tracker such as the EKF or UKF. Due to their poor performance in some situations, various modifications have been proposed, including use of a pseudo measurement [23,21,27,32], an alternative linearization of the measurement prediction function [8], and sequentially

processing the converted position and range rate measurements (applied to the EKF [21,27,32] and the UKF [22,38]).

4.2.1 Proposed Approach

Based on the success of the CMKF for tracking with range and bearing measurements, it is understandable that many existing approaches for tracking with range, bearing and range rate use a converted measurement approach for the position portion of the measurements. However, by leaving the range rate measurement as a nonlinear function of the state, the resulting filters have the potential for inconsistent performance and divergence. The question asked in the development of the proposed tracker is whether the converted measurement approach can be extended to include the range rate measurement, resulting in a converted measurement that is fully linear with respect to the Cartesian state, thus allowing for the use of a linear Kalman filter.

The answer lies in the intuition that range rate is simply a velocity measurement along the true line of sight of the target. This velocity measurement can be rotated from the line of sight coordinate system to the tracking coordinate system to provide a measure of Cartesian velocity that is clearly linear with the state. The issue, of course, is that the true line of sight is unknown. One can, however, use the measured line of sight angle for the rotation as long as the uncertainty in this measurement is accounted for in the converted measurement error covariance.

With this approach, it can be seen that the target velocity perpendicular to the line of sight (cross range rate) has an impact on the accuracy of the line of sight velocity measurement. To account for this, a non-informative cross range rate measurement is introduced. Using this non-informative measurement in the derivation, in conjunction with a priori knowledge of target speed, one can derive the measurement error covariance for the conversion of range rate to Cartesian velocity.

The result is a converted measurement approach that converts range, bearing and range rate to Cartesian position and velocity. This converted measurement, now linear with respect to the state, is used in a linear Kalman filter. The resulting filter exhibits advantages over the current state of the art for cases with poor angle accuracy. The contribution of this chapter is the introduction of this new measurement conversion approach that extends the CMKF of [15] to include measurement of range rate, allowing the use of a linear Kalman filter.

The method proposed here addresses all nonlinearities with this new measurement conversion approach described in Section 4.4. The converted measurement is then used in a linear Kalman filter as described in Section 4.5 and evaluated with respect to the existing state of the art in Section 4.6.

4.3 Background

4.3.1 Problem Statement

Active sonar and radar systems produce measurements in polar (or spherical) coordinates, often with the additional measurement of range rate:

$$\mathbf{z}_{\text{RAW}} = \begin{bmatrix} r_m \\ \alpha_m \\ \dot{r}_m \end{bmatrix} = \mathbf{h}(\mathbf{x}) + w_{\text{RAW}} \tag{4.1}$$

where r_m, α_m, and $\dot{r}_m$ are the measured range, bearing and range rate; $\mathbf{h}$ is the measurement function, and $\mathbf{x}$ is the target state. (A list of symbols used in this chapter can be found in Table 4.1.) The measurement error for the raw measurements, w_{RAW}, is assumed to be Gaussian with covariance matrix

$$R_{\text{RAW}} = \begin{bmatrix} \sigma_r^2 & 0 & \rho\sigma_r\sigma_{\dot{r}} \\ 0 & \sigma_\alpha^2 & 0 \\ \rho\sigma_r\sigma_{\dot{r}} & 0 & \sigma_{\dot{r}}^2 \end{bmatrix} \tag{4.2}$$

where σ_r, σ_α, and $\sigma_{\dot{r}}$ are the standard deviations of the range, bearing and range rate measurement noise. The correlation coefficient for the correlation between the range and range rate measurement noise is ρ [24].

Table 4.1: List of Symbols Used

Symbol	**Meaning**
r	Range
$\dot{r}$	Range rate
α	Bearing
θ	Elevation
$\dot{c}$	Cross range rate
	(across line of sight horizontally)
$\dot{e}$	Cross range rate
	(across line of sight in the vertical plane)

4.3.2 Existing Techniques

Since target motion is linear in Cartesian coordinates, state estimation is best performed in this coordinate system. The most straightforward approach is to address this problem with the EKF directly. The Kalman filter for a nearly constant velocity target motion assumption is described in [3]. Defining the state as $\mathbf{x} = \begin{bmatrix} x & y & \dot{x} & \dot{y} \end{bmatrix}'$, using H_k to represent the measurement prediction matrix (the Jacobian of the measurement function, detailed in the sequel) and P_k to represent the state estimate's covariance matrix, the (extended) Kalman gain and covariance update steps are

$$S_{k+1} = R_{k+1} + H_{k+1} P_{k+1|k} H'_{k+1} \tag{4.3}$$

$$W_{k+1} = P_{k+1|k} H'_{k+1} S^{-1}_{k+1} \tag{4.4}$$

$$P_{k+1|k+1} = P_{k+1|k} - W_{k+1} S_{k+1} W'_{k+1} \tag{4.5}$$

$$\hat{\mathbf{x}}_{\mathbf{k+1|k+1}} = \hat{\mathbf{x}}_{\mathbf{k+1|k}} + W_{k+1} \left[\mathbf{z_k} - \mathbf{h} \left(\hat{\mathbf{x}}_{\mathbf{k+1|k}} \right) \right] \tag{4.6}$$

Note that all of the measurements are a nonlinear function of the Cartesian target state. An approach to limit the nonlinearity to the range rate measurement is to convert the range and bearing into Cartesian coordinates (time indices are omitted where this causes no confusion).

$$\mathbf{z}_{\text{CONV}} = \begin{bmatrix} x_m \\ y_m \\ \eta_m \end{bmatrix} = \begin{bmatrix} r_m \cos \alpha_m \\ r_m \sin \alpha_m \\ f\left(\dot{r}_m\right) \end{bmatrix} \tag{4.7}$$

After this conversion, the position portion of the measurement is now linear with respect to the target dynamics, while the range rate based measurement remains a nonlinear function of the state, precluding the use of the traditional (linear) Kalman filter. There are numerous variations of this approach which are described next.

An examination of popular and state of the art techniques shows that various approaches are used for the conversion of range and bearing, the use of range rate, the order of processing and the calculation of the measurement prediction matrix. An overview of these distinctions follows.

Range and Bearing Conversion

In [39], it was shown that the conventional conversion from polar to Cartesian coordinates used in (4.7) introduces a bias in the expected value of the converted measurement. Various remedies to this bias have been proposed. An additive debiasing term was prescribed in [39,49] and applied to tracking with range rate in [21,38]. In [45] the bias was shown to be truly multiplicative in nature, and the resulting multiplicative debiasing term was applied to range rate tracking in [27]. A modification to this technique was described in [44,20] and used in tracking

with range rate in [32]. A comparison of these methods was made in [15] along with a proposed decorrelated, unbiased measurement conversion. This method has not previously been applied to tracking with range rate, and the methodology is incorporated into the proposed measurement conversion in Section 4.4.

Range Rate Conversion

The range rate measurement is a nonlinear function of the target state

$$\dot{r}_m = \frac{x\dot{x} + y\dot{y}}{\sqrt{x^2 + y^2}} + w_{\dot{r}} \tag{4.8}$$

where $w_{\dot{r}}$ is the range rate measurement noise.

To reduce the nonlinearity between the state and the measurement, replacement of the range rate measurement, $\dot{r}_m$, with a pseudo measurement consisting of $r_m\dot{r}_m$ has been proposed [23] and applied to the second order EKF in [21,27,32].

$$\eta_m^{\text{pseudo}} = r_m\dot{r}_m = h_\eta^{\text{pseudo}}(\mathbf{x}) + w_\eta = x\dot{x} + y\dot{y} - \rho\sigma_r\sigma_{\dot{r}} + w_\eta \tag{4.9}$$

where $\rho\sigma_r\sigma_{\dot{r}}$ is a debiasing term.

According to [38], this pseudo measurement is appropriate when the range and range rate measurement noises are statistically independent, but for certain waveforms, this independence assumption is not accurate [2]. For these cases, use of the UKF has been proposed [22,38] to handle the strong nonlinearities with the use of range rate instead of the range, range rate product. In this case η_m is

simply the range rate measurement, $\dot{r}_m$,

$$\eta_m^{\text{raw}} = \dot{r}_m = h_\eta^{\text{raw}}(\mathbf{x}) + w_{\dot{r}} = \frac{x\dot{x} + y\dot{y}}{\sqrt{x^2 + y^2}} + w_{\dot{r}} \tag{4.10}$$

Sequential Processing

Traditionally, the Kalman filter processes all measurements in a scan (in this case range, bearing and range rate) simultaneously. In some cases, sequentially processing the measurements is advantageous. Sequentially processing the position measurements (range and bearing or their converted counterparts) first, followed by processing of range rate has been proposed for the EKF using the pseudo measurement (4.9) in [21,27,32] and for the UKF using the raw range rate measurement [22,38]. In order to process these measurements sequentially, the range rate based measurement, η_m^{pseudo} or η_m^{raw}, must first be decorrelated from the position components of the measurement (see Appendix B).

Measurement Prediction Matrix

The range rate, η_m^{raw}, can be treated as a linear measurement [4] in order to use a linear Kalman filter. The measurement matrix H_{L} for this filter is

$$H_{\text{L}} = \begin{bmatrix} 1 & 0 & 0 & 0 \\ 0 & 1 & 0 & 0 \\ 0 & 0 & \cos\alpha_m & \sin\alpha_m \end{bmatrix} \tag{4.11}$$

While it is desirable to use the linear Kalman filter, this approach is only valid for accurate angle measurements. Assuming a maximum target speed of $|v|_{max}$, the required bearing accuracy, in radians, is [4]

$$\sigma_\alpha < \frac{0.2\sigma_{\dot{r}}}{|v|_{max}} \tag{4.12}$$

In cases where this inequality does not hold, a nonlinear filter (e.g. the EKF or UKF) has been prescribed.

In its most basic form, the EKF with linear state dynamics and nonlinear measurement prediction uses the Jacobian of the measurement prediction function, evaluated at the predicted state, in (4.3) – (4.4),

$$H_{\text{EKF}} = \begin{bmatrix} 1 & 0 & 0 & 0 \\ 0 & 1 & 0 & 0 \\ \frac{\partial h}{\partial x} & \frac{\partial h}{\partial y} & \frac{\partial h}{\partial \dot{x}} & \frac{\partial h}{\partial \dot{y}} \end{bmatrix} \tag{4.13}$$

In an attempt to overcome degraded EKF performance due to strong nonlinearities, an alternative version of the Jacobian has been proposed. Examination of the third row of H_{EKF} shows that $H_{\text{EKF}}\hat{\mathbf{x}}$ includes the terms $\frac{\partial h}{\partial x}\hat{x}+\frac{\partial h}{\partial y}\hat{y}+\frac{\partial h}{\partial \dot{x}}\hat{\dot{x}}+\frac{\partial h}{\partial \dot{y}}\hat{\dot{y}}$. Based on the idea that the expected value of the first two terms sum to zero, $E\left[\frac{\partial h}{\partial x}\hat{x} + \frac{\partial h}{\partial y}\hat{y}\right] = 0$ [8], one can use the following alternative linearization[1]

[1] This yields (4.11) with the predicted bearing rather than the measured one.

$$H_{\text{AEKF}} = \begin{bmatrix} 1 & 0 & 0 & 0 \\ 0 & 1 & 0 & 0 \\ 0 & 0 & \frac{\partial h}{\partial \dot{x}} & \frac{\partial h}{\partial \dot{y}} \end{bmatrix} \tag{4.14}$$

For the second order EKF with decorrelated pseudo range rate measurements, (4.3) – (4.6) are processed for the converted position portion of the measurements. The state estimate, $\hat{\mathbf{x}}^{\text{p}} = \begin{bmatrix} \hat{x} & \hat{y} & \hat{\dot{x}} & \hat{\dot{y}} \end{bmatrix}'$, and state covariance, $P^{\text{p}}_{k+1|k+1}$, updated using the position measurement only, are subsequently processed using the pseudo range rate measurement in a second order EKF [21] (see Appendix C).

Similarly, in the sequential UKF, (4.3) – (4.6) are processed for the converted position portion of the measurements. The state estimate and state covariance estimate, updated using the position measurement only, are subsequently processed by the raw range rate measurement using the second order unscented transform [38]. Sigma points are generated using the state and covariance estimate that has been updated by the position estimates and then passed through the nonlinear function, $h^{\text{raw}}_{\varepsilon}$, to provide the time and measurement update.

Additional Approaches

There have been additional noteworthy approaches for exploitation of range rate measurement that also try to overcome the difficulties of the nonlinearity. The work of [57] only utilizes the position measurements for estimation, but employs

range rate for track initialization and data association in a integrated probabilistic data association framework. The resulting tracker has improved performance with respect to the number of false tracks and computational load.

A denoising of the pseudo measurement was applied to the second order sequential EKF approach in [62]; however this approach relies on a constant velocity assumption. In [61], the concept is extended to a constant acceleration assumption. This approach relies on two separate filters (i.e. the results of one filter do not influence the other filter) running simultaneously with the filters' outputs being combined outside the filter recursion.

Summary of Existing Techniques: The proposed variations of the EKF and UKF reduce the detrimental effects that result from a nonlinear filter; however, they do not eliminate the nonlinearity itself. None of the approaches results in a single, linear Kalman filter that is robust to large measurement errors and independent of the target motion assumption. The following section proposes an approach that achieves these goals.

4.4 New Converted Measurement Approach with Range Rate Measurements

In order to successfully employ a single linear filter, one approach would be to convert the range rate measurement directly into a form that is linear in the Cartesian state. The raw measurement needs to be converted in a manner that is

unbiased and consistent, and that allows for and describes the correlation between the range and range rate measurement errors. The converted measurement error covariance estimate should also be evaluated at the prediction (as opposed to the measurement) to avoid estimation bias [15].

A conversion of the raw measurement of range, bearing and range rate into a measurement of position and velocity in Cartesian coordinates is a valid candidate. In order to develop this conversion, consider the inclusion of a non-informative cross range rate measurement, $\dot{c}$. The conversion function to Cartesian is therefore[2],

$$\mathbf{z}_{\mathrm{C}} = \begin{bmatrix} x_m \\ y_m \\ \dot{x}_m \\ \dot{y}_m \end{bmatrix} = \mathbf{D}\left(\alpha_{\mathbf{m}}\right) \begin{bmatrix} r_m \\ 0 \\ \dot{r}_m \\ \dot{c}_m \end{bmatrix} \tag{4.15}$$

where D is the direction cosine matrix,

$$\begin{bmatrix} \cos\alpha_m & -\sin\alpha_m & 0 & 0 \\ \sin\alpha_m & \cos\alpha_m & 0 & 0 \\ 0 & 0 & \cos\alpha_m & -\sin\alpha_m \\ 0 & 0 & \sin\alpha_m & \cos\alpha_m \end{bmatrix} \tag{4.16}$$

Cross range rate is non-informative because it is not truly measured, but

[2] Clearly the second column of D and corresponding 0 in the measurement vector are not required in (4.15). It is written in this form to allow for a common definition of D in the subsequent equations (4.20) – (4.21).

a priori knowledge about the distribution of expected cross range rates (based on knowledge of possible target speeds) can be used in calculating the converted measurement error covariance as described in 4.4.2.

4.4.1 Estimation of the Mean

The expected value of (4.15), using the noise assumptions of (4.2) (i.e. range and bearing measurement noises are uncorrelated), indicates that the conversion introduces a bias

$$E\left\{ D\left(\alpha_m\right) \begin{bmatrix} r_m \\ 0 \\ \dot{r}_m \\ \dot{c}_m \end{bmatrix} \right\} = e^{-{\sigma^2}_\alpha/2} \begin{bmatrix} x_m \\ y_m \\ \dot{x}_m \\ \dot{y}_m \end{bmatrix} \tag{4.17}$$

This is evident from noting that $E\left[\cos\left(\alpha + w_\alpha\right)\right] = \cos\left(\alpha\right) e^{-{\sigma_\alpha}^2/2}$ and $E\left[\sin\left(\alpha + w_\alpha\right)\right] = \sin\left(\alpha\right) e^{-{\sigma_\alpha}^2/2}$ [3]. An unbiased version of the measurement conversion (4.15) can be developed as an extension of the Unbiased Converted Measurement for position [45,3]

$$\mathbf{z}_{\mathrm{U}} = \begin{bmatrix} x_m \\ y_m \\ \dot{x}_m \\ \dot{y}_m \end{bmatrix} = e^{\sigma_\alpha^2/2} D\left(\alpha_m\right) \begin{bmatrix} r_m \\ 0 \\ \dot{r}_m \\ \dot{c}_m \end{bmatrix} \tag{4.18}$$

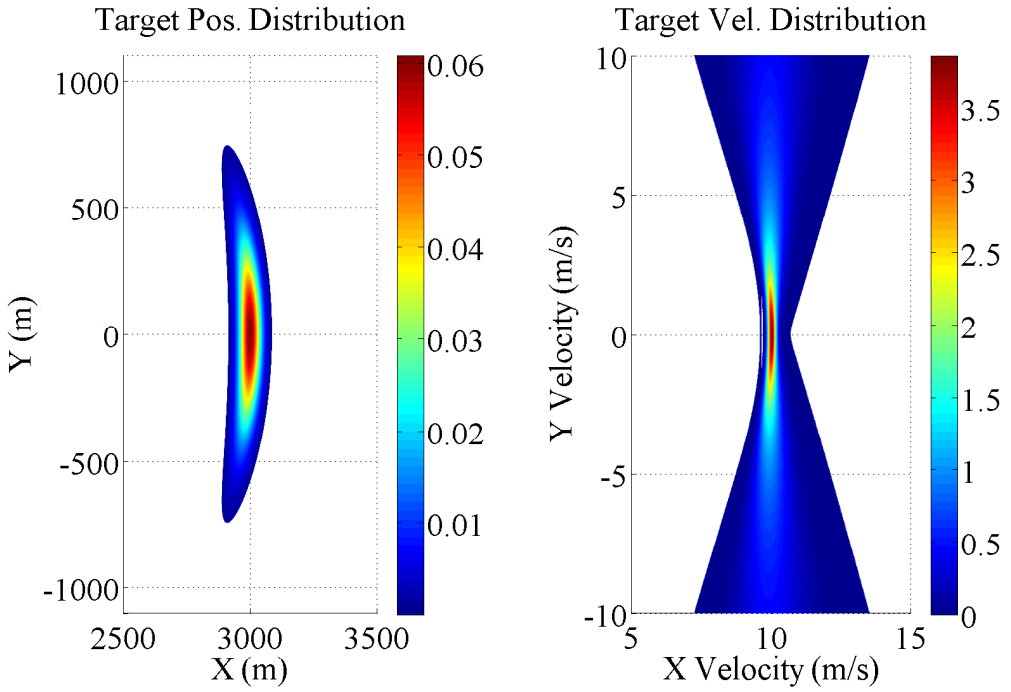

Fig. 4.1: Probability distribution functions (pdf) for the true target position and velocity given a measurement of $r_m = 3{,}000$m, $\alpha_m = 0°$, $\dot{r}_m = 10$ and $\dot{c}_m = 0$. Measurement errors are normal and independent with $\sigma_r = 30$m, $\sigma_\alpha = 5°$, $\sigma_{\dot{r}} = 0.1$m/s, and $\sigma_{\dot{c}} = 30$m/s. Pdf not displayed for values less than a threshold.

4.4.2 Estimation of the Covariance

The probability distribution functions for the true target position and velocity given a measurement are shown in Fig. 4.1.

For convenience, the converted measurement error covariance, R_{C}, will be developed in a coordinate system along the line of sight (LOS) to the target, R_{R}, and then converted to Cartesian coordinates, i.e.

$$R_{\mathrm{C}} = D(\alpha) R_{\mathrm{R}} D(\alpha)' \tag{4.19}$$

The calculation of the components of R_{C} requires the true target velocity and position. Since this is not available in practice, the evaluation is performed at the predicted target state, $\hat{\mathbf{x}}_{k+1|k}$. This is because evaluation at the measurement results in correlation between the converted measurement error covariance and converted measurement error itself, which leads to a biased Kalman gain and introduces estimation bias [43,26,15]. Therefore, evaluation at the predicted estimate is preferred.

First the predicted target state and covariance are rotated into the estimate's LOS coordinate system:

$$\hat{\mathbf{x}}_{\mathrm{R}} = D(\alpha_t)' \hat{\mathbf{x}}_{k+1|k} \tag{4.20}$$

$$P_{\mathrm{R}} = D(\alpha_t)' P_{k+1|k} D(\alpha_t) \tag{4.21}$$

where the predicted target bearing is

$$\alpha_t = \tan^{-1}\left(\frac{\hat{\mathbf{x}}^2_{k+1|k}}{\hat{\mathbf{x}}^1_{k+1|k}}\right) \tag{4.22}$$

and $\hat{\mathbf{x}}^n$ is the nth component of $\hat{\mathbf{x}}$.

The individual components of R_{R} evaluated at the prediction are as follows (see Appendix D),

$$
\begin{aligned}
R_{\mathrm{R}}^{11} &= \frac{1}{2}\left[\left(\hat{\mathbf{x}}_{\mathrm{R}}^{1}\right)^{2}+P_{\mathrm{R}}^{11}+\sigma_{r}^{2}\right]\left(1+e^{-2\sigma_{\alpha}^{2}}e^{-2\sigma_{\alpha_t}^{2}}\right)e^{\sigma_{\alpha}^{2}} \\
&\quad -\frac{1}{2}\left[\left(\hat{\mathbf{x}}_{\mathrm{R}}^{1}\right)^{2}+P_{\mathrm{R}}^{11}\right]\left(1+e^{-2\sigma_{\alpha_t}^{2}}\right) \qquad (4.23)\\
R_{\mathrm{R}}^{12} &= 0 \qquad (4.24)\\
R_{\mathrm{R}}^{13} &= \frac{1}{2}\left(\hat{\mathbf{x}}_{\mathrm{R}}^{1}\hat{\mathbf{x}}_{\mathrm{R}}^{3}+P_{\mathrm{R}}^{13}+\rho\sigma_{r}\sigma_{\dot{r}}\right)\left(1+e^{-2\sigma_{\alpha}^{2}}e^{-2\sigma_{\alpha_t}^{2}}\right)e^{\sigma_{\alpha}^{2}} \\
&\quad -\frac{1}{2}\left(\hat{\mathbf{x}}_{\mathrm{R}}^{1}\hat{\mathbf{x}}_{\mathrm{R}}^{3}+P_{\mathrm{R}}^{13}\right)\left(1+e^{-2\sigma_{\alpha_t}^{2}}\right) \qquad (4.25)\\
R_{\mathrm{R}}^{22} &= \frac{1}{2}\left[\left(\hat{\mathbf{x}}_{\mathrm{R}}^{1}\right)^{2}+P_{\mathrm{R}}^{11}+\sigma_{r}^{2}\right]\left(1-e^{-2\sigma_{\alpha}^{2}}e^{-2\sigma_{\alpha_t}^{2}}\right)e^{\sigma_{\alpha}^{2}} \\
&\quad -\frac{1}{2}\left[\left(\hat{\mathbf{x}}_{\mathrm{R}}^{1}\right)^{2}+P_{\mathrm{R}}^{11}\right]\left(1-e^{-2\sigma_{\alpha_t}^{2}}\right) \qquad (4.26)\\
R_{\mathrm{R}}^{23} &= \frac{1}{2}\left(\hat{\mathbf{x}}_{\mathrm{R}}^{1}\hat{\mathbf{x}}_{\mathrm{R}}^{4}+P_{\mathrm{R}}^{14}\right)\left(1-e^{-2\sigma_{\alpha}^{2}}e^{-2\sigma_{\alpha_t}^{2}}\right)e^{\sigma_{\alpha}^{2}} \\
&\quad -\frac{1}{2}\left(\hat{\mathbf{x}}_{\mathrm{R}}^{1}\hat{\mathbf{x}}_{\mathrm{R}}^{4}+P_{\mathrm{R}}^{14}\right)\left(1-e^{-2\sigma_{\alpha_t}^{2}}\right) \qquad (4.27)\\
R_{\mathrm{R}}^{33} &= \frac{1}{2}\left[\left(\hat{\mathbf{x}}_{\mathrm{R}}^{3}\right)^{2}+P_{\mathrm{R}}^{33}+\sigma_{\dot{r}}^{2}\right]\left(1+e^{-2\sigma_{\alpha}^{2}}e^{-2\sigma_{\alpha_t}^{2}}\right)e^{\sigma_{\alpha}^{2}} \\
&\quad -\frac{1}{2}\left[\left(\hat{\mathbf{x}}_{\mathrm{R}}^{3}\right)^{2}+P_{\mathrm{R}}^{33}\right]\left(1+e^{-2\sigma_{\alpha_t}^{2}}\right) \\
&\quad +\frac{1}{2}\left[\left(\hat{\mathbf{x}}_{\mathrm{R}}^{4}\right)^{2}+P_{\mathrm{R}}^{44}+\sigma_{\dot{c}}^{2}\right]\left(1-e^{-2\sigma_{\alpha}^{2}}e^{-2\sigma_{\alpha_t}^{2}}\right)e^{\sigma_{\alpha}^{2}} \\
&\quad -\frac{1}{2}\left[\left(\hat{\mathbf{x}}_{\mathrm{R}}^{4}\right)^{2}+P_{\mathrm{R}}^{44}\right]\left(1-e^{-2\sigma_{\alpha_t}^{2}}\right) \qquad (4.28)
\end{aligned}
$$

where $\sigma_{\alpha_t}^2$ is the approximate bearing variance of the predicted track estimate based on a linearization of P_{R},

$$\sigma_{\alpha_t}^{2}=\frac{P_{\mathrm{R}}^{22}}{\left(\hat{\mathbf{x}}_{\mathrm{R}}^{1}\right)^{2}} \qquad (4.29)$$

$\hat{\mathbf{x}}_{\mathrm{R}}^{n}$ is the nth component of $\hat{\mathbf{x}}_{\mathrm{R}}$ and P_{R}^{nm} is the nm element of P_{R}.

Since the cross range rate measurement, $\dot{c}_m$, is non-informative, its standard deviation, $\sigma_{\dot{c}}$, is infinite. One can, however, set the value of $\sigma_{\dot{c}}$ used in (4.28) based on an a priori estimate of the standard deviation of target cross range rate to capture the effect that the cross range rate has on the ability to measure the line of sight velocity. The remaining components of the measurement noise covariance in the LOS coordinate system, R_{R} (e.g. R_{R}^{44}, R_{R}^{34}), are are set to infinity to capture that $\dot{c}_m$ is non-informative. It is therefore useful to deal with the inverse of R_{R} and note that for a positive definite covariance matrix,

$$\left[\begin{array}{cc} \sigma_1^2 & \rho\sigma_1\sigma_2 \\ \rho\sigma_1\sigma_2 & \sigma_2^2 \end{array}\right]^{-1}\Bigg|_{\sigma_2\to\infty} = \left[\begin{array}{cc} (\sigma_1^2)^{-1} & 0 \\ 0 & 0 \end{array}\right] \tag{4.30}$$

therefore

$$R_{\mathrm{R}}{}^{-1} = \left[\begin{array}{ccc} & & 0 \\ & \left(R_{\mathrm{R}}^{1:3,1:3}\right)^{-1} & 0 \\ & & 0 \\ 0 & 0 \quad 0 & 0 \end{array}\right] \tag{4.31}$$

Since the inverse of the direction cosine matrix, $D(\alpha_m)$, is its transpose, the measurement noise covariance for (4.18), R_{C}, is

$$R_{\mathrm{C}}{}^{-1} = D(\alpha_t)\, R_{\mathrm{R}}{}^{-1} D(\alpha_t)' \tag{4.32}$$

Since $R_{\mathrm{C}}{}^{-1}$ is not invertible, R_{C} is not available for use in the Kalman filter gain calculation (4.3); one has to use the information form of the Kalman filter, described in 4.5.1.

4.4.3 Extension to 3D

The extension of the measurement conversion function from polar to spherical raw measurements is tedious, yet straightforward. An assumption that the sensor's bearing accuracy σ_α was not a function of the target bearing was made in the 2D case. This implicitly is making an assumption about the sensor array geometry (i.e. a circular array). For the 3D case, this assumption warrants additional discussion. If we assume that the sensor's angular measurement accuracies, with respect to true target line of sight, are independent of the true target spherical coordinates' bearing and elevation (a reasonable assumption for a spherical array), then in the spherical coordinates the bearing accuracy is a function of elevation, i.e.

$$\sigma_\alpha = \sigma_{\alpha\mathrm{LOS}} / \cos(\theta) \tag{4.33}$$

Figure 4.2 depicts $\sigma_{\alpha\mathrm{LOS}}$, the angular accuracy referenced to the line of sight to the target, and σ_α, the bearing error in spherical coordinates. The elevation accuracy, however is the same regardless of bearing or elevation, i.e. $\sigma_\theta = \sigma_{\theta\mathrm{LOS}}$. Figure 4.3 provides a visualization of the error volume for the constant σ_α and constant $\sigma_{\alpha\mathrm{LOS}}$ assumption. In the derivation of the 3D converted measurement error covariance, a constant, known $\sigma_{\alpha\mathrm{LOS}}$ and $\sigma_{\theta\mathrm{LOS}}$ is assumed.

As in the 2D case, a non-informative cross range rate measurement, $\dot{c}$, is used for the horizontal plane. In addition a second cross range rate measurement,

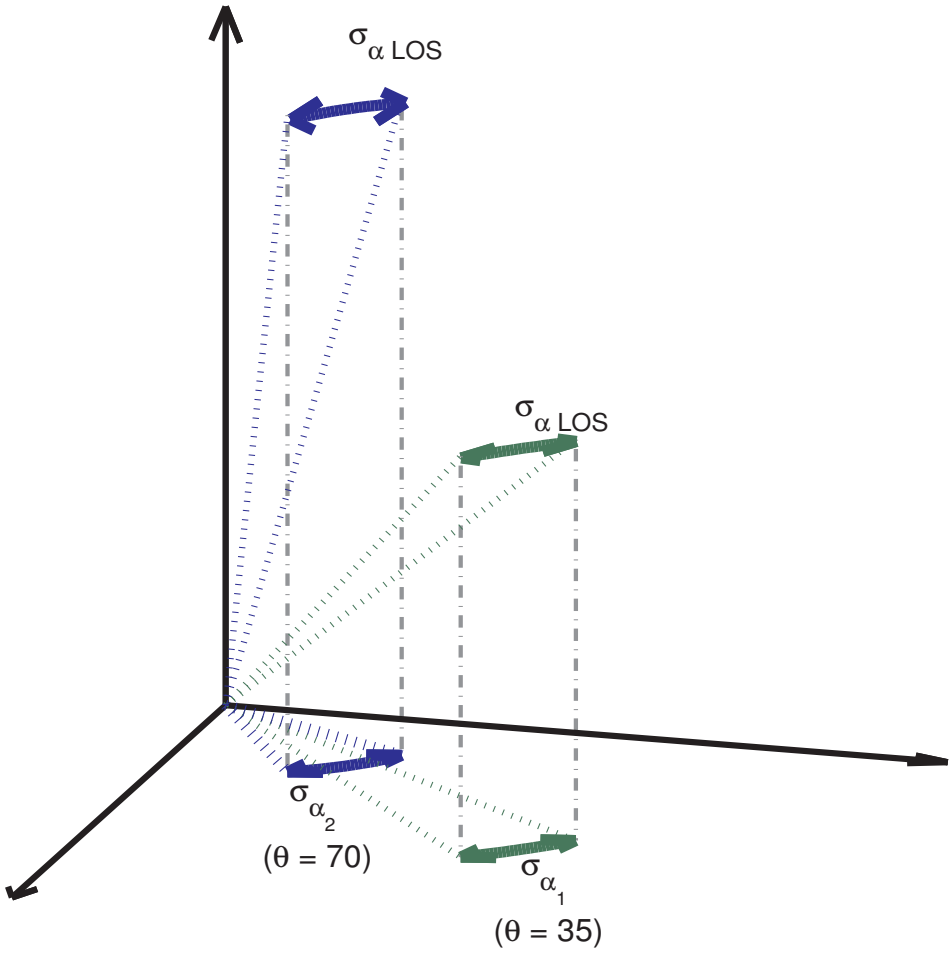

Fig. 4.2: Definition of σ_α and $\sigma_{\alpha\text{LOS}}$ displayed for an elevation of 35 and 70° with a constant $\sigma_{\alpha\text{LOS}}$. Although the angular error with respect to the line of sight of the target, $\sigma_{\alpha\text{LOS}}$, is constant, when projected to a bearing error in spherical coordinates, σ_α is a function of elevation (i.e. $\sigma_\alpha = \sigma_{\alpha\text{LOS}}/\cos(\theta)$).

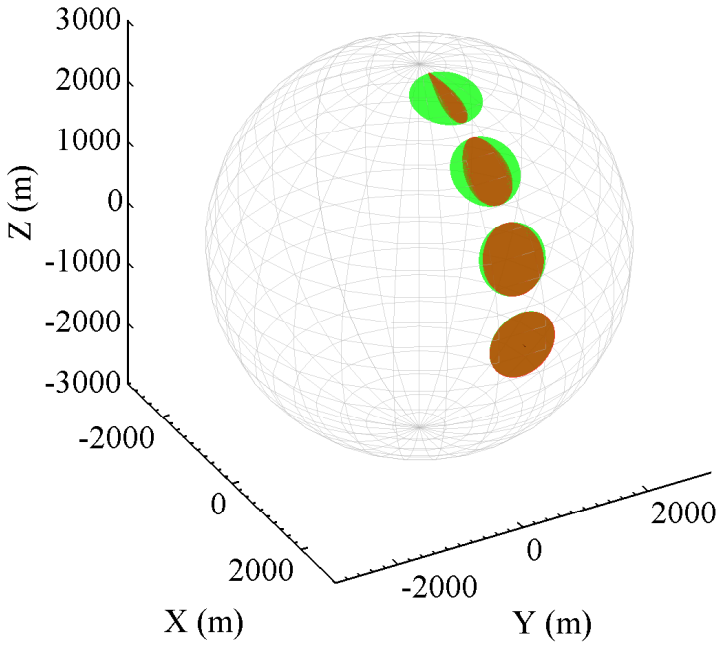

Fig. 4.3: Error volumes for a constant σ_α (red) and constant $\sigma_{\alpha\text{LOS}}$ (green) for an elevation of 0, 25, 50 and 75° and a range of 3000m, with a bearing and elevation accuracy of $\sigma = 10°$ and a range accuracy of $\sigma_r = 30$m. A 3000m radius sphere is included for reference. Using a constant σ_α (red) assumption leads to the angular accuracy with respect to the line of sight shrinking with elevation by a factor of $\cos(\theta)$. This is because in spherical coordinates σ_α is defined in the x-y plane, and the angular accuracy along the line of sight is projected into the x-y plane. A constant $\sigma_{\alpha\text{LOS}}$ (green) is a more realistic assumption for a spherical array.

$\dot{e}$, with standard deviation $\sigma_{\dot{e}}$, is used for the vertical plane. Defining the state as

$$\mathbf{x}_{\mathrm{3D}} = \begin{bmatrix} x & y & z & \dot{x} & \dot{y} & \dot{z} \end{bmatrix}' \tag{4.34}$$

with the associated state estimate covariance matrix P_{R3D}, the unbiased measurement conversion is

$$\mathbf{z}_{\mathrm{U3D}} = \begin{bmatrix} x_m \\ y_m \\ z_m \\ \dot{x}_m \\ \dot{y}_m \\ \dot{z}_m \end{bmatrix} = e^{\frac{\sigma_\alpha^2}{2}} e^{\frac{\sigma_\theta^2}{2}} D_{\mathrm{3D}}\left(\alpha_m, \theta_m\right) \begin{bmatrix} r_m \\ 0 \\ 0 \\ \dot{r}_m \\ \dot{c}_m \\ \dot{e}_m \end{bmatrix} \tag{4.35}$$

The converted measurement error covariance matrix, R_{R3D} can be calculated as follows.

The 3D direction cosine matrix is,

$$D_{\mathrm{3D}} = \begin{bmatrix} D_1 & 0 \\ 0 & D_1 \end{bmatrix} \tag{4.36}$$

where

$$D_1 = \begin{bmatrix} \cos\alpha_m \cos\theta_m & -\sin\alpha_m & -\cos\alpha_m \sin\theta_m \\ \sin\alpha_m \cos\theta_m & \cos\alpha_m & -\sin\alpha_m \sin\theta_m \\ \sin\theta_m & 0 & \cos\theta_m \end{bmatrix}$$

The predicted target state and covariance are rotated into the estimate's LOS coordinate system:

$$\hat{\mathbf{x}}_{\mathrm{R3D}} = D_{\mathrm{3D}}\left(\alpha_t, \theta_t\right)' \hat{\mathbf{x}}_{k+1|k} \tag{4.37}$$

$$P_{\mathrm{R3D}} = D_{\mathrm{3D}}\left(\alpha_t, \theta_t\right)' P_{k+1|k} D_{\mathrm{3D}}\left(\alpha_t, \theta_t\right) \tag{4.38}$$

where the predicted target bearing and elevation are

$$\alpha_t = \tan^{-1}\left(\frac{\hat{\mathbf{x}}^2_{k+1|k}}{\hat{\mathbf{x}}^1_{k+1|k}}\right) \tag{4.39}$$

$$\theta_t = \tan^{-1}\left(\frac{\hat{\mathbf{x}}^3_{k+1|k}}{\sqrt{\left(\hat{\mathbf{x}}^1_{k+1|k}\right)^2 + \left(\hat{\mathbf{x}}^2_{k+1|k}\right)^2}}\right) \tag{4.40}$$

and $\hat{\mathbf{x}}^n$ is the nth component of $\hat{\mathbf{x}}$.

The individual components of R_{R} evaluated at the prediction are as follows,

$$
\begin{aligned}
R^{11}_{\mathrm{R3D}} &= \frac{1}{4}\left[\left(\hat{\mathbf{x}}^1_{\mathrm{R3D}}\right)^2 + P^{11}_{\mathrm{R3D}} + \sigma_r^2\right]\left(1 + e^{-2\sigma_\alpha^2}e^{-2\sigma_{\alpha_t}^2}\right)e^{\sigma_\alpha^2} \\
&\quad \cdot \left(1 + e^{-2\sigma_\theta^2}e^{-2\sigma_{\theta_t}^2}\right)e^{\sigma_\theta^2} \\
&\quad - \frac{1}{4}\left[\left(\hat{\mathbf{x}}^1_{\mathrm{R3D}}\right)^2 + P^{11}_{\mathrm{R3D}}\right]\left(1 + e^{-2\sigma_{\alpha_t}^2}\right)\left(1 + e^{-2\sigma_{\theta_t}^2}\right) \qquad (4.41) \\
R^{12}_{\mathrm{R3D}} &= 0 \qquad (4.42) \\
R^{13}_{\mathrm{R3D}} &= 0 \qquad (4.43) \\
R^{14}_{\mathrm{R3D}} &= \frac{1}{4}\left(\hat{\mathbf{x}}^1_{\mathrm{R3D}}\hat{\mathbf{x}}^4_{\mathrm{R3D}} + P^{14}_{\mathrm{R3D}} + \rho\sigma_r\sigma_{\dot{r}}\right)\left(1 + e^{-2\sigma_\alpha^2}e^{-2\sigma_{\alpha_t}^2}\right)e^{\sigma_\alpha^2} \\
&\quad \cdot \left(1 + e^{-2\sigma_\theta^2}e^{-2\sigma_{\theta_t}^2}\right)e^{\sigma_\theta^2} \\
&\quad - \frac{1}{4}\left(\hat{\mathbf{x}}^1_{\mathrm{R3D}}\hat{\mathbf{x}}^4_{\mathrm{R3D}} + P^{14}_{\mathrm{R3D}}\right)\left(1 + e^{-2\sigma_{\alpha_t}^2}\right)\left(1 + e^{-2\sigma_{\theta_t}^2}\right) \qquad (4.44) \\
R^{22}_{\mathrm{R3D}} &= \frac{1}{4}\left[\left(\hat{\mathbf{x}}^1_{\mathrm{R3D}}\right)^2 + P^{11}_{\mathrm{R3D}} + \sigma_r^2\right]\left(1 - e^{-2\sigma_\alpha^2}e^{-2\sigma_{\alpha_t}^2}\right)e^{\sigma_\alpha^2} \\
&\quad \cdot \left(1 + e^{-2\sigma_\theta^2}e^{-2\sigma_{\theta_t}^2}\right)e^{\sigma_\theta^2} \\
&\quad - \frac{1}{4}\left[\left(\hat{\mathbf{x}}^1_{\mathrm{R3D}}\right)^2 + P^{11}_{\mathrm{R3D}}\right]\left(1 - e^{-2\sigma_{\alpha_t}^2}\right)\left(1 + e^{-2\sigma_{\theta_t}^2}\right) \qquad (4.45) \\
R^{23}_{\mathrm{R3D}} &= 0 \qquad (4.46) \\
R^{24}_{\mathrm{R3D}} &= \frac{1}{2}\left(\hat{\mathbf{x}}^1_{\mathrm{R3D}}\hat{\mathbf{x}}^5_{\mathrm{R3D}} + P^{15}_{\mathrm{R3D}}\right)\left(1 - e^{-2\sigma_\alpha^2}e^{-2\sigma_{\alpha_t}^2}\right)e^{\sigma_\alpha^2} \\
&\quad - \frac{1}{2}\left(\hat{\mathbf{x}}^1_{\mathrm{R3D}}\hat{\mathbf{x}}^5_{\mathrm{R3D}} + P^{15}_{\mathrm{R3D}}\right)\left(1 - e^{-2\sigma_{\alpha_t}^2}\right) \qquad (4.47)
\end{aligned}
$$

$$
\begin{aligned}
R^{33}_{\mathrm{R3D}} &= \frac{1}{2}\left[\left(\hat{\mathbf{x}}^{1}_{\mathrm{R3D}}\right)^{2} + P^{11}_{\mathrm{R3D}} + \sigma_r^2\right]\left(1 - e^{-2\sigma_\theta^2}e^{-2\sigma_{\theta_t}^2}\right)e^{\sigma_\theta^2} \\
&\quad - \frac{1}{2}\left[\left(\hat{\mathbf{x}}^{1}_{\mathrm{R3D}}\right)^{2} + P^{11}_{\mathrm{R3D}}\right]\left(1 - e^{-2\sigma_{\theta_t}^2}\right) \qquad (4.48) \\
R^{34}_{\mathrm{R3D}} &= \frac{1}{2}\left(\hat{\mathbf{x}}^{1}_{\mathrm{R3D}}\hat{\mathbf{x}}^{6}_{\mathrm{R3D}} + P^{16}_{\mathrm{R3D}}\right)\left(1 - e^{-2\sigma_\theta^2}e^{-2\sigma_{\theta_t}^2}\right)e^{\sigma_\theta^2} \\
&\quad - \frac{1}{2}\left(\hat{\mathbf{x}}^{1}_{\mathrm{R3D}}\hat{\mathbf{x}}^{6}_{\mathrm{R3D}} + P^{16}_{\mathrm{R3D}}\right)\left(1 - e^{-2\sigma_{\theta_t}^2}\right) \qquad (4.49) \\
R^{44}_{\mathrm{R3D}} &= \frac{1}{4}\left[\left(\hat{\mathbf{x}}^{4}_{\mathrm{R3D}}\right)^{2} + P^{44}_{\mathrm{R3D}} + \sigma_{\dot{r}}^2\right]\left(1 + e^{-2\sigma_\alpha^2}e^{-2\sigma_{\alpha_t}^2}\right)e^{\sigma_\alpha^2} \\
&\quad \cdot \left(1 + e^{-2\sigma_\theta^2}e^{-2\sigma_{\theta_t}^2}\right)e^{\sigma_\theta^2} \\
&\quad - \frac{1}{4}\left[\left(\hat{\mathbf{x}}^{4}_{\mathrm{R3D}}\right)^{2} + P^{44}_{\mathrm{R3D}}\right]\left(1 + e^{-2\sigma_{\alpha_t}^2}\right)\left(1 + e^{-2\sigma_{\theta_t}^2}\right) \\
&\quad + \frac{1}{2}\left[\left(\hat{\mathbf{x}}^{5}_{\mathrm{R3D}}\right)^{2} + P^{55}_{\mathrm{R3D}} + \sigma_{\dot{c}}^2\right]\left(1 - e^{-2\sigma_\alpha^2}e^{-2\sigma_{\alpha_t}^2}\right)e^{\sigma_\alpha^2} \\
&\quad - \frac{1}{2}\left[\left(\hat{\mathbf{x}}^{5}_{\mathrm{R3D}}\right)^{2} + P^{55}_{\mathrm{R3D}}\right]\left(1 - e^{-2\sigma_{\alpha_t}^2}\right) \\
&\quad + \frac{1}{4}\left[\left(\hat{\mathbf{x}}^{6}_{\mathrm{R3D}}\right)^{2} + P^{66}_{\mathrm{R3D}} + \sigma_{\dot{e}}^2\right]\left(1 + e^{-2\sigma_\alpha^2}e^{-2\sigma_{\alpha_t}^2}\right)e^{\sigma_\alpha^2} \\
&\quad \cdot \left(1 - e^{-2\sigma_\theta^2}e^{-2\sigma_{\theta_t}^2}\right)e^{\sigma_\theta^2} \\
&\quad - \frac{1}{4}\left[\left(\hat{\mathbf{x}}^{6}_{\mathrm{R3D}}\right)^{2} + P^{66}_{\mathrm{R3D}}\right]\left(1 + e^{-2\sigma_{\alpha_t}^2}\right)\left(1 - e^{-2\sigma_{\theta_t}^2}\right) \qquad (4.50)
\end{aligned}
$$

where $\sigma^2_{\alpha_t}$, as in the 2D case, is the approximate bearing variance of the predicted track estimate (4.29) and $\sigma^2_{\theta_t}$ is the approximate elevation variance of the predicted track estimate,

$$\sigma^2_{\theta_t} = \frac{P^{33}_{\mathrm{R}}}{\left(\hat{\mathbf{x}}^{1}_{\mathrm{R}}\right)^{2}} \qquad (4.51)$$

Since the cross range rate measurements, $\dot{c}_m$ and $\dot{e}_m$, are non-informative, the remaining components of the measurement noise covariance in the LOS coordinate system are infinite. Again, we deal with this by using the inverse of

R_{R3D}

$$R_{\mathrm{R3D}}{}^{-1} = \begin{bmatrix} & & & & 0 & 0 \\ & \left(R_{\mathrm{R3D}}^{1:4,1:4}\right)^{-1} & & & 0 & 0 \\ & & & & 0 & 0 \\ 0 & 0 & 0 & 0 & 0 & 0 \\ 0 & 0 & 0 & 0 & 0 & 0 \end{bmatrix} \tag{4.52}$$

and

$$R_{\mathrm{C3D}}{}^{-1} = D_{3D}\left(\alpha_t, \theta_t\right) R_{\mathrm{R3D}}{}^{-1} D_{3D}\left(\alpha_t, \theta_t\right)' \tag{4.53}$$

4.5 Application to Tracking

4.5.1 Information Form of the Kalman Filter

The information form of the Kalman filter [3] (IF) propagates the inverse of the state covariance and uses the inverse of the measurement error covariance. The utility in this context is the use of the *inverse* measurement error covariance. This allows the use of $R_{\mathrm{C}}{}^{-1}$ (4.32) in the 2D case and $R_{\mathrm{C3D}}{}^{-1}$ (4.53) in the 3D case directly, in place of R_{C} or R_{C3D}, which are unavailable. The calculation of the Kalman gain in the Kalman filter (4.3) – (4.4) is replaced with

$$W_{k+1} = \left[P_{k+1|k}^{-1} + H' R_{k+1}^{-1} H\right]^{-1} H' R_{k+1}^{-1} \tag{4.54}$$

and the state covariance update (4.5) is replaced with

$$P_{k+1|k+1} = [P^{-1}_{k+1|k} + H' R^{-1}_{k+1} H]^{-1} \tag{4.55}$$

4.5.2 Converted Measurement Kalman Filter with Range Rate

With the use of the measurement conversion function (4.18), each component of the state is observed directly. When applied to the information form Kalman filter, one has H as the identity matrix. The converted measurement is therefore linear with respect to the target state, eliminating the need for the extended (or unscented) Kalman filter with its pitfalls [3].

The proposed Converted Measurement Kalman Filter with Range Rate (CMKFRR) is implemented as follows:

1. Convert the raw measurements of range, bearing and range rate to Cartesian position and velocity with (4.18), using $\dot{c}_m = 0$, and use the result[3], $\mathbf{z} = \mathbf{z}_{\mathrm{U}}$, in (4.6).

2. Use the information form of the Kalman filter (4.54)–(4.55) with $R^{-1} = {R_{\mathrm{C}}}^{-1}$ from (4.32).

3. Set the measurement prediction matrix, $H = I_{4\times4}$, in (4.54)–(4.55).

[3] Since the appropriate terms of R_{R}^{-1} are set to zero, the values used for $\dot{c}_m$ and $\dot{e}_m$ are arbitrary, since R_{R} mitigates their impact on the Kalman update. This is an important property of the IF. The values of 0 are used for convenience.

4. Let $h(\hat{\mathbf{x}}) = \hat{\mathbf{x}}$ in (4.6).

The extension to 3D is as follows:

1. Convert the raw measurements of range, bearing, elevation and range rate to Cartesian position and velocity with (4.35), using $\dot{c}_m = 0$ and $\dot{e}_m = 0$, and use the result, $\mathbf{z} = \mathbf{z}_{\text{U3D}}$, in (4.6).

2. Use the information form of the Kalman filter (4.54)–(4.55) with $R^{-1} = {R_{\text{C3D}}}^{-1}$ from (4.53).

3. Set the measurement prediction matrix, $H = I_{6\times 6}$, in (4.54)–(4.55).

4. Let $h(\hat{\mathbf{x}}) = \hat{\mathbf{x}}$ in (4.6).

The use of a priori information in CMKFRR for (4.28) and (4.50) requires additional discussion. In practice, having some a priori target information is unlikely to be problematic (are you tracking commercial aircraft or military; swimmers or submarines?) and is presumably used in determining the appropriate process noise for the assumed target dynamics. An assumption for maximum target speed, in conjunction with the transmitted waveform bandwidth, is used in determining the bandwidth of the receiver. If the distribution of target velocities is known to be zero mean with standard deviation σ_s, as is the case in the performance evaluations to follow, $\sigma_{\dot{c}}$ and $\sigma_{\dot{e}}$ should be set to σ_s. Otherwise, $\sigma_{\dot{c}}$ should be based on an assumed maximum target speed. The effect of underestimating $\sigma_{\dot{c}}$

(and $\sigma_{\dot{e}}$) is that the range rate measurement will have more influence on the state update and the tracker will be overconfident (ANEES greater than one). Overestimating will result in the the range rate measurement having less influence, and in the extreme case $\sigma_{\dot{c}} = \infty$, the tracker will converge to the one using position measurements only.

Since $\sigma_{\dot{c}}$ has the overall effect of controlling the gain of the range rate measurement, the use of this a priori knowledge has a similar effect to the common practice of using artificial process noise or pseudo-noise in an EKF [3]. However, while the EKF practice is completely heuristic, the use of $\sigma_{\dot{c}}$ proposed here has a theoretical basis and physical interpretation. Furthermore, the gain is adjusted automatically as a function of σ_α, while the pseudo-noise approach can only be optimized for one value of σ_α.

4.6 Evaluation

4.6.1 Measurement Conversion Consistency Evaluation

The consistency of the conversion method was examined using the Normalized Error Squared (NES) [3]. The NES was evaluated by performing 1,000 measurement conversions under the following conditions:

1. True target range, r = 3,000m.

2. True target bearing, α, varying from 0° to 360°.

3. True target heading uniformly distributed from $-\pi$ to π.

4. True target speed χ_2 distributed, scaled by σ_s, set to 20m/s.

5. Sensor range accuracy, $\sigma_r = 30$m.

6. Sensor bearing accuracy, $\sigma_\alpha = 1°$, $5°$ and $10°$.

7. Sensor range rate accuracy, $\sigma_{\dot{r}} = 0.1$m/s.

8. Correlation coefficient between range and range rate errors of 0.5.

9. The a priori standard deviation of target cross range rate, $\sigma_{\dot{c}}$, set to 20m/s.

The distribution of target speeds, parameterized here as σ_s, is assumed to be known a priori, and used to set $\sigma_{\dot{c}}$ in (4.28).

For the calculation of R_{R}, a predicted estimate is required. To simulate this the predicted estimate, $\hat{\mathbf{x}}$, was set to the ground truth state corrupted by normally distributed independent noise with $\sigma_x = \sigma_y = 15$m and $\sigma_{\dot{x}} = \sigma_{\dot{y}} = 0.05$m/s. Correlation coefficient between the x and y components was 0.2. P was set appropriately based on this noise.

$$P = \begin{bmatrix} 15^2 & 0.2 \cdot 15^2 & 0 & 0 \\ 0.2 \cdot 15^2 & 15^2 & 0 & 0 \\ 0 & 0 & 0.05^2 & 0.2 \cdot 0.05^2 \\ 0 & 0 & 0.2 \cdot 0.05^2 & 0.05^2 \end{bmatrix} \tag{4.56}$$

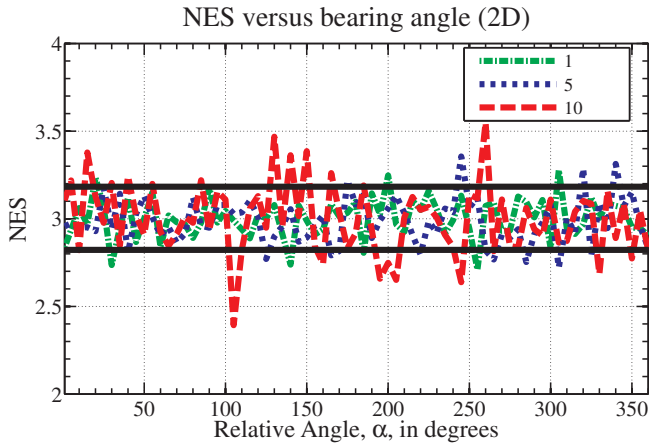

Fig. 4.4: Normalized Error Squared (NES) of the 2D measurement conversion for sensor bearing accuracy, $\sigma_\alpha = 1°$, $5°$ and $10°$. Plots include chi-square 0.99 probability bounds.

Although the converted measurement has dimension 4, the expected NES [3, eq. (10.4.3-26)] is 3, since velocity errors along the cross range rate are multiplied by zero.

Fig. 4.4 shows the results of the Monte Carlo evaluation, which indicates that the converted measurement error covariance is statistically consistent with converted measurement errors for a range of bearing accuracies.

For evaluation of the 3D conversion, the parameters for the 2D case were used with the following modifications/additions

1. True target elevation of $0°$, $30°$ and $60°$.

2. True target pitch uniformly distributed from $-\pi$ to π.

3. True target speed χ_3 distributed, scaled by σ_s, set to 20m/s.

4. Sensor bearing accuracy, $\sigma_{\alpha\text{LOS}} = 1^\circ$, 5° and 10°.

5. Sensor elevation accuracy, $\sigma_\theta = 1^\circ$, 5° and 10°.

6. Predicted σ_z and $\sigma_{\dot{z}}$ set to 15m and 0.05m/s.

7. The a priori standard deviations of target cross range rates, $\sigma_{\dot{c}}$ and $\sigma_{\dot{e}}$, set to 20m/s.

Again, the distribution of target speeds, parameterized here as σ_s, is assumed to be known a priori, and used to set $\sigma_{\dot{c}}$ and $\sigma_{\dot{e}}$ in (4.50).

Although the converted measurement has dimension 6, the expected NES is 4, since the cross range velocity errors are multiplied by zero. Fig. 4.5 shows the results of the Monte Carlo evaluation, which indicates that the measurement conversion technique is fairly consistent for a wide range of bearing and elevation accuracies and at various elevations. The conversion is slightly optimistic for small elevations and slightly conservative for large elevations.

4.6.2 Tracking Performance Comparisons

The performance of the proposed Converted Measurement Kalman Filter with Range Rate (CMKFRR) has been evaluated with respect to the current state-of-art techniques. The CMKFRR was compared to

1. CMKF using range and bearing measurements only (POS)

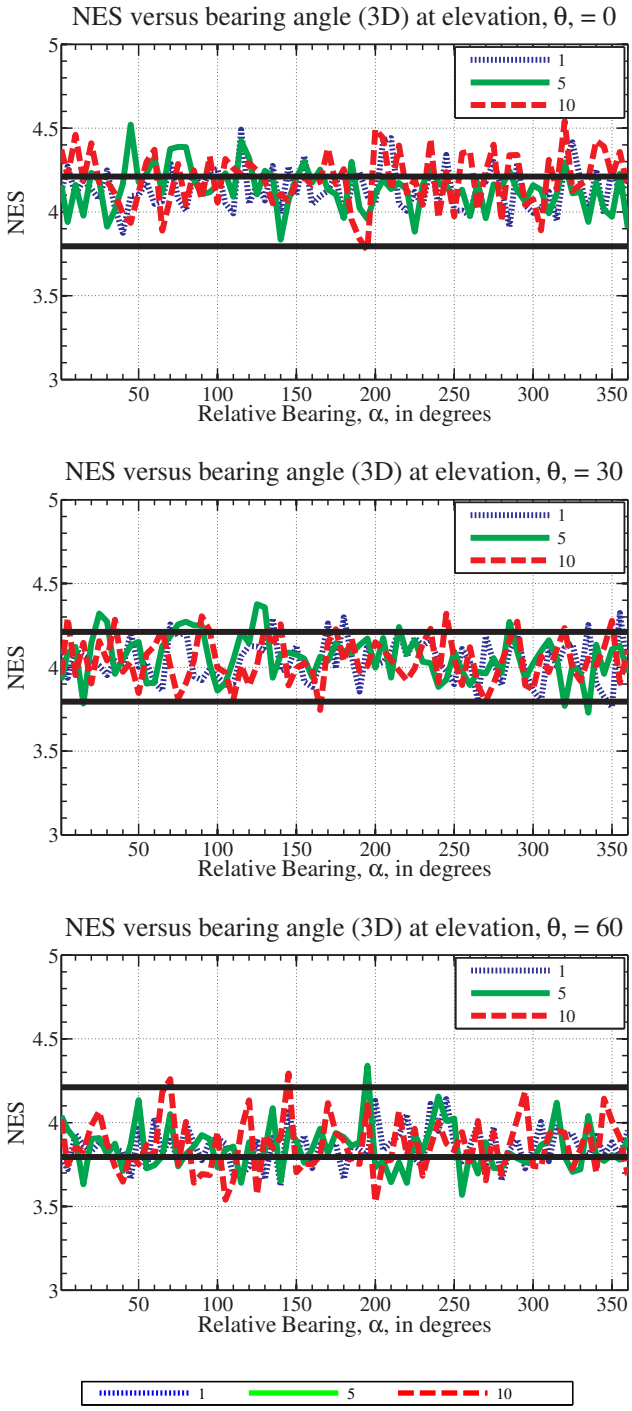

Fig. 4.5: NES of the 3D measurement conversion for sensor angle accuracy, $\sigma_{\alpha \mathrm{LOS}}$ $= \sigma_\theta = 1°$, $5°$ and $10°$. Plots include chi-square 0.99 probability bounds.

2. Sequential EKF using pseudo range rate (i.e. range, range rate product) as described in 4.3.2 (SEKF)

3. Sequential UKF using range rate as described in 4.3.2 (SUKF)

4. Posterior Cramer-Rao lower bound, as defined in [50], for range and bearing measurements only (PCRLBPOS)

5. Posterior Cramer-Rao lower bound for range, bearing and range rate measurements (PCRLBPOSRR)

The sequential EKF was chosen as the EKF representative since the performance of this filter exceeded that of the EKF using (4.13) and (4.14). To allow for direct comparison, all of the existing trackers were implemented with the conversion of range and bearing to Cartesian coordinates using the method described in [20,32]. The conclusions hold for other conversion methods.

Measures of performance include mean square error (MSE) for the target position and velocity estimates. An additional measure of performance is the tracker consistency based on the Average Normalized Estimation Error Squared (ANEES). The ANEES scaled by the state dimension, n, is [3]

$$\text{ANEES} = \frac{1}{Nn}\sum_{i=1}^{N}\tilde{\mathbf{x}}_i^T P_i^{-1}\tilde{\mathbf{x}}_i \tag{4.57}$$

where $\tilde{\mathbf{x}}_i$ is the estimation error and P_i is the error covariance for trial i. The ANEES of a consistent estimator is close to 1. Tracker consistency is important

not only for analysis of results, but also for measurement to track association in multitarget tracking scenarios in clutter.

The tracking scenario is set up as follows:

1. True target range, r, normally distributed with mean 4,000m and standard deviation of 30m.
2. True target bearing uniformly distributed from $-\pi$ to π
3. True target heading uniformly distributed from $-\pi$ to π
4. True target speed χ_2 distributed, scaled by σ_s, set to 10m/s
5. Sensor range accuracy, $\sigma_r = 30$m
6. Sensor bearing accuracy, $\sigma_\alpha = 1°$, $2.5°$, $5°$, $8°$ and $16°$.
7. Sensor range rate accuracy, $\sigma_{\dot{r}} = 0.1$m/s
8. Correlation between range and range rate errors, $\rho = -0.2$.

The target follows a nearly constant velocity track and all trackers employ a discrete continuous white noise acceleration (DWNA) model [3] with power spectral density $\tilde{q} = 0.1904 m^2/s^3$. As discussed in Sec. 4.4.2, it is assumed that there is some a priori knowledge about the range of possible target speeds, parametrized in this scenario as σ_s. To ensure a fair comparison of the trackers, all trackers use this knowledge during tracker initialization. One-point initialization

is employed using the measured position and an initial velocity estimate of 0 m/s and standard deviation of σ_s m/s in each component. The proposed tracker, due to its formulation, can also take advantage of this knowledge by setting $\sigma_{\dot{c}} = \sigma_s$ in the calculation of the converted measurement error covariance.

Figs. 4.6, 4.7 and 4.8 show the results of 5,000 Monte Carlo runs of the trackers. In each of the test cases, the proposed CMKFRR achieved performance that was equal to or better than the existing methods. For small angle error, the performance of the CMKFRR matched the existing methods (results overlap on plots), and all trackers were fairly consistent. As the angle accuracy degraded, the CMKFRR performance was better in terms of MSE, and considerably better in terms of consistency. Even for severely degraded angle accuracy, $\sigma_\alpha = 16°$, the CMKFRR maintained consistency.

4.6.3 Tracking Performance as a Function of Angle Accuracy

As to be expected, MSE performance is a function of angle accuracy. An analysis of the MSE performance as a function of angle accuracy shows that the performance of SEKF and SUKF is actually worse than the performance of a tracker with position only (range and bearing) measurements when angle accuracy degrades. Fig. 4.9 shows the MSE of the SEKF, SUKF and CMKFRR relative to the position only based tracker for $\rho = 0, -0.3, -0.6$, and -0.9 (Plot is the MSE at

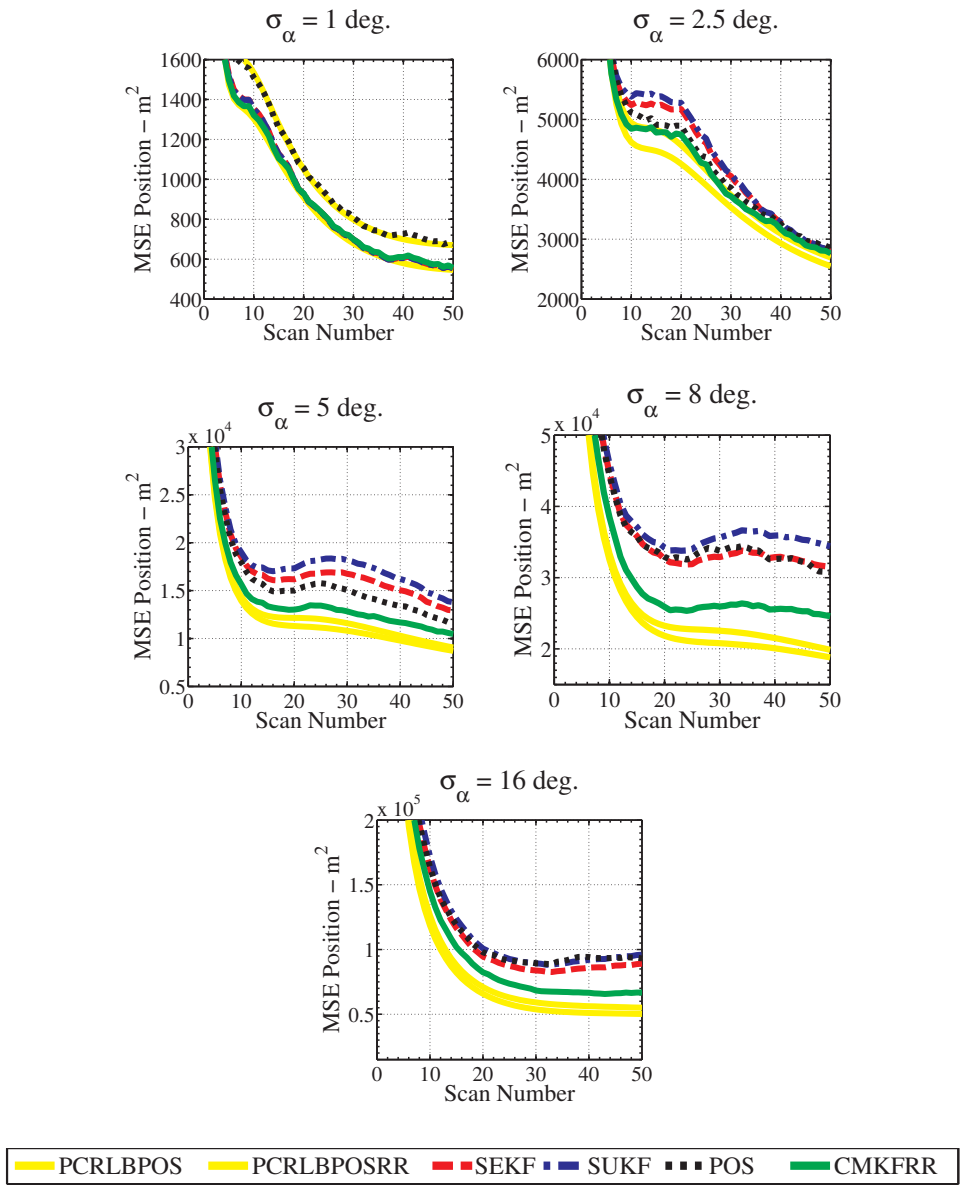

Fig. 4.6: Position MSE for the position only based tracker (POS), sequential EKF using pseudo range rate (SEKF), sequential UKF using range rate (SUKF), and the new Converted Measurement Kalman Filter with Range Rate (CMKFRR). The PCRLB for position only and position and range rate measurements is also shown.

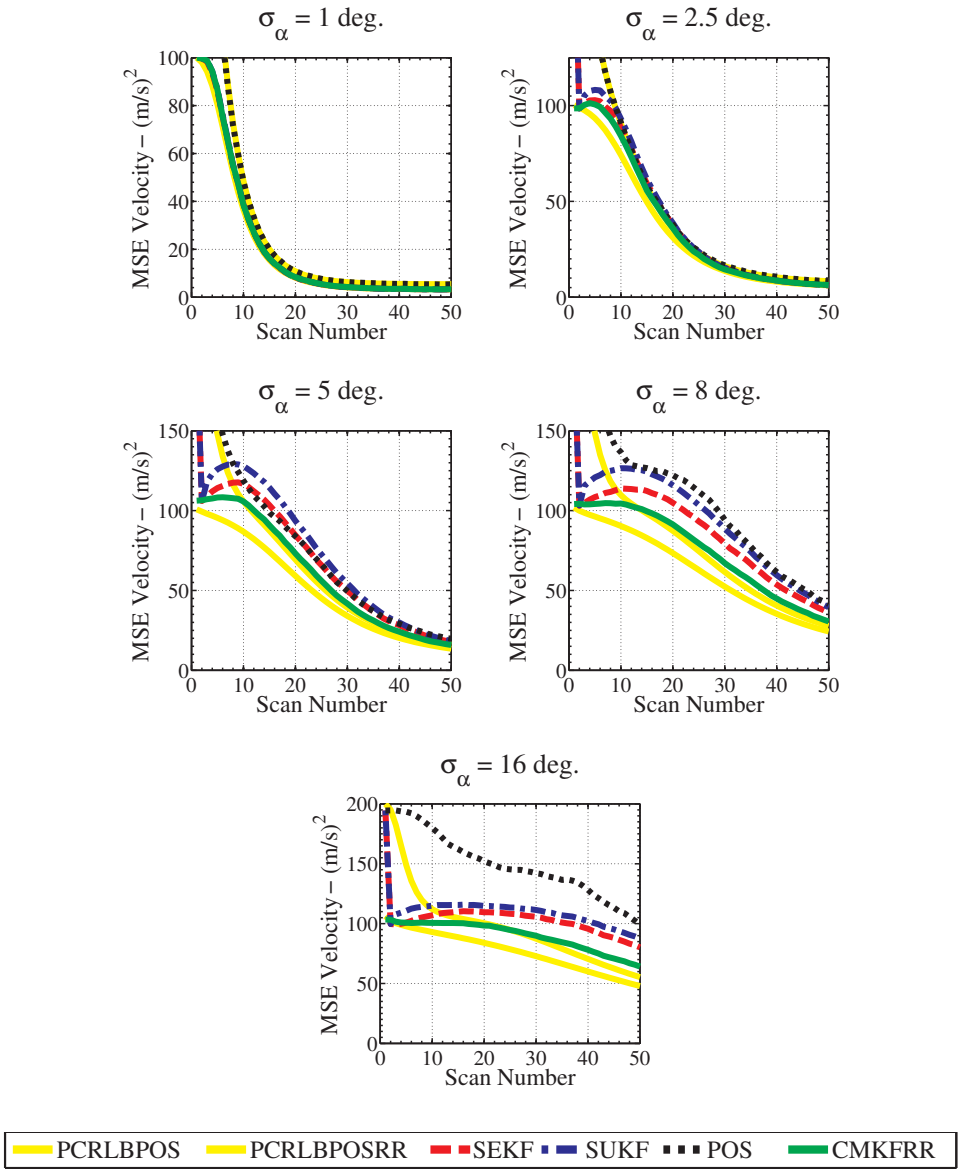

Fig. 4.7: Velocity MSE for the position only based tracker (POS), sequential EKF using pseudo range rate (SEKF), sequential UKF using range rate (SUKF), and the new Converted Measurement Kalman Filter with Range Rate (CMKFRR). The PCRLB for position only and position and range rate measurements is also shown.

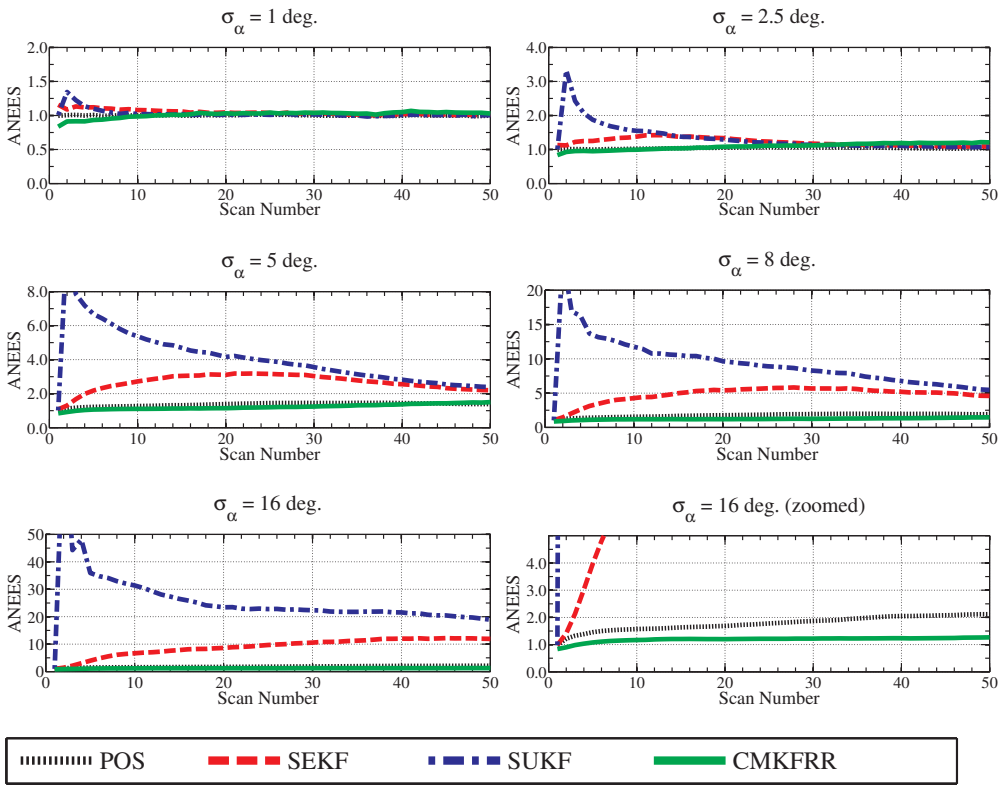

Fig. 4.8: ANEES for the position only based tracker (POS), sequential EKF using pseudo range rate (SEKF), sequential UKF using range rate (SUKF), and the new Converted Measurement Kalman Filter with Range Rate (CMKFRR).

the 10th scan)[4]. The plot shows that the new CMKFRR is the only tracker using range rate whose performance exceeds that of the position only based tracker for all angle accuracies. This is a key finding as a system whose angle accuracy is not constant could use the new tracker without the concern of range rate degrading performance in those cases where angle accuracy is degraded.

4.6.4 Tracking Performance as a Function of Range - Range Rate Correlation

Performance as a function of range - range rate correlation coefficient ρ was also examined, with results shown in Fig. 4.10. For small σ_α, the SEKF and SUKF performance degrades as the magnitude of the (negative) correlation increases. Although some of the variation in performance is due to the finite number of trials (exhibited in the position only based tracker that does not utilize range rate), the performance degradation trend of the SEKF and SUKF is still evident. This trend is in spite of the fact that negative correlation provides a theoretical advantage over no, or positive, correlation. The degradation is less pronounced in the SUKF, presumably since the use of the range-range rate product in the SEKF magnifies the error of the range rate [38]. The new CMKFRR does not show a degradation in performance for increased (negative) correlation.

[4] Commonly used waveforms, such as the upsweep linear FM, have a *negative* correlation between the range and range rate measurement noises [2].

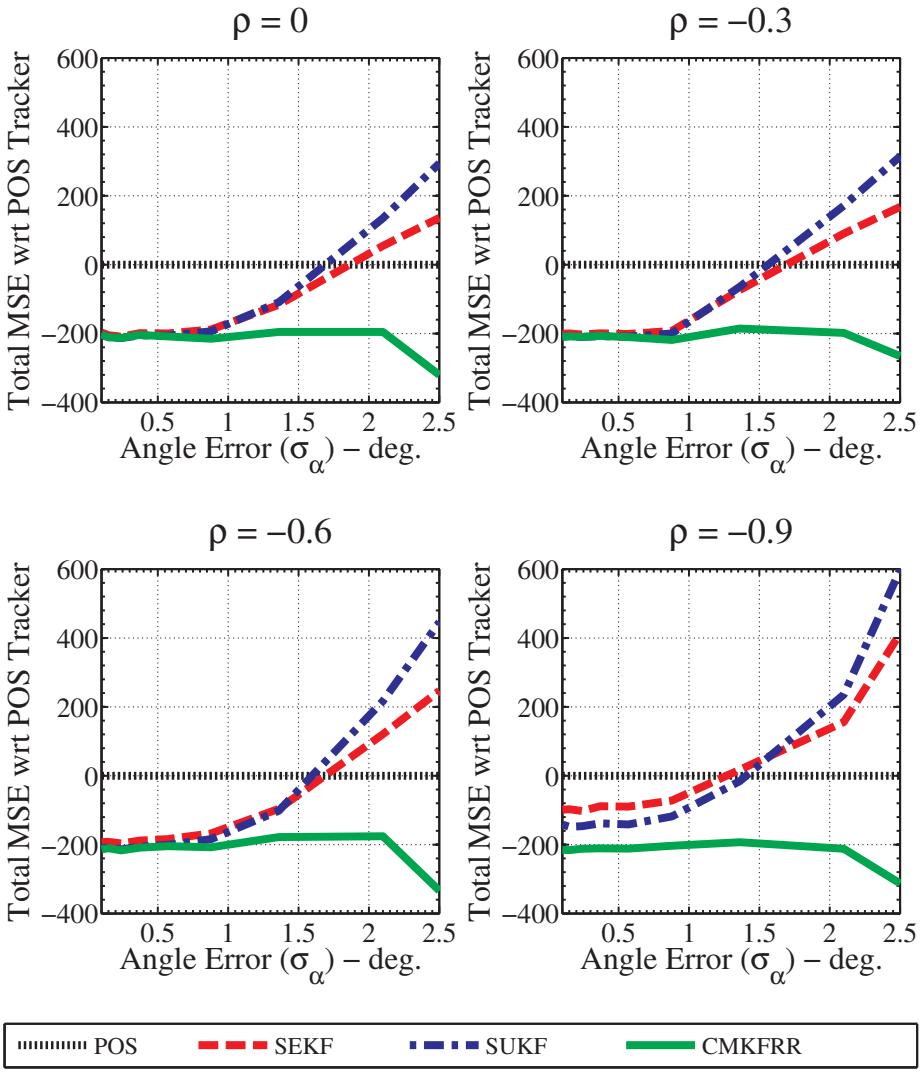

Fig. 4.9: MSE relative to the position only based tracker (POS) as a function of angle error, σ_α, of the sequential EKF using pseudo range rate (SEKF), sequential UKF using range rate (SUKF), and the proposed Converted Measurement Kalman Filter with Range Rate (CMKFRR) for various correlation coefficients between range and range rate, ρ. The plots are the MSE of each tracker minus the MSE of the POS tracker.

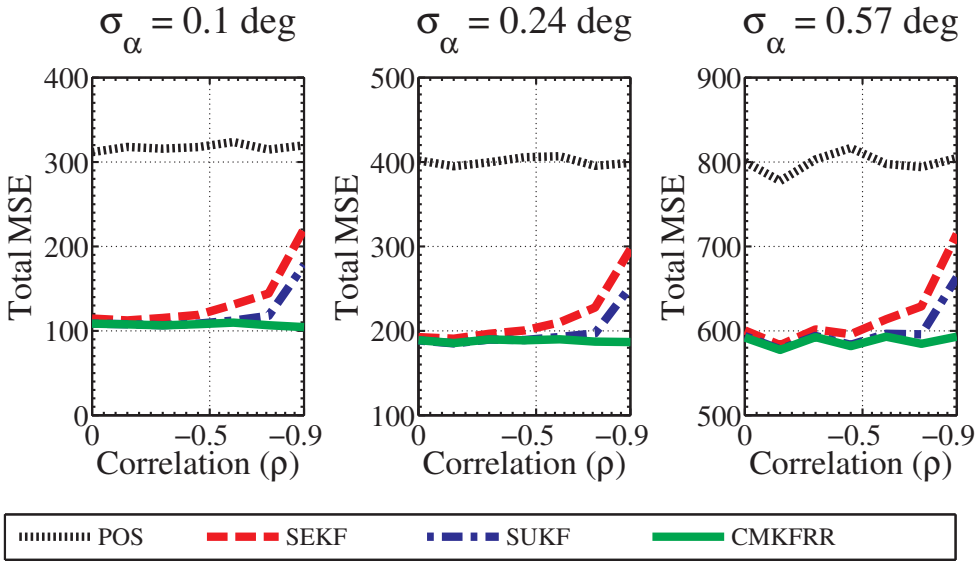

Fig. 4.10: MSE as a function of range and range rate correlation coefficient, ρ, for the position only based tracker (POS), the sequential EKF using pseudo range rate (SEKF), sequential UKF using range rate (SUKF), and the new Converted Measurement Kalman Filter with Range Rate (CMKFRR) for various angular errors, σ_α.

4.7 Conclusion

When tracking with measurements of range, bearing and range rate, various filtering techniques have been proposed. For cases with poor bearing accuracy, the valid approaches have been limited to nonlinear filters, such as the EKF and UKF or a bank of two filters. This chapter has shown that a single linear Kalman filter can be employed to tackle this estimation problem by using a new converted measurement technique and the information form of the Kalman filter. The conversion process avoids conversion bias by using an unbiased converted measurement, and precludes estimation bias by evaluating the converted measurement error covariance at the prediction. Simulations show that this linear Kalman filter has advantages over current state of the art trackers, such as the sequential EKF using pseudo range rate and the sequential UKF, for tracking scenarios with poor angle measurement accuracy. For small angle errors the performance of the proposed filter matches the existing techniques; however, for poor angle measurement accuracy (common in certain real world systems) the proposed filter exhibits improved MSE performance and significantly better consistency. Unlike these state of the art trackers, the performance of the new CMKFRR is improved with the respect to position only tracking even for severely degraded angle accuracy.

Chapter 5

Converted Measurement Sigma Point Kalman Filter for Bi-Static Sonar and Radar Tracking

5.1 Abstract

Tracking with bi-static sonar or radar measurements is challenging due to the fact that the measurements are nonlinear functions of the Cartesian state. The performance of existing approaches, including the Extended Kalman Filter (EKF) and sigma point Kalman filters such as the Unscented Kalman Filter (UKF) and Cubature Kalman Filter (CKF), may not be acceptable in terms of mean square error or tracker consistency (i.e. the tracker's state estimation error covariance is not statistically consistent with the actual estimation errors). This work generalizes the sigma point Kalman filter (SPKF) as a converted measurement SPKF. The resulting CMSPKF is demonstrated to have improved performance over the conventional SPKF when employed in a bi-static tracking scenario.

5.2 Introduction

In tracking problems it is common for the state dynamic equation to be linear while the measurements are nonlinear functions of the state. Perhaps the most common example of this is target tracking with a Cartesian state using a nearly constant velocity (or acceleration) dynamic model with measurements of range and bearing. Another important example is when measurements are from a bi-static sonar or radar system. There are many approaches to deal with nonlinear measurements that can be put into two broad categories: the converted measurement approach and the converted prediction approach.

In the converted measurement approach the measurement is transformed from the sensor's measurement coordinate system into the state coordinate system (e.g. Cartesian) using a nonlinear transformation. The converted measurement, now a linear function of the state, can be used in a standard (linear) Kalman filter. The challenges of this approach are accounting for biases in the conversion and calculating an approximation to the converted measurement error covariance. Approximation is required since the bias introduced by the conversion (for bi-static cases) and the converted measurement error covariance (for both bi-static and mono-static cases) are both functions of the the true state, not available in practice.

The EKF and numerical approximation approaches such as the UKF [34]

and CKF [1] are converted prediction approaches[1]. In these approaches the state prediction is converted into the measurement coordinate system using the nonlinear observation function. The innovation is also calculated in the measurement coordinate system and the innovation covariance and cross-covariance are approximated using a first or second order series expansion (EKF and second order EKF) or by using numerical integration (UKF and CKF).

The premise of this chapter is that, for certain problems, the converted measurement approach is superior in terms of mean square error and consistency. This has been confirmed in tracking with a single sensor that provides measurements in polar or spherical coordinates [4,15]. A Converted Measurement Sigma Point Kalman Filter (CMSPKF) is developed in the present chapter for cases, such as the bi-static case, in which it is not possible to derive an unbiased measurement conversion and converted measurement error covariance. Of particular interest is the case when the bi-static system has good range accuracy, but relatively poor angle accuracy. This is relevant for small sensors, as the range accuracy is primarily a function of waveform design, while the angle accuracy is a function of aperture (size of the sensor array/antenna).

The Converted Measurement Sigma Point Kalman Filter (CMSPKF) does not simply employ the Unscented Transform (UT) to convert the measurement from measurement coordinates to Cartesian coordinates. The reasons for this are

[1] Also called mixed coordinate filtering [3].

two-fold. The first is that the UT does not provide an unbiased estimate of the truth [33,15]. The second is that employing the UT to approximate the converted measurement error covariance results in a dependency between the measurement error covariance estimate and the measurement error itself, leading to an estimation bias when the converted measurement is used in tracking [15]. Estimation bias refers to a bias in an estimator that is introduced through the use of a covariance that is a function of the measurement noise. This results in a bias in the gain of Kalman filter, or in the weights of a linear least squares estimator.

To resolve these issues, the proposed CMSPKF estimates the conversion bias and the converted measurement error covariance with a sigma point transform using a combination of the tracker's predicted estimate and the raw measurement error covariance. This chapter extends the previous work of [13–15] by developing a method that takes advantage of the unbiased conversion and mitigation of estimation bias without the need to derive the conversion bias and converted measurement error covariance. This is achieved through a novel use of the unscented (or cubature) transform.

The remainder of this chapter is organized as follows. Sections 5.3 and 5.4 introduce the bi-static tracking problem and describe existing approaches based on sigma point transformations. Section 5.5 derives the CMSPKF, shows the implementation of the filter and describes the approximations used in its development. Section 5.6 shows the results of a Monte-Carlo evaluation of the CMSPKF

with respect to existing methods and demonstrates the advantage of the technique for four specific bi-static tracking cases.

5.3 Background

5.3.1 Bi-static sonar and radar — 2D

Active bi-static sonar and radar systems produce raw measurements (designated by subscript 2B for the 2D bi-static case) of bi-static range and bearing

$$\mathbf{z}_{2\mathrm{B}} = \begin{bmatrix} b_m \\ \\ \alpha_m \end{bmatrix} = \mathbf{h}_2(\mathbf{x}) + w_{2\mathrm{B}} \tag{5.1}$$

where b_m and α_m are the measured bi-static range and bearing; $\mathbf{h}_2$ is the measurement function; $\mathbf{x}$ is the target state, and $w_{2\mathrm{B}}$ is the measurement noise. Figure 5.1 describes the bi-static geometry. We will assume that the target dynamics can be represented with a nearly constant velocity model (with state $\mathbf{x} = [x \;\; y \;\; \dot{x} \;\; \dot{y}]'$). Extending the concepts to higher order models is straightforward. Without loss of generality, the receiver is assumed to be at the origin and the transmitter is at a location in Cartesian coordinates at (L,0). If this is not the case, tracking can be done in a local coordinate system that matches these assumptions, using

$$L = \sqrt{(x_{\mathrm{tx}} - x_{\mathrm{rx}})^2 + (y_{\mathrm{tx}} - y_{\mathrm{rx}})^2} \tag{5.2}$$

where tx and rx stand for transmitter and receiver, respectively. The resulting local estimate can then be transformed into a global coordinate system (see Fig.

5.2).

The measurement function, $\mathbf{h}_2$, is [17]

$$\mathbf{h}_2(\mathbf{x}) = \begin{bmatrix} \sqrt{x^2+y^2} + \sqrt{(L-x)^2+y^2} \\ \tan^{-1}(y/x) \end{bmatrix} \tag{5.3}$$

The bi-static range measurement is a measurement of the total range from transmitter to target to receiver. This is accomplished by measuring the time delay between transmit and receive and converting to range using the speed of transmission. The measurement error, $w_{2\mathrm{B}}$, for the raw measurements (in the bi-static coordinates, designated by 2B for the 2D bi-static case) is assumed to be zero-mean Gaussian with covariance matrix

$$R_{2\mathrm{B}} = \begin{bmatrix} \sigma_b^2 & 0 \\ 0 & \sigma_\alpha^2 \end{bmatrix} \tag{5.4}$$

State estimation is performed in Cartesian coordinates since the target motion is linear in this coordinate system. The relationship between the measured bi-static range and bearing and the position portion of the Cartesian state is as follows [17].

$$\begin{bmatrix} x \\ y \end{bmatrix} = \mathbf{g}_2(\mathbf{z}_{2\mathrm{B}}) \triangleq {\mathbf{h}_2}^{-1}(\mathbf{z}_{2\mathrm{B}}) \triangleq \begin{bmatrix} r_1 \cos\alpha \\ r_1 \sin\alpha \end{bmatrix} \tag{5.5}$$

where r_1 is a function of the bi-static range, b, the bearing, α, and the distance between the receiver and the transmitter (see Appendix E).

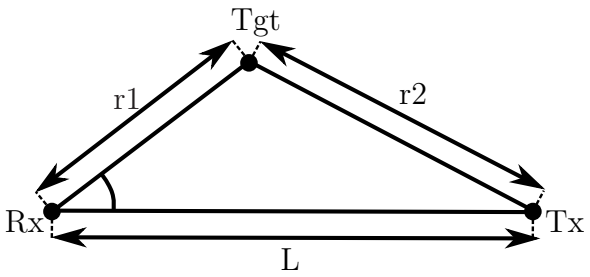

Fig. 5.1: Geometry of the target, Tgt, transmitter, Tx, and receiver, Rx for the bi-static case. Bi-static measurements include the bearing to the target, α and the bi-static range, $b = r_1 + r_2$. The locations of the transmitter and receiver, and therefore the distance between them, L, is assumed to be known.

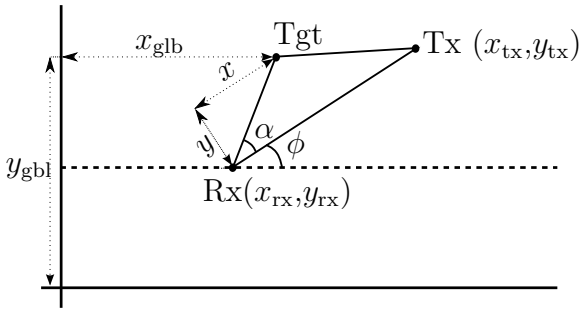

Fig. 5.2: Geometry of the target, Tgt, transmitter, Tx, and receiver, Rx for arbitrary locations. Tracking is performed in the local coordinates (x, y) and transformed to global coordinates $(x_{\text{GBL}}, y_{\text{GBL}})$.

$$r_1 = \frac{L^2 - b^2}{2\left(L\cos(\alpha) - b\right)} \tag{5.6}$$

The state estimate, $\hat{\mathbf{x}}_{k+1|k+1}$, and state covariance, $P_{k+1|k+1}$, (in local coordinates) can be converted into global coordinates: Define the receiver state as

$$\mathbf{x}_{\text{rx}} = \begin{bmatrix} x_{\text{rx}} \\ y_{\text{rx}} \\ 0 \\ 0 \end{bmatrix} \tag{5.7}$$

and the rotation, ϕ, as

$$\phi = \tan^{-1}\left(\frac{y_{\text{tx}} - y_{\text{rx}}}{x_{\text{tx}} - x_{\text{tx}}}\right) \tag{5.8}$$

The conversion of the state and covariance is:

$$\hat{\mathbf{x}}_{\text{glb,k+1|k+1}} = D\left(\phi\right)\hat{\mathbf{x}}_{k+1|k+1} - \mathbf{x}_{\text{rx}} \tag{5.9}$$

$$P_{\text{glb,k+1|k+1}} = D\left(\phi\right)P_{k+1|k+1}D\left(\phi\right)' \tag{5.10}$$

where D is the direction cosine matrix,

$$\begin{bmatrix} \cos\phi & \sin\phi & 0 & 0 \\ -\sin\phi & \cos\phi & 0 & 0 \\ 0 & 0 & \cos\phi & \sin\phi \\ 0 & 0 & -\sin\phi & \cos\phi \end{bmatrix} \tag{5.11}$$

5.3.2 Bi-static sonar and radar — 3D

In many radar systems, as well as some sonar systems, the receiver also provides a measurement of elevation angle, θ. The following changes from the 2D case are made to include this measurement. The raw measurement (designated by subscript 3B) is now

$$\mathbf{z}_{3\mathrm{B}} = \begin{bmatrix} b_m \\ \alpha_m \\ \theta_m \end{bmatrix} = \mathbf{h_3}(\mathbf{x}) + w_{3\mathrm{B}} \tag{5.12}$$

The inclusion of elevation allows for estimation in three dimensions using a nearly constant velocity (with state $\mathbf{x} = [x \;\; y \;\; z \;\; \dot{x} \;\; \dot{y} \;\; \dot{z}]'$), or nearly constant velocity and attitude/depth ($\mathbf{x} = [x \;\; y \;\; z \;\; \dot{x} \;\; \dot{y}]'$). In either case the measurement function is

$$\mathbf{h}_3(\mathbf{x}) = \begin{bmatrix} \sqrt{x^2+y^2+z^2} + \sqrt{(L-x)^2+y^2+z^2} \\ \tan^{-1}\left(\frac{y}{x}\right) \\ \tan^{-1}\left(\frac{z}{\sqrt{x^2+y^2}}\right) \end{bmatrix} \tag{5.13}$$

where

$$L = \sqrt{(x_{\mathrm{tx}} - x_{\mathrm{rx}})^2 + (y_{\mathrm{tx}} - y_{\mathrm{rx}})^2 + (z_{\mathrm{tx}} - z_{\mathrm{rx}})^2} \tag{5.14}$$

As in the 2D case, the measurement error is assumed to be Gaussian with

covariance matrix

$$R_{3\mathrm{B}} = \begin{bmatrix} \sigma_b^2 & 0 & 0 \\ 0 & \sigma_\alpha^2 & 0 \\ 0 & 0 & \sigma_\theta^2 \end{bmatrix} \tag{5.15}$$

The conversion from the measurement to Cartesian state for 3D is

$$\begin{bmatrix} x \\ y \\ z \end{bmatrix} = \mathbf{g_3}\left(\mathbf{z}_{3\mathrm{B}}\right) \triangleq \mathbf{h_3}^{-1}\left(\mathbf{z}_{3\mathrm{B}}\right) \triangleq \begin{bmatrix} r_1 \cos\alpha \cos\theta \\ r_1 \sin\alpha \cos\theta \\ r_1 \sin\theta \end{bmatrix} \tag{5.16}$$

where

$$r_1 = \frac{L^2 - b^2}{2\left(L\cos(\alpha)\cos(\theta) - b\right)} \tag{5.17}$$

The local coordinates can be converted into global coordinates in a similar manner to the 2D case.

5.4 Existing Techniques

Due to the nonlinearity of the bi-static problem, one must resort to a nonlinear filter. Although there are numerous nonlinear filtering techniques, this work focuses on a family of filters, sometimes referred to as "sigma point filters" [52], that include the UKF and CKF. These filters employ a deterministic sampling approach (forms of quadrature integration) to approximate the mean and covariance of a random variable that has undergone nonlinear transformation. For clarity, the term sigma point transform (SPT) will be used to refer to the sampling based

approximation and sigma point filter will refer to a filter that employs such a transform.

5.4.1 Sigma Point Transform

The SPT, a generalization of the unscented transform [34], uses a deterministic set of point masses in the approximation of the mean and covariance of a random variable $\mathbf{x}$ that has been transformed by a nonlinear function $\mathbf{f}$. It is assumed that the covariance of the random variable, P_{xx}, and an estimate of its mean, $\hat{\mathbf{x}}$, before the transformation, are available. The steps of the transform are

1. Generate a set of m sigma points around $\hat{\mathbf{x}}$

$$\mathbf{s}_i = \hat{\mathbf{x}} + \boldsymbol{\Delta}_i \tag{5.18}$$

   where $\boldsymbol{\Delta}_i$ is a function of the covariance of the random variable, P_{xx}, and differs for the unscented and cubature techniques (see Appendix F).

2. Pass each point through the nonlinear function

$$\mathbf{t}_i = \mathbf{f}(\mathbf{s}_i) \tag{5.19}$$

3. Estimate the mean of the transformed variable using a weighted sum

$$\hat{\mathbf{z}} = \sum_{i=0}^{m-1} \mathrm{w}_i \mathbf{t}_i \tag{5.20}$$

   where w_i, a function of the state dimension, n, also differs for the unscented and cubature techniques (see Appendix F).

4. Estimate the covariance of the transformed variable

$$P_{zz} = \sum_{i=0}^{m-1} \mathrm{w}_i \left(\mathbf{t}_i - \hat{\mathbf{z}}\right) \left(\mathbf{t}_i - \hat{\mathbf{z}}\right)' \tag{5.21}$$

5. Estimate the cross-covariance

$$P_{xz} = \sum_{i=0}^{m-1} \mathrm{w}_i \left(\mathbf{s}_i - \hat{\mathbf{x}}\right) \left(\mathbf{t}_i - \hat{\mathbf{z}}\right)' \tag{5.22}$$

For convenience, the notation

$$\left(\hat{\mathbf{z}}, P_{zz}, P_{xz}\right) = \mathrm{SPT}\left(\hat{\mathbf{x}}, P_{xx}, \mathbf{f}\right) \tag{5.23}$$

will be used to represent this transform in the sequel.

5.4.2 Tracking Approaches using the Sigma Point Transform

Sigma Point Kalman Filter (SPKF)

For the specific case of tracking with linear target dynamics and measurements that are a nonlinear function of the target state, the SPKF differs from the traditional Kalman filter in the measurement update steps. The standard state prediction functions are executed, resulting in a state prediction for time $k+1$, $\hat{\mathbf{x}}_{k+1|k}$, and an associated state prediction covariance, $P_{k+1|k}$. The state update steps are as follows:

1. Use the SPT to estimate the predicted measurement, $\hat{\mathbf{z}}_{k+1|k}$, the predicted measurement covariance, P_{zz}, and the cross-covariance, P_{xz}

$$\left(\hat{\mathbf{z}}_{k+1|k}, P_{zz}, P_{xz}\right) = \mathrm{SPT}\left(\hat{\mathbf{x}}_{k+1|k}, P_{k+1|k}, \mathbf{h}\right) \tag{5.24}$$

2. Estimate the Kalman gain

$$W_k = P_{xz}\left(P_{zz} + R_{\mathrm{B}}\right)^{-1} \tag{5.25}$$

3. Update the state estimate

$$\hat{\mathbf{x}}_{k+1|k+1} = \hat{\mathbf{x}}_{k+1|k} + W_k\left(\mathbf{z}_{\mathrm{B},k} - \hat{\mathbf{z}}_{k+1|k}\right) \tag{5.26}$$

4. Update the state covariance

$$P_{k+1|k+1} = P_{k+1|k} - W_k\left(P_{zz} + R_{\mathrm{B}}\right)W_k{}' \tag{5.27}$$

For the 2D case, $R_{2\mathrm{B}}$ from (5.4) is used for R_{B}, while $R_{3\mathrm{B}}$ from (5.15) is used in the 3D case. Similarly, $\mathbf{h_2}$ or $\mathbf{h_3}$ is used for $\mathbf{h}$ appropriately.

Kalman Filter Using a Sigma Point Transform of the Measurements (SPTKF)

Since previous work on mono-static tracking has shown that it is advantageous to first convert the raw measurement into Cartesian coordinates (denoted by subscript C) and utilize a (linear) Kalman filter [39], it is tempting to use a SPT in this manner for the bi-static case [41]. In this approach the raw measurement is first converted into Cartesian, for time step $k+1$

$$\left(\hat{\mathbf{z}}_{\mathrm{C}}, R_{\mathrm{C}}\right) = \mathrm{SPT}\left(\mathbf{z}_{\mathrm{B}}, R_{\mathrm{B}}, \mathbf{g}\right) \tag{5.28}$$

The cross-covariance estimate from the SPT is not required. The relationship between the converted measurement and the Cartesian state is now linear

$$\hat{z}_{\mathrm{C},k+1} = H\mathbf{x}_{k+1} + w_{k+1} \tag{5.29}$$

where

$$H = \begin{bmatrix} 1 & 0 & 0 & 0 \\ 0 & 1 & 0 & 0 \end{bmatrix} \tag{5.30}$$

and R_{C} is an estimate of the covariance of w_{k+1}. The standard Kalman measurement update step can then be used

1. Calculate the Kalman gain

$$W_{k+1} = P_{k+1|k}H' \left(R_{\mathrm{C},k+1} + HP_{k+1|k}H'\right)^{-1} \tag{5.31}$$

2. Update the state estimate

$$\hat{\mathbf{x}}_{k+1|k+1} = \hat{\mathbf{x}}_{k+1|k} + W_{k+1}\left(\mathbf{z}_{\mathrm{C}} - H\hat{\mathbf{x}}_{k+1|k}\right) \tag{5.32}$$

3. Update the state covariance

$$P_{k+1|k+1} = P_{k+1|k} - W_{k+1}(R_{\mathrm{C,k+1|k}} + HP_{k+1|k}H'){W_{k+1}}' \tag{5.33}$$

This approach will be refered to as the Sigma Point Transform Kalman Filter (SPTKF), to distinguish it from the traditional SPKF.

5.5 The Converted Measurement Sigma Point Kalman Filter (CMSPKF)

5.5.1 Motivation

While the approach described in Sec. 5.4.2 may be advantageous in some situations, there are two issues with the implementation that limit its effectiveness. The first issue is that the SPT does not provide an unbiased estimate of the truth [33], leading to a conversion bias when used in a Kalman filter [15]. Figure 5.3 shows the results of a Monte-Carlo evaluation of the UT for bi-static sonar. The bi-static measurements fall roughly on an ellipse when mapped into Cartesian coordinates ($\mathbf{g}(\mathbf{z}_{\mathrm{B}})$). Due to the curvature of this ellipse, the expected value of these measurement, $E[\mathbf{g}(\mathbf{z}_{\mathrm{B}})]$, is biased towards the receiver and transmitter. Use of the unscented transform yields $E[\hat{\mathbf{z}}_{\mathrm{C}}]$ with an even larger bias.

The second issue is that the estimate of the converted measurement error covariance, R_{C}, is evaluated at the measurement. This dependency of R_{C} on the measurement leads to a bias in the Kalman gain resulting in a bias away from the transmitter and receiver. Due to this estimation bias, a static target will, on average, initially appear to be moving away from the transmitter and receiver [15].

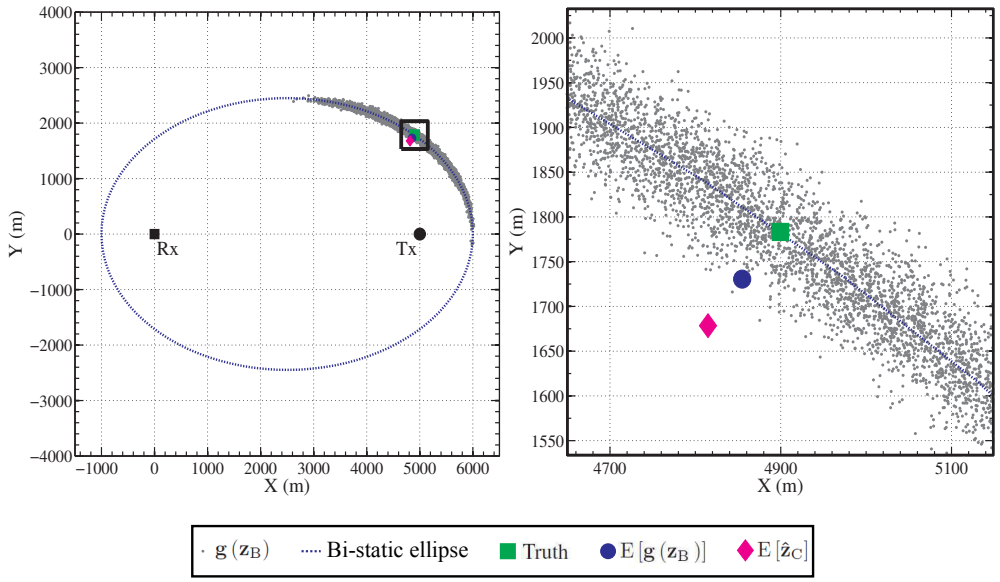

Fig. 5.3: 10,000 measurement Monte Carlo evaluation of the expected value for the conversion from bi-static range and bearing to Cartesian for the conventional conversion, $\mathbf{g}(z_{\mathrm{B}})$, and the conversion using the Unscented Transform $\hat{\mathbf{z}}_{\mathrm{C}}$ from (5.28). The bi-static range standard deviation, σ_b, and bearing standard deviation, σ_α, are $50m$ and $6°$, respectively. The individual conversions and the bi-static ellipse are shown for reference. The black square in the upper figure is zoomed in on the lower figure.

5.5.2 Proposed New Filter, CMSPKF

In order to rectify the issues of conversion and estimation bias, a new use of sigma point transformation is proposed. Since the bias and covariance of the converted measurements are dependent on the target state, an estimate of these values can be calculated using the raw measurement error covariance and the predicted estimate of the target state. That is, the sigma point transform is used to estimate the state dependent bias and covariance using the current state prediction. These quantities are then utilized in the Kalman filter equations as follows:

1. Prior to employing the sigma point transform, convert the predicted state from Cartesian coordinates into the measurement coordinate system,

$$\hat{\mathbf{z}}_{\mathrm{B},k+1|k} = \mathbf{h}(\hat{\mathbf{x}}_{k+1|k}) \tag{5.34}$$

2. Use the sigma point transform to estimate the expected value and covariance of the random variable with mean $\hat{\mathbf{z}}_{\mathrm{B}}$ and covariance R_{B}, transformed by the function $\mathbf{g}$ (for $k+1|k$) from sensor (bi-static range, bearing, and possibly elevation) to state (Cartesian)

$$\left(\hat{\mathbf{z}}_{\mathrm{C}}, \check{R}_{\mathrm{C}}\right) = \mathrm{SPT}\left(\hat{\mathbf{z}}_{\mathrm{B}}, R_{\mathrm{B}}, \mathbf{g}\right) \tag{5.35}$$

where $\mathbf{g}$ is defined in (5.5).

3. Estimate the bias and modify the converted measurement error covariance to account for debiasing[2]

$$\hat{\mu}_{k+1|k} = \hat{\mathbf{z}}_{\mathrm{C},k+1|k} - H\hat{\mathbf{x}}_{k+1|k} \tag{5.36}$$

$$R_{\mathrm{C},k+1|k} = \check{R}_{\mathrm{C},k+1|k} + \hat{\mu}_{k+1|k}\hat{\mu}'_{k+1|k} \tag{5.37}$$

4. Calculate the Kalman gain

$$W_{k+1} = P_{k+1|k}H' \left(R_{\mathrm{C},k+1|k} + HP_{k+1|k}H'\right)^{-1} \tag{5.38}$$

5. Calculate the (unbiased) innovation

$$\nu_{k+1} = \mathbf{g}\left(\mathbf{z}_{\mathrm{B},k+1}\right) - \hat{\mu}_{k+1|k} - H\hat{\mathbf{x}}_{k+1|k} \tag{5.39}$$

$$= \mathbf{g}\left(\mathbf{z}_{\mathrm{B},k+1}\right) - \mathbf{z}_{\mathrm{C},k+1} \tag{5.40}$$

6. Update the state estimate

$$\hat{\mathbf{x}}_{k+1|k+1} = \hat{\mathbf{x}}_{k+1|k} + W_{k+1}\nu_{k+1} \tag{5.41}$$

7. Update the state covariance

$$P_{k+1|k+1} = P_{k+1|k} - W_{k+1}(R_{\mathrm{C,k+1|k}} + HP_{k+1|k}H')W_{k+1}{}' \tag{5.42}$$

A block diagram of the proposed method is shown in Fig. 5.4, inspired by figure 5.2.4-1 in [3]. A depiction of the process in Fig. 5.5. The figures depict

[2] Since the estimate is debiased with respect to the truth, while $\check{R}_{\mathrm{C}}$ is estimated with respect to $E\left[\mathbf{g}\left(\hat{\mathbf{z}}_{\mathrm{B}}\right)\right]$, the addition of the term $\hat{\mu}_{k+1|k}\hat{\mu}'_{k+1|k}$ is required to achieve consistency.

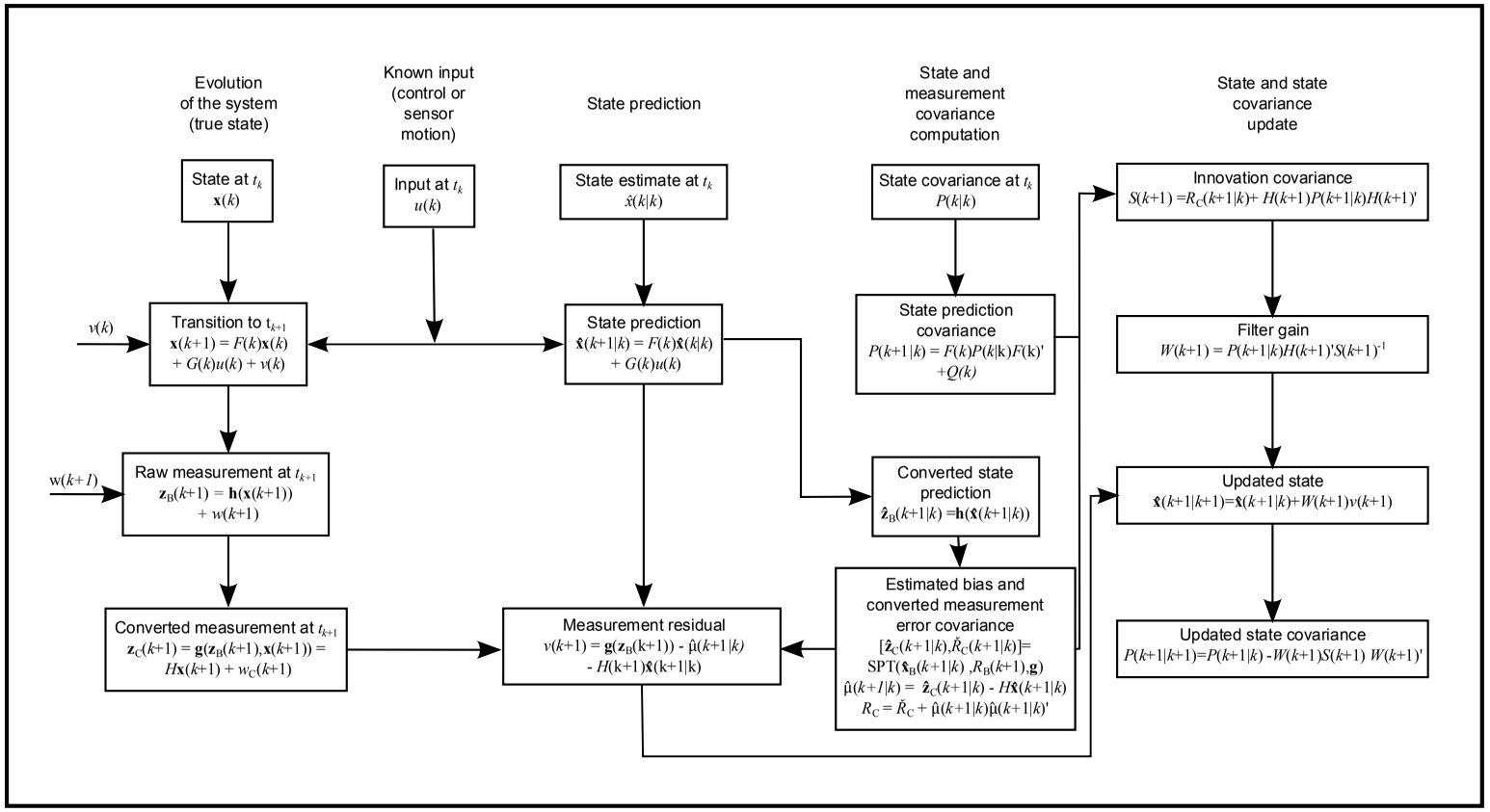

Fig. 5.4: Block Diagram of one cycle of the CMSPKF

the conversion process and include the underlying measurement error probability density function as a color gradient. The first sub-figure shows the true target position, the predicted estimate and the bi-static ellipse in Cartesian coordinates. The second sub-figure shows the truth in bi-static coordinates and the predicted estimate converted from Cartesian to bi-static. The true measurement error covariance, R_{B}, is displayed as an ellipse plotted at a Mahalanobis distance of 1.5. The four sigma points, calculated based on the predicted estimate converted to bi-static coordinates, used in the Cubature transform are also shown. The third sub-figure shows these sigma points, converted to Cartesian, and their mean, $\hat{\mathbf{z}}_{\mathrm{C},k+1|k}$. The difference between $\hat{\mathbf{z}}_{\mathrm{C},k+1|k}$ and $\hat{\mathbf{x}}_{k+1|k}$ provides an estimate of the bias introduced by the conversion. The covariance calculated using the sigma points with (R_{C}) and without ($\check{R}_{\mathrm{C}}$) bias correction are shown as ellipses. The true converted measurement error covariance is shown for comparison.

5.5.3 Approximations

There are two important approximations to be aware of with this approach. The obvious one is the use of the sigma-point transform to approximate the bias and converted measurement covariance at $\hat{\mathbf{x}}_{k+1|k}$, which for an exact result would require integration of the probability density function for the random variable $\mathbf{z}_{\mathrm{B}}$. The second approximation is that the SPT is employed using the one-step prediction as a surrogate for the truth. This is a departure from [15], the basis for

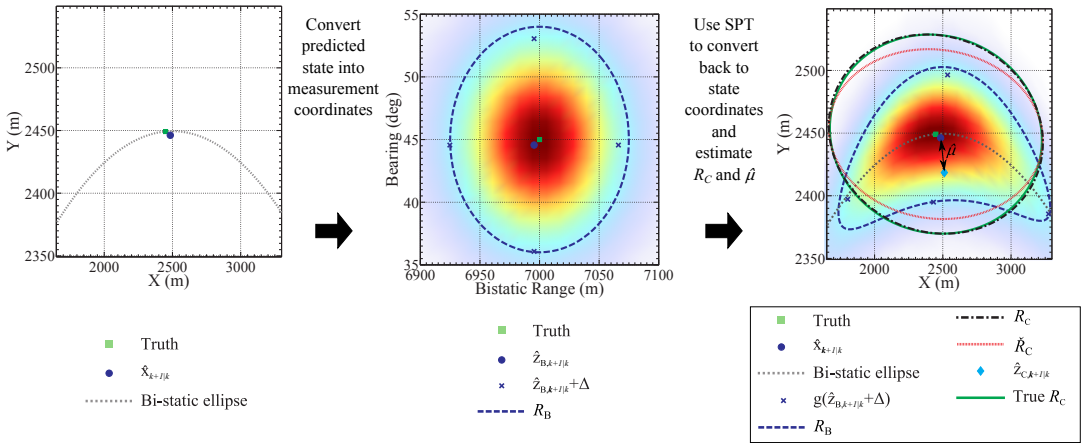

Fig. 5.5: The steps used in the CMSPKF are shown here graphically. (1) The predicted state is used as a surrogate for the truth and converted into measurement coordinates; (2) Using the measurement error covariance, R_{B}, sigma points are placed around the predicted state (in measurement coordinates); (3) The sigma points are converted into state coordinates and the mean, $\hat{\mathbf{z}}_{\mathrm{C},k+1|k}$, and converted measurement error covariance, $\check{R}_{\mathrm{C}}$, are estimated using the SPT; (4) Using $\hat{\mathbf{z}}_{\mathrm{C},k+1|k}$ and the original state estimate, $\hat{\mathbf{x}}_{k+1|k}$, the bias introduced by the conversion, $\hat{\mu}$, is estimated; and (5) The bias estimate is used to debias the converted measurement and inflate the converted measurement error covariance to account for debiasing.

this CMSPKF, which accounts for the error in the prediction. The effect of this approximation is examined in Section 5.6.

5.6 Evaluation

The evaluation of the proposed technique includes the analysis of (1) the static conversion and (2) the use of the converted measurement in a dynamic tracking scenario.

5.6.1 Evaluation of the conversion

To examine the performance of the conversion, a mono-static and bi-static evaluation was performed. Analysis of the mono-static case is instructive since the bias and converted measurement error covariance can be derived explicitly without the use of a SPT.

The metric for conversion evaluation is consistency, which is examined with Monte Carlo evaluation. The Normalized Error Squared (NES) is used as a measure of consistency [3],

$$\text{NES} = \frac{1}{N}\sum_{i=1}^{N} \tilde{\mathbf{z}}_i' R_{\text{C},i}^{-1} \tilde{\mathbf{z}}_i \tag{5.43}$$

where $\tilde{\mathbf{z}}_i$ is the converted measurement error,

$$\tilde{\mathbf{z}}_i = H\mathbf{x} - \left(\mathbf{g}\left(\mathbf{z}_{\text{B},i}\right) - \hat{\mu}_i\right) \tag{5.44}$$

$R_{\mathrm{C},i}$ is the converted measurement error covariance estimate for trial i, and is calculated from (5.37). N is the number of trials. The NES of a consistent estimator should be close to the state dimension, n, which in this case is 2, and (if $\tilde{\mathbf{z}}_i$ is zero-mean Gaussian with covariance $R_{\mathrm{C},i}$) be chi-square distributed with nN degrees of freedom.

Polar to Cartesian

For the instructive case of converting from polar to Cartesian (equivalent to setting $L = 0$, and using $r_1 = b/2$), it is possible to compare the proposed method with the explicit method of [15]. The NES was evaluated by performing 5,000 measurement conversions under the following conditions:

1. True target range, $r = 3{,}000$m;
2. True target bearing, α, varying from $0°$ to $90°$;
3. Sensor range accuracy, $\sigma_b = 60$m ($\sigma_{r_1} = 30$m); and
4. Sensor bearing accuracy, $\sigma_\alpha = 1°$, $4°$ and $8°$.

To complete the conversion a predicted position is required. To simulate this, the predicted position, $H\hat{\mathbf{x}}$, was set to the ground truth state corrupted by normally distributed independent noise with the following covariance matrix

$$P = \gamma \begin{bmatrix} 30^2 & 0.1 \cdot 30^2 \\ 0.1 \cdot 30^2 & 30^2 \end{bmatrix} \tag{5.45}$$

The value of γ was set to 1, 10 and 100 to examine the effects that error in the predicted position have on consistency. The results are shown in Fig. 5.6 for the proposed method (using the cubature transform) and for the method in [15]. As seen in the figure, the conversion is consistent for even moderate errors in the prediction. As these errors increase to very large levels ($\gamma = 100$), the method shows signs of inconsistency when compared to the decorrelated, unbiased, converted measurement (DUCM) [15]. The new method is consistent for cases with large measurement errors ($\sigma_\alpha = 8$) and small errors in the predicted position ($\gamma = 1$). This indicates that the inconsistencies are caused primarily by errors in the predicted position, not the in measurement. Since the size of the converted measurement error covariance (i.e. the eigenvalues of $R_{\mathrm{C,k+1|k}}$) are a function of σ_b and σ_α, the inconsistency is due to $R_{\mathrm{C,k+1|k}}$ being rotated relative to the true converted measurement error covariance; a result of using $H\hat{\mathbf{x}}$ as the best available surrogate for the truth.

The conclusion is that the method of [15] should be used when the conversion bias and the converted measurement error covariance can be derived explicitly (as in the polar to Cartesian case), but *the method proposed here is the only one viable for cases (such as the bi-static case) in which direct evaluation is not possible.*

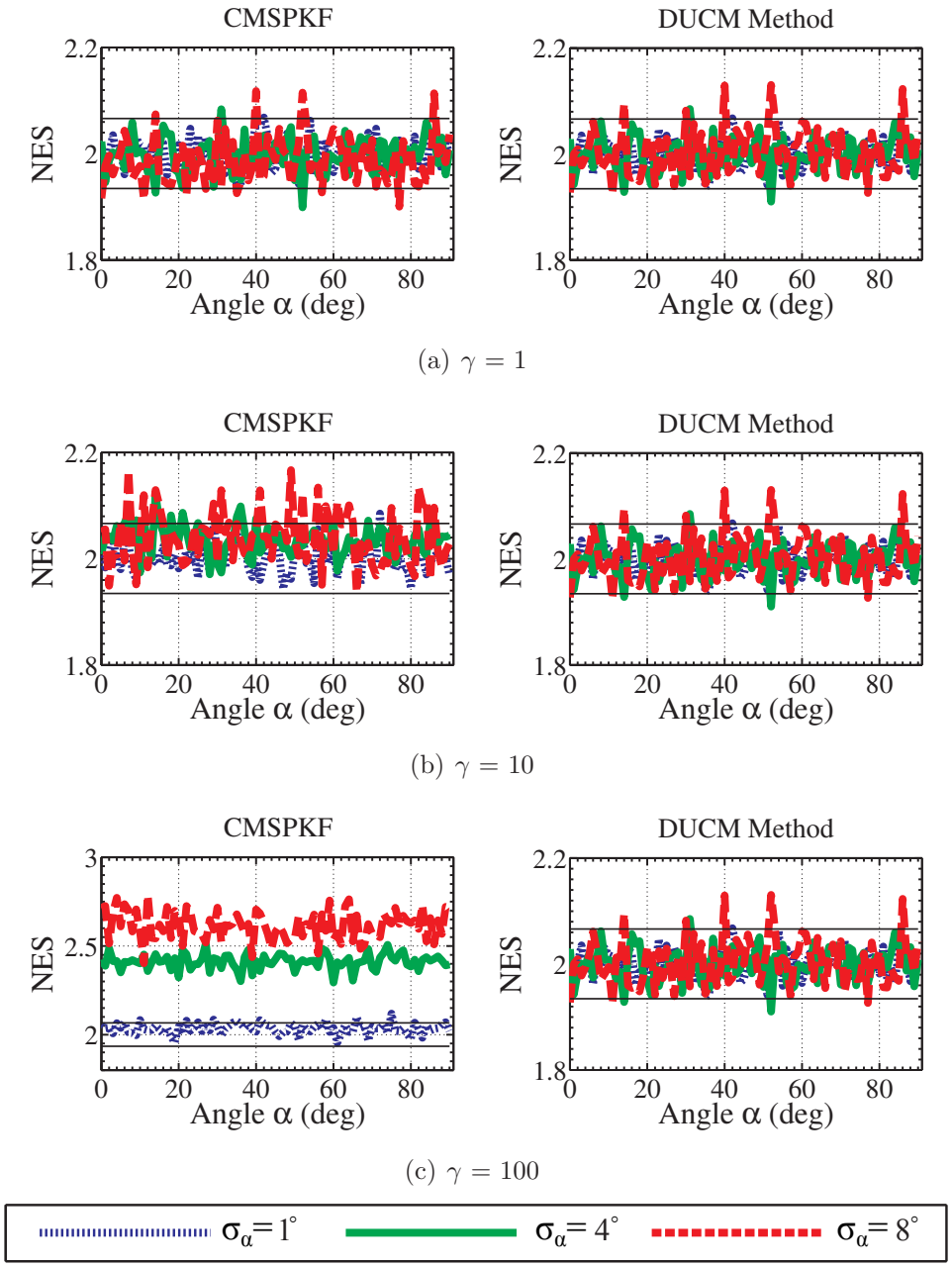

Fig. 5.6: NES of the polar to Cartesian measurement conversion for the CM-SPKF approximation and the DUCM method. Plots are for various cases of error in the one-step prediction and σ_α; they include the Chi-square upper (0.99) and lower (0.01) probability region bounds.

Bi-static Range and Bearing to Cartesian

For the case studied in this paper, namely, converting from bi-static range and bearing to Cartesian, the converted measurement error covariance cannot be derived, so an approximation is required. The NES of the conversion using the cubature transform was evaluated by performing 5,000 measurement conversions under the following conditions:

1. True target range, $r = 8{,}000$m;
2. True target bearing, α, varying from 0° to 90°;
3. Sensor range accuracy, $\sigma_b = 60$m;
4. Sensor bearing accuracy, $\sigma_\alpha = 1^\circ$, 4° and 8°; and
5. Transmitter to receiver separation, $L = 2500$m.

To complete the conversion a predicted state is required. To simulate this, the predicted state, $\hat{\mathbf{x}}$, was set to the ground truth state corrupted by normally distributed independent noise with the following covariance matrix

$$P = \gamma \begin{bmatrix} 60^2 & 0.1 \cdot 60^2 \\ 0.1 \cdot 60^2 & 60^2 \end{bmatrix} \tag{5.46}$$

Again, γ was set to 1 (Case I), 10 (Case II) and 100 (Case III) to examine the effects that the error in the predicted estimate have on consistency. The results are shown in Fig. 5.7. As seen in the figure, the conversion is consistent for even

moderate errors in the prediction. As these errors increase to very large levels ($\gamma = 100$), the method starts to show signs of inconsistency. The conclusion is that the method proposed here is viable for cases (such as the bi-static case) in which direct evaluation is not possible, but performance may be degraded in cases in which the error in the predicted state is much larger than the measurement error. It is important to note that converted estimate approaches (UKF and CKF) also suffer performance degradation as the errors in the predicted state increase, as these methods calculate the Kalman gain with P_{xx} and P_{xz} based on the predicted state.

5.6.2 Evaluation of the CMSPKF

To evaluate tracking performance, two test cases are examined for 2D in which

1. True initial target range, r, is normally distributed;
2. True initial target bearing is uniformly distributed ($-\pi$ to π);
3. True target heading is uniformly distributed ($-\pi$ to π); and
4. True target speed is χ_2 distributed, scaled by σ_s

Additional test cases, in 3D, were used in which the true initial target elevation angle is uniformly distributed (3 to 4 degrees)

The target follows a nearly constant velocity track and is estimated using filters with a discretized continuous white noise acceleration model [3]. For the

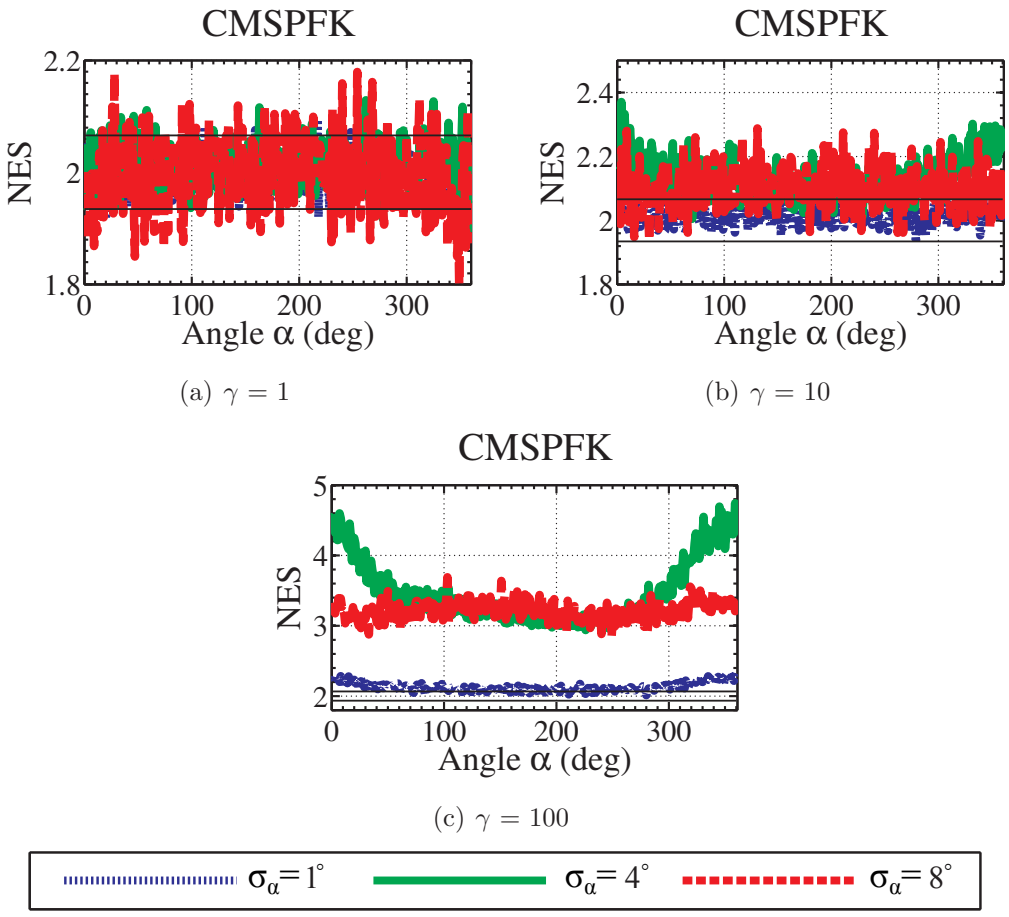

(a) $\gamma = 1$

(b) $\gamma = 10$

(c) $\gamma = 100$

Fig. 5.7: NES of the bi-static range and bearing to Cartesian measurement conversion using the CMSPKF approximation. Plots are for various cases of error for the one-step prediction and σ_α; they include the Chi-square upper (0.99) and lower (0.01) probability region bounds. Note: DUCM cannot be used in this case since it requires explicit expressions that are not available.

Table 5.1: CMKF Test Cases - 2D

Parameter	**Test Case I**	**Test Case II**
Initial Target Range ($\mu \pm \sigma$)	500 ± 10km	6000 ± 30m
Target Speed σ_s	50m/s	3m/s
Sensor σ_r	0.5m	20 m
Sensor σ_α	$\frac{3}{15}^\circ$	8°
Tracker Process Noise $\tilde{q}$	$19\text{m}^2/\text{s}^3$	$0.0027\text{m}^2/\text{s}^3$
Scan Rate	2 sec/scan	3 sec/scan
Source-Receiver Separation L	250km	2500m

3D case, the target also follows a nearly constant attitude/depth. One-point initialization of the tracker, using the SPT to convert the first measurement into Cartesian, is used with an initial velocity estimate of 0 and standard deviation of σ_s in each component. The parameters for each test case are listed in Tables 5.1 and 5.2.

The measures of performance examined are the mean square error (MSE) of the position and velocity components of the state estimate, and the average normalized estimation error squared. The ANEES scaled by the state dimension,

Table 5.2: CMKF Test Cases - 3D

Parameter	**Test Case III**	**Test Case IV**
Initial Target Range ($\mu \pm \sigma$)	500 ± 10km	6000 ± 30m
Target Speed σ_s	50m/s	3m/s
Sensor σ_r	0.5m	20 m
Sensor σ_α,σ_θ	$\frac{3}{15}^\circ$	8°
Tracker Process Noise $\tilde{q}$	$19\text{m}^2/\text{s}^3$	$0.0027\text{m}^2/\text{s}^3$
Scan Rate	2 sec/scan	3 sec/scan
Source-Receiver Separation L	225km	2500m

n, is [3]

$$\text{ANEES} = \frac{1}{Nn}\sum_{i=1}^{N}\tilde{\mathbf{x}}_i^T P_i^{-1}\tilde{\mathbf{x}}_i \tag{5.47}$$

where $\tilde{\mathbf{x}}_i$ is the estimation error and P_i is the error covariance for trial i. The expected value of (5.47) is unity.

Three trackers are used in the evaluation. The SPKF (described in 5.4.2), the Kalman Filter using a Sigma Point Transform (described in 5.4.2) and the new CMSPKF (described in 5.5). In all cases, the cubature transform was used.

The results of the evaluation are shown in Figs. 5.8 and 5.9. For the first test case, the CMSPKF exhibits improved consistency with an ANEES close to one. The SPTKF had reasonable consistency, while the SPKF was clearly inconsistent. The CMSPKF also had the best MSE performance for position and velocity. The SPKF, despite its consistency problems, outperformed the SPTKF in MSE.

For test case II, the CMSPKF again had the best consistency performance and MSE position performance. The MSE velocity performance was mixed with the SPKF initially having the best performance. After the initial scans, the MSE velocity performance of the SPKF and CMSPKF were comparable.

For the first 3D case (test case III), both the SPKF and CMSPKF performed well in terms of consistency and efficiency. The SPTKF was overconfident (ANEES greater than one) and had the worst MSE performance. For the other 3D case (test case IV), the CMSPKF again had the best consistency performance and MSE position performance. As in test case II, the MSE velocity performance

was mixed with the SPKF initially having the best performance. After the initial scans, the MSE velocity performance of the SPKF and CMSPKF were comparable.

5.7 Conclusion

The converted measurement Kalman filter (CMKF) has previously been shown to have superior performance over other nonlinear filtering techniques if two sources of bias, conversion bias and estimation bias, are mitigated. Previous work has only addressed cases in which an unbiased conversion and a converted measurement error covariance could be explicitly derived. For certain problems, such as tracking with bi-static measurements, this is not possible. This work has extended the CMKF to handle these cases by an innovative employment of the sigma point transform. Monte Carlo simulations show that this new CMSPKF method has improved performance over the traditional SPKF and SPTKF in terms of tracker consistency. The method also has improved MSE position performance and MSE velocity performance that is competitive with the SPKF.

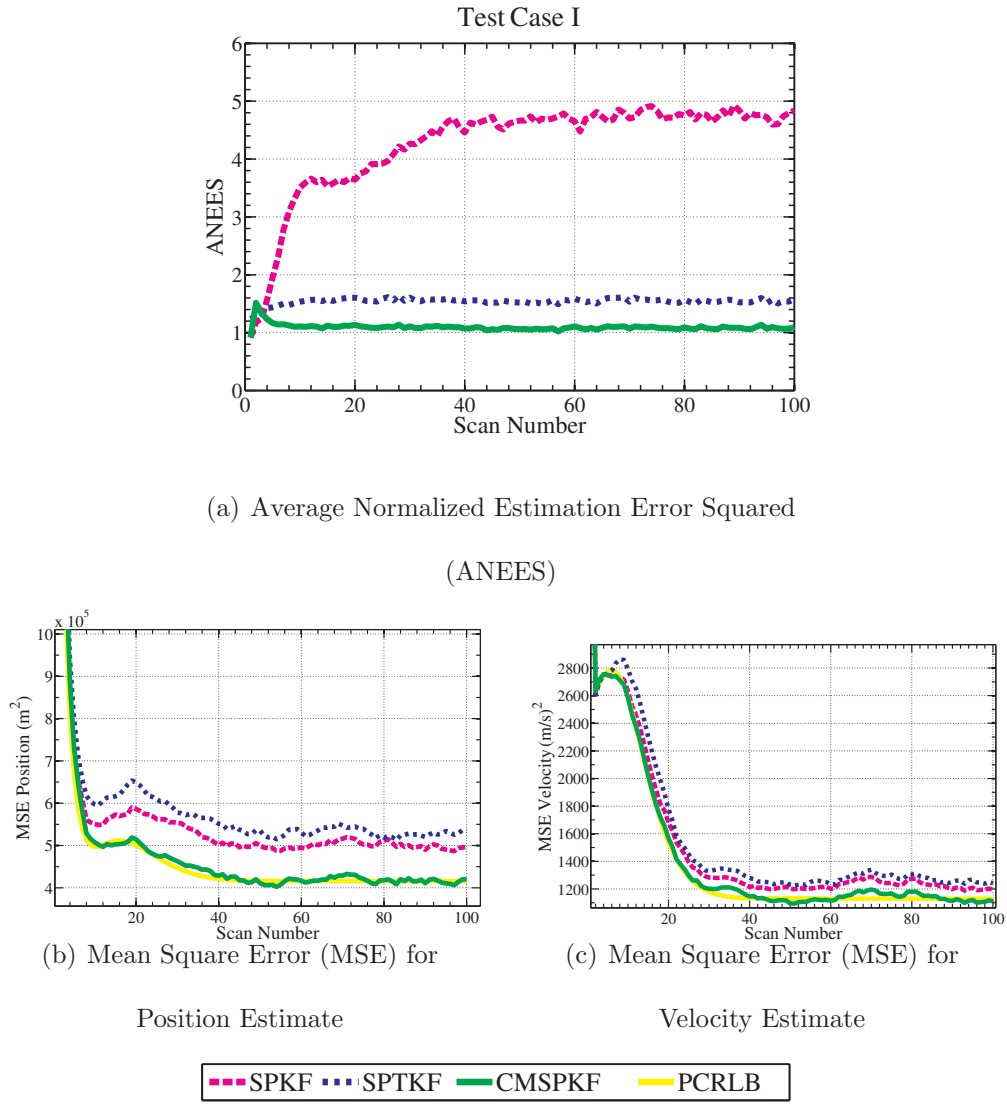

(a) Average Normalized Estimation Error Squared (ANEES)

(b) Mean Square Error (MSE) for Position Estimate

(c) Mean Square Error (MSE) for Velocity Estimate

Fig. 5.8: 5,000 run Monte Carlo evaluation for test case I of the Cubature Kalman Filter (SPKF), a Kalman filter using the Cubature Transform (SPTKF) and the proposed Converted Measurement Sigma Point Kalman Filter using the Cubature transform (CMSPKF). The ANEES and MSE performance are shown as well as the PCRLB.

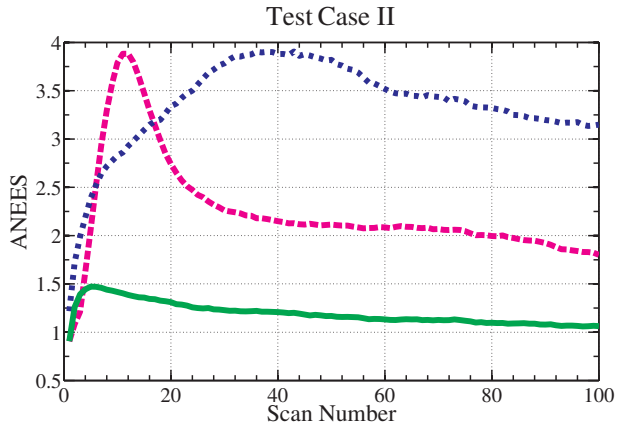

(a) Average Normalized Estimation Error Squared (ANEES)

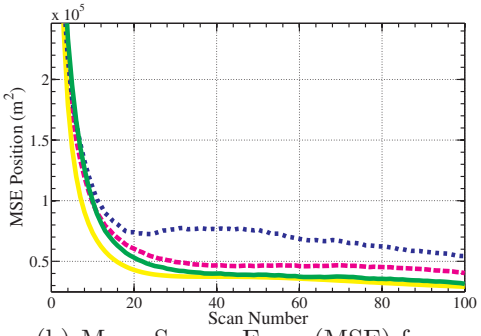

(b) Mean Square Error (MSE) for Position Estimate

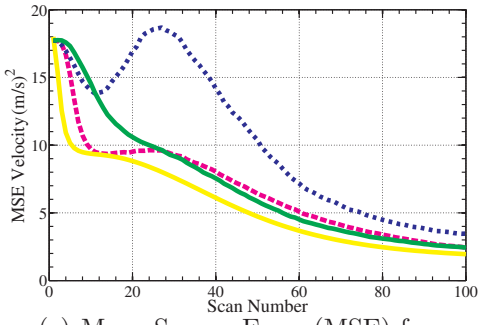

(c) Mean Square Error (MSE) for Velocity Estimate

Fig. 5.9: 5,000 run Monte Carlo evaluation for test case II of the Cubature Kalman Filter (SPKF), a Kalman filter using the Cubature Transform (SPTKF) and the proposed Converted Measurement Sigma Point Kalman Filter using the Cubature transform (CMSPKF). The ANEES and MSE performance are shown as well as the PCRLB.

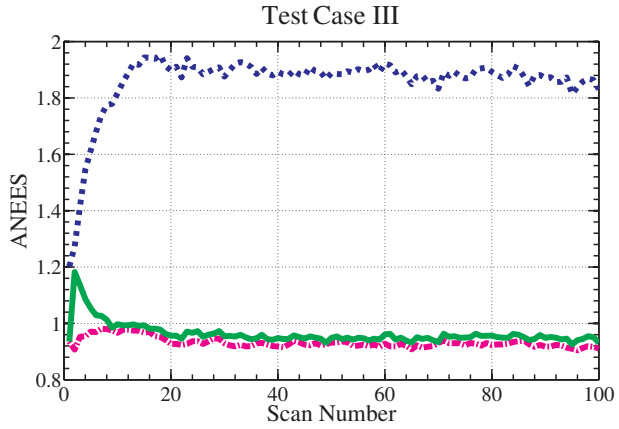

(a) Average Normalized Estimation Error Squared (ANEES)

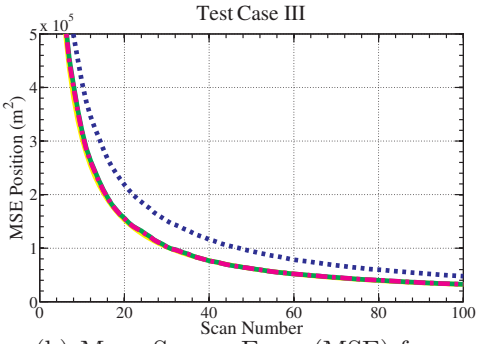

(b) Mean Square Error (MSE) for Position Estimate

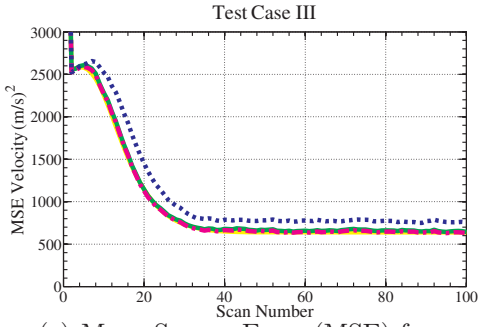

(c) Mean Square Error (MSE) for Velocity Estimate

Fig. 5.10: 5,000 run Monte Carlo evaluation for test case III (3D) of the Cubature Kalman Filter (SPKF), a Kalman filter using the Cubature Transform (SPTKF) and the proposed Converted Measurement Sigma Point Kalman Filter using the Cubature transform (CMSPKF). The ANEES and MSE performance are shown as well as the PCRLB.

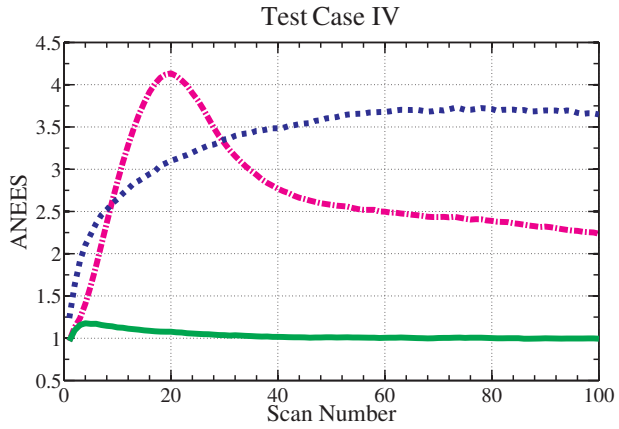

(a) Average Normalized Estimation Error Squared (ANEES)

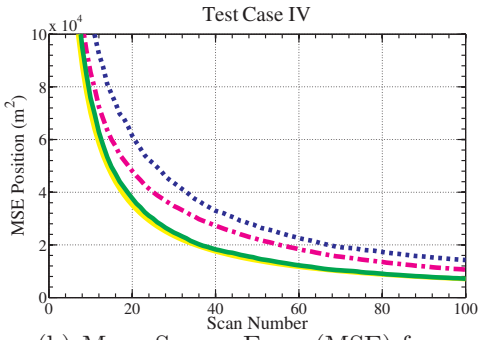

(b) Mean Square Error (MSE) for Position Estimate

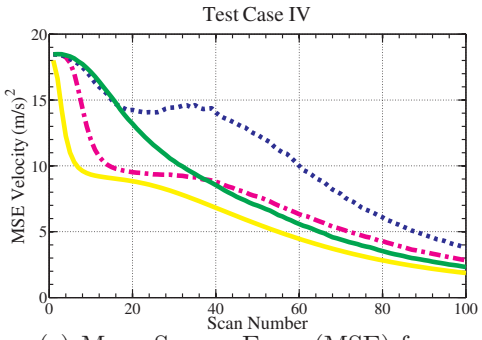

(c) Mean Square Error (MSE) for Velocity Estimate

Fig. 5.11: 5,000 run Monte Carlo evaluation for test case IV (3D) of the Cubature Kalman Filter (SPKF), a Kalman filter using the Cubature Transform (SPTKF) and the proposed Converted Measurement Sigma Point Kalman Filter using the Cubature transform (CMSPKF). The ANEES and MSE performance are shown as well as the PCRLB.

Chapter 6

Extended Object Tracking with Exploitation of Range Rate Measurements

6.1 Abstract

In active sonar and radar target tracking, measurements consist of position and often also include range rate. Tracking algorithms use these measurements over time to estimate target state comprising position, velocity and, where applicable, turn rate. In most cases there is an underlying assumption in the tracking algorithm that the target is a "point target" (i.e. the target has no physical extent). Another common assumption is that at most one measurement per scan originates from the target. For certain combinations of transmitted waveform and target type, the resolution of the waveform is such that the target is "over-resolved" (i.e. the error in the measurements is small enough that the spatial characteristics of the target can be measured). For such cases the point target assumption must be replaced with an extended target assumption. This work provides a methodology to exploit the extended nature of the target for the case of a rigid target whose

spatial characteristics are fixed with respect to the line of motion. By employing a combination of the expectation maximization (EM) algorithm and allowing more than one measurement per scan to originate from the target, a technique is developed that uses a single scan of raw measurements that include range, bearing and range rate to provide an estimate of target position, velocity, heading and turn rate. This single scan estimate is then used in a nearly constant turn rate extended Kalman filter to provide a multi-scan estimate of the target state.

6.2 Introduction

In active sonar and radar target tracking systems, the goal is often to provide an estimate of the target's state using measurements of range, bearing and range rate. Target dynamics are best modeled in Cartesian coordinates and consist of position, velocity and often include acceleration or turn rate. Common models for target dynamics are the nearly constant velocity, nearly constant acceleration and coordinated turn models [3].

In the formulation of the tracking algorithm it is common to assume that the target has no physical extent. This assumption is reasonable if the resolution of the transmitted waveform is greater than or equal to the size of the target. If, however, the resolution of the measurements is small enough that the spatial characteristics of the target can be measured, this "point target" assumption must be relaxed.

If the sensor is capable of resolving individual measurement sources within an extended target and detailed knowledge is available to model these sources, the target can be modeled as discrete measurements within an extended object [5]. An alternative is to estimate the overall shape of the target as opposed to individual components. Within this shape estimation approach, numerous models exist. Two approaches that represent the extended target as an ellipse are [36], which uses symmetric, positively definite (SPD) random matrices; and the approach of [6] which employs a random hypersurface model (RHM). The RHM approach has been extended to more complex shapes in [5] by using star-convex RHMs. Irregular shapes are handled in [37] by using multiple (possibly overlapping) ellipses. Another approach to modeling spatial extent uses the assumption that the number of target measurements is Poisson distributed, with the measurement(s) drawn from a spatial distribution [28–30].

While these approaches are excellent and fairly liberal with regards to shape, a different approach is chosen here that aims to fully exploit the range rate measurements at the expense of using a somewhat more restrictive target model. The target model chosen in this research is that of a target "template" that characterizes the locations of target highlights (i.e. the active reflectors of the target). While the size and orientation of the target is unknown, the relative locations of the highlights are assumed to be known a priori. It is also assumed that the target is rigid and has spatial characteristics that are fixed with respect to the line

of motion. (The model can be viewed as a parameterized version of a "discrete" spatial distribution, as discussed in [10], [29]). With this parametrized model, a single scan estimate of position, velocity, heading and turn rate can be made. This single scan estimate can then be utilized in a multi-scan tracker (e.g. an extended Kalman filter) with a coordinated turn motion model (nearly constant turn rate) [3].

To provide the target estimate, the measurements from the extended target must be assigned to the individual target highlights. This is achieved by employing a combination of the EM algorithm and a version of the probabilistic multi-hypothesis tracker (PMHT) association model [48]. Unlike many tracking approaches, the PMHT (even for a single point target) does not assume there is at most a single measurement per target. There is therefore a natural compatibility between the PMHT and extended objects, which have multiple measurements per target. Also advantageous is that the algorithm is very flexible and easy to extend [56]. A pertinent example of this is that the PMHT has been successfully employed in extended object tracking using random matrices [54,55]. The relationship of the PMHT association model with spatial distributions is also discussed in [29] and [28].

The combination of this target extent model and EM based estimation results in an algorithm with similar characteristics to one from a different field (image processing). This concept of aligning measured points to a template can

be viewed as a version of surface registration. The iterative closest point algorithm (ICP) [58] is a common approach for surface registration. Its extension, the multi-scale EM-ICP [31], uses a similar formulation to the one proposed here; however, the approach of the present chapter allows for the more general measurement error model needed for radar/sonar processing and utilizes range rate measurements.

The remainder of this chapter is organized as follows: Section 6.3 introduces the model for the extended target and the measurements; Section 6.4 describes the approach for single and multi-scan estimation; Section 6.5 provides a simulation of the algorithm and examines the resulting performance and Section 6.6 provides some concluding remarks. This chapter extends [16] by (i) modifying the measurement model to improve performance, (ii) providing an estimate of the converted measurement error covariance using the observed information matrix and (iii) utilizing the converted measurement in an extended Kalman filter.

6.3 The Model

6.3.1 Extended Target Model with Discrete Reflectors

In active radar and sonar processing, the transmitted signal is reflected off the target and returns to the receiver, resulting in measurements of range, bearing and range rate. The reflections are due to a finite number of strong reflectors, such as the nose and engines of an aircraft or the bow and sail of a submarine.

For waveforms with high spatial resolution, it is possible to resolve the individual reflectors from the target as opposed to the integration of all the reflectors. In many cases there is general knowledge of the relative locations of the primary reflectors for a given target class (e.g. a military aircraft), that can reasonably represent a number of targets in that class. Using this premise, an extended target model approach can be developed.

The target is therefore represented as a set of M highlights (i.e. reflectors) forming a template for a general target. Each reflector, $j = 1 \cdots M$, is specified with a probability of detection, α_j, and a position in 2D Cartesian coordinates,

$$\mathbf{t}_j = \begin{bmatrix} x_t(j) \\ \\ y_t(j) \end{bmatrix} \tag{6.1}$$

relative to the center of the target. While the shape of the target is known, the orientation, ψ, location (of the center), $\mathbf{x} = [x\ y]^{\mathrm{T}}$, and size, s, are unknown. Fig. 6.1 shows an example.

An assumption is made that the direction of travel of the object is along the orientation, ψ, of the target (i.e. the plane flies forward, not sideways). Furthermore, we assume the target is following a coordinated turn (nearly constant speed and turn rate) motion model. Using these assumptions the turn rate, $\dot{\psi}$, and speed, v, can be estimated using a single scan of data.

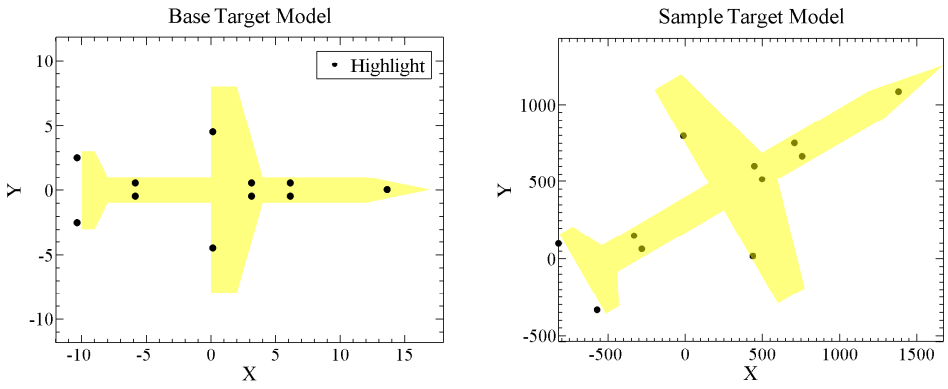

Fig. 6.1: General target template (left), and template scaled by the size $s = 100$, rotated by the orientation $\psi = 30°$, and centered at $[200\ 400]^{\mathrm{T}}$ (right).

6.3.2 Measurement Model

The measurement vector for a single scan of N measurements for time step k is

$$\mathbf{z_{RAW}}_i(k) = \begin{bmatrix} r_m(i,k) \\ \alpha_m(i,k) \\ \dot{r}_m(i,k) \end{bmatrix} \quad i = 1, \ldots, N \tag{6.2}$$

where the measurement vector includes range, r, bearing, α, and range rate, $\dot{r}$.

The measurement error for the raw measurements is assumed to be Gaussian with covariance matrix

$$R_{\mathrm{RAW}} = \begin{bmatrix} \sigma_r^2 & 0 & \rho\sigma_r\sigma_{\dot{r}} \\ 0 & \sigma_\alpha^2 & 0 \\ \rho\sigma_r\sigma_{\dot{r}} & 0 & \sigma_{\dot{r}}^2 \end{bmatrix} \tag{6.3}$$

where σ_r, σ_α, and $\sigma_{\dot{r}}$ are the standard deviations of the range, bearing and range

rate measurement noise. The correlation coefficient between the range and range rate measurement noise is ρ.

6.4 Estimation Approach

An overview of the new approach is shown in Fig. 6.2. First the raw measurements from a single scan are converted to Cartesian coordinates using the approach of [13]. These converted measurements are used in an EM algorithm for a single scan estimate of target position, size, heading, velocity and turn rate. The observed information matrix is calculated and used as a surrogate for the error covariance of this estimate. Finally, an extended Kalman filter with a coordinated turn motion model is used to combine the single scan estimates into a multi-scan estimate of the target state.

6.4.1 Measurement Conversion for an Individual Measurement

It is advantageous to first convert the raw measurements into Cartesian before processing. The raw measurements are converted into measurements of Cartesian position, x and y, and velocity, $\dot{x}$ and $\dot{y}$ using a simplified version of the method described in [13].

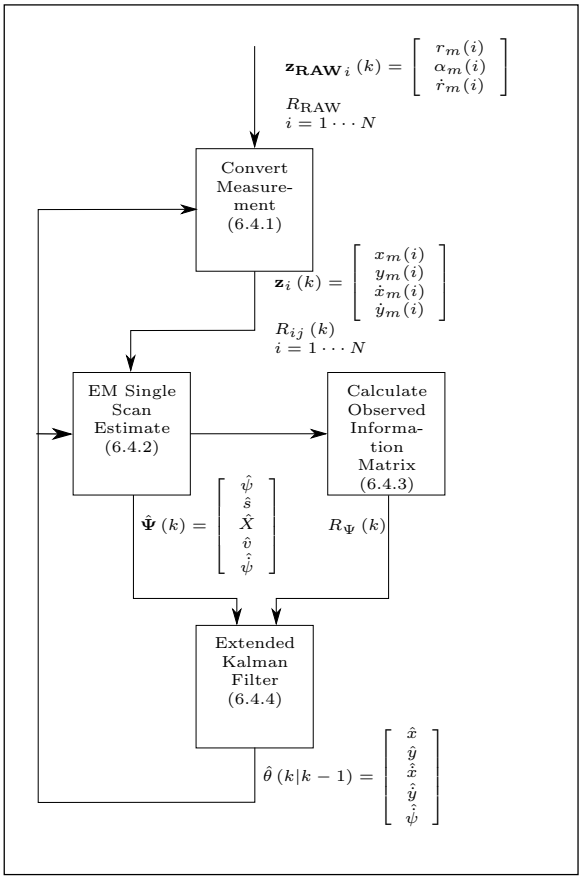

Fig. 6.2: Overview of the extended target tracking approach.

$$\mathbf{z}_i(k) = \begin{bmatrix} x_m(i,k) \\ y_m(i,k) \\ \dot{x}_m(i,k) \\ \dot{y}_m(i,k) \end{bmatrix} \tag{6.4}$$

$$= e^{\sigma_\alpha^2/2} \begin{bmatrix} r_m(i,k)\cos\alpha_m(i,k) \\ r_m(i,k)\sin\alpha_m(i,k) \\ \dot{r}_m(i,k)\cos\alpha_m(i,k) \\ \dot{r}_m(i,k)\sin\alpha_m(i,k) \end{bmatrix} \tag{6.5}$$

The conversion from range rate into Cartesian velocity assumes that the cross range rate is zero and accounts for any error in this assumption by setting the variance in the cross range rate dimension to infinity (or equivalently, setting the inverse to zero). This is implemented using the inverse converted measurement covariance, $R_{ij}(k)^{-1}$, which has a dimension of four by four, but is rank 3.

The converted measurement error covariance, $R_{ij}(k)$, is calculated according to Appendix G.

6.4.2 EM Single Scan Estimate from Multiple Measurements

Likelihood Model

Using the set of N measurements in combination with the target model, a single scan estimate of target position, speed, size and turn rate can be calculated. The

unknown parameters to be estimated form the vector $\mathbf{\Psi}$

$$\mathbf{\Psi} = \left[\mathbf{x}^{\mathrm{T}}\ s\ \psi\ v\ \dot{\psi}\right]^{\mathrm{T}} \tag{6.6}$$

The following probabilistic model is used for the likelihood function of $\mathbf{\Psi}$:

$$p_{\mathbf{z}}\left(\mathbf{z}_i|\mathbf{\Psi}\right) = \sum_{j=1}^{M} \pi_j p_{ij}\left(\mathbf{z}_i|\mathbf{\Psi}\right) \tag{6.7}$$

where, π_j is treated as the prior probability of a measurement originating from reflector j and $p_{\mathbf{z}}$ is the conditional probability density for a single measurement given $\mathbf{\Psi}$. This value is approximated using the probabilities of detection ($\alpha_j, j = 1, \ldots, M$) by assuming each measurement comes from one of the reflectors, namely,

$$\pi_j = \frac{\alpha_j}{\sum_{l=1}^{M} \alpha_l} \tag{6.8}$$

The probability density function (pdf) for a given measurement–to–reflector combination, p_{ij} is given by

$$p_{ij}\left(\mathbf{z}_i|\mathbf{\Psi}\right) = |2\pi R_{ij}|^{-\frac{1}{2}} \exp\left\{-\frac{1}{2}\nu_{ij}\left(\mathbf{\Psi}, \mathbf{z}_i\right)^{\mathrm{T}} R_{ij}^{-1} \nu_{ij}\left(\mathbf{\Psi}, \mathbf{z}_i\right)\right\} \tag{6.9}$$

where $\nu_{ij}\left(\mathbf{\Psi}, \mathbf{z}_i\right)$, the difference between measurement i and reflector j, is

$$\nu_{ij}\left(\mathbf{\Psi}, \mathbf{z}_i\right) = \mathbf{z}_i - \begin{bmatrix} sD\left(\psi\right)\mathbf{t}_j + \mathbf{x} \\ v\cos\psi - s\dot{\psi}|\mathbf{t}_j|\sin\left(\psi + \theta_j\right) \\ v\sin\psi + s\dot{\psi}|\mathbf{t}_j|\cos\left(\psi + \theta_j\right) \end{bmatrix} \tag{6.10}$$

where

$$D(\psi) = \begin{bmatrix} \cos\psi & -\sin\psi \\ \sin\psi & \cos\psi \end{bmatrix} \tag{6.11}$$

is the rotation matrix,

$$|\mathbf{t}_j| = \sqrt{x_t(j)^2 + y_t(j)^2} \tag{6.12}$$

is the distance from reflector j to the target center,

$$\theta_j = \tan^{-1} \frac{y_t(j)}{x_t(j)} \tag{6.13}$$

is the angle of the line from the center to reflector j; relative to the reference direction, and R_{ij} is the converted measurement error covariance matrix (see appendix G).

The term $sD(\psi)\,\mathbf{t}_j + \mathbf{x}$ provides the position of target highlight j, scaled by the size, s, rotated by the heading ψ, and translated by the position of the target center $\mathbf{x}$.

In order to simultaneously estimate target speed (along its heading) and turn rate, the contribution of these terms to the measured instantaneous velocity must be separated. The terms $v\cos\psi$ and $v\sin\psi$ are the contributions of the target center's velocity to measured velocity. The terms $s\dot{\psi}|\mathbf{t}_j|\sin(\psi+\theta_j)$ and $s\dot{\psi}|\mathbf{t}_j|\cos(\psi+\theta_j)$ are the contributions due to turn rate. Fig. 6.3 shows the path of the target on the left. When the motion of the target center is removed (as shown on the right), the motion of the individual highlights due to turn rate is evident.

The incomplete-data log-likelihood of $\mathbf{\Psi}$ based on all the measurements $\mathcal{Z}$ is given by [7]:

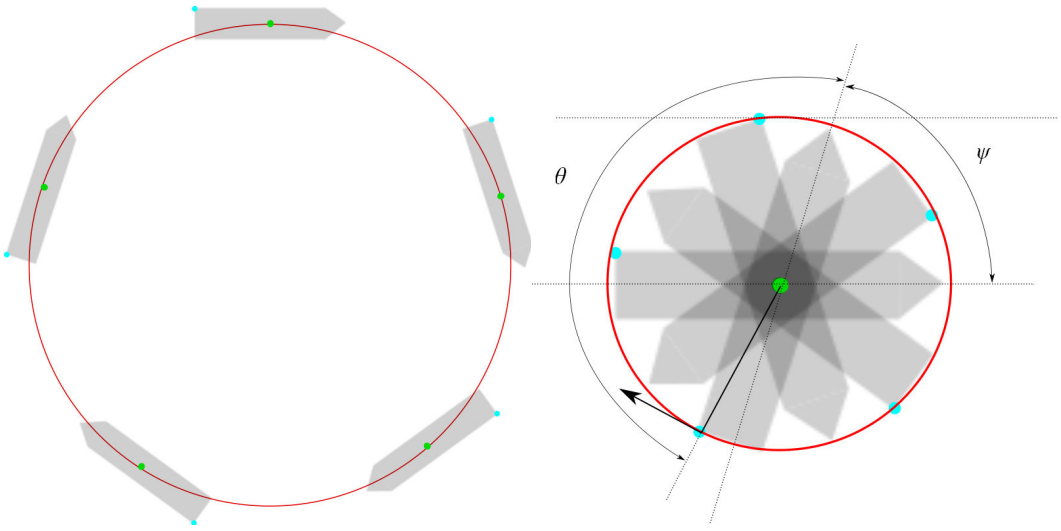

Fig. 6.3: Turn rate contribution to range rate.

$$\begin{aligned}\ln \mathcal{L}\left(\mathbf{\Psi};\mathcal{Z}\right) &= \ln p_{\mathcal{Z}}\left(\mathcal{Z}|\mathbf{\Psi}\right) \\ &= \ln \prod_{i=1}^{N} p_{\mathbf{z}}\left(\mathbf{z}_i|\mathbf{\Psi}\right) \\ &= \sum_{i=1}^{N} \ln\left(\sum_{j=1}^{M} \pi_j p_{ij}\left(\mathbf{z}_i|\mathbf{\Psi},\mathbf{t_j}\right)\right) \end{aligned} \tag{6.14}$$

where $p_{\mathcal{Z}}$ is the conditional probability density of the set of measurements $\mathcal{Z}$, given $\mathbf{\Psi}$. For each measurement, $\mathbf{z}_i$, one has here the summation of its pdf if originated from reflector j and weighted by π_j.

Solving for $\mathbf{\Psi}$

To estimate $\mathbf{\Psi}$, one can find the vector that maximizes (6.14). The difficulty with (6.14) is the log of a sum. However, by recognizing (6.7) as a mixture model, the problem can be approached with the EM algorithm. The inside summation can

be rewritten according to the EM approach using binary multipliers as missing data. The "missing" data are association variables that declare which reflector produced each measurement [42]. These association variables are expressed as binary vectors where each element in the binary vector corresponds to a reflector.

The binary vectors are defined as

$$\mathcal{Y} = \left[\mathbf{y}_1{}^{\mathrm{T}}, \cdots, \mathbf{y}_N{}^{\mathrm{T}}\right]^{\mathrm{T}} \tag{6.15}$$

where $\mathbf{y}_i = [y_{i1}, \ldots, y_{iM}]^{\mathrm{T}}$ is a M-dimensional binary vector (0 or 1), such that y_{ij} is one if measurement i is a reflection from reflector j, and zero otherwise. The complete log-likelihood, based also on $\mathcal{Y}$ is

$$\begin{aligned}
\ln \mathcal{L}_{\mathrm{c}}\left(\mathbf{\Psi}; \mathcal{Z}, \mathcal{Y}\right) &= \ln p_{\mathrm{c}}\left(\mathcal{Z}, \mathcal{Y} | \mathbf{\Psi}\right) \\
&= \sum_{i=1}^{N} \ln \left(\sum_{j=1}^{M} y_{ij} \pi_j p_{ij}\left(\mathbf{z}_i | \mathbf{\Psi}\right) \right) \\
&= \sum_{i=1}^{N} \sum_{j=1}^{M} y_{ij} \ln \left(\pi_j p_{ij}\left(\mathbf{z}_i | \mathbf{\Psi}\right) \right)
\end{aligned} \tag{6.16}$$

where p_{c} is the conditional probability density of the complete data, $\mathcal{Z}$ and $\mathcal{Y}$, given $\mathbf{\Psi}$. If we view the missing data, $\mathcal{Y}$, as random variables, the EM $\mathcal{Q}$ function can now be found. In the EM algorithm, the $\mathcal{Q}$ function is iteratively maximized. This function is the expectation of the complete log-likelihood, with the expectation operation conducted with respect to the unknown data $\mathcal{Y}$, given the observed data, $\mathcal{Z}$, and the estimate of $\mathbf{\Psi}$ from the previous iteration, $\mathbf{\Psi}^{(l)}$, namely,

$$\mathcal{Q}\left(\mathbf{\Psi};\mathbf{\Psi}^{(l)},\mathcal{Z}\right)=E\left\{\ln\mathcal{L}_{\mathrm{c}}\left(\mathbf{\Psi};\mathcal{Z},\mathcal{Y}\right)|\mathcal{Z},\mathbf{\Psi}^{(l)}\right\} \tag{6.17}$$

$$\begin{aligned}\mathcal{Q}\left(\mathbf{\Psi};\mathbf{\Psi}^{(l)},\mathcal{Z}\right)=&\sum_{i=1}^{N}\sum_{j=1}^{M}w_{ij}\left(\mathbf{\Psi}^{(l)},\mathbf{z}_i\right)\ln\left(\pi_j p_{ij}\left(\mathbf{z}_i|\mathbf{\Psi}\right)\right)\\ =&\sum_{i=1}^{N}\sum_{j=1}^{M}w_{ij}\left(\mathbf{\Psi}^{(l)},\mathbf{z}_i\right)\left[\ln(\pi_j)-\frac{1}{2}\ln(|2\pi R_{ij}|)\right.\\ &\left.-\frac{1}{2}\nu_{ij}\left(\mathbf{\Psi},\mathbf{z}_i\right)^{\mathrm{T}}R_{ij}^{-1}\nu_{ij}\left(\mathbf{\Psi},\mathbf{z}_i\right)\right]\end{aligned} \tag{6.18}$$

where w_{ij} is the estimate of the posterior association probabilities y_{ij} given the measurements and the previous estimate $\mathbf{\Psi}^{(l)}$, allowing for more than one measurement to be a reflection from a single reflector. Since this association model allows for more than one measurement to be a reflection from a single reflector, the model is an application of the PMHT association model [48]. The association probabilities are

$$\begin{aligned}w_{ij}\left(\mathbf{\Psi}^{(l)},\mathbf{z}_i\right)=&p_y\left(y_{ij}|\mathbf{z}_i,\mathbf{\Psi}^{(l)}\right)\\ =&\frac{\pi_j p_{ij}\left(\mathbf{z}_i|\mathbf{\Psi}^{(l)}\right)}{\sum_{m=1}^{M}\pi_m p_{im}\left(\mathbf{z}_i|\mathbf{\Psi}^{(l)}\right)}\end{aligned} \tag{6.19}$$

where p_y is the conditional probability of an association pair, given $\mathbf{\Psi}^{(l)}$ and measurement $\mathbf{z}_i$. The w_{ij} calculation given above assumes a clutter free environment. The extension to a cluttered environment is quite straightforward and simply re-

quires an additional clutter distribution term in the denominator of the expression for w_{ij} [48] and the appropriate modification to $\mathcal{Y}$.

For the M step of EM, the $\mathcal{Q}$ function is maximized with respect to $\mathbf{\Psi}$. The $\mathbf{\Psi}$ that maximizes (6.18) can be found by solving

$$\nabla_{\mathbf{\Psi}} \mathcal{Q}\left(\mathbf{\Psi}; \mathbf{\Psi}^{(l)}, \mathcal{Z}\right) = 0 \tag{6.20}$$

to yield $\mathbf{\Psi}^{(l+1)}$, where

$$\begin{aligned}\nabla_{\mathbf{\Psi}} \mathcal{Q}\left(\mathbf{\Psi}; \mathbf{\Psi}^{(l)}, \mathcal{Z}\right) = -\frac{1}{2}\Bigg[\nabla_{\mathbf{\Psi}} \sum_{i=1}^{N}\sum_{j=1}^{M} w_{ij}\left(\mathbf{\Psi}^{(l)}, \mathbf{z}_i\right) \\ \cdot \nu_{ij}\left(\mathbf{\Psi}, \mathbf{z}_i\right)^{\mathrm{T}} R_{ij}^{-1} \nu_{ij}\left(\mathbf{\Psi}, \mathbf{z}_i\right)\Bigg]\end{aligned} \tag{6.21}$$

Since R_{ij}^{-1} is symmetric and using

$$\nabla_{\mathbf{x}}\left\{f(\mathbf{x}^{\mathrm{T}}) A f(\mathbf{x})\right\} = 2\left(\nabla_{\mathbf{x}} f(\mathbf{x})\right)^{\mathrm{T}} A f(\mathbf{x}) \tag{6.22}$$

one can simplify (6.21)

$$\nabla_{\mathbf{\Psi}} \mathcal{Q}\left(\mathbf{\Psi}; \mathbf{\Psi}^{(l)}, \mathcal{Z}\right) = -\sum_{i=1}^{N}\sum_{j=1}^{M} w_{ij}\left(\mathbf{\Psi}^{(l)}, \mathbf{z}_i\right)\left(\nu'_{ij}\left(\mathbf{\Psi}\right)\right)^{\mathrm{T}} R_{ij}^{-1} \nu_{ij}\left(\mathbf{\Psi}, \mathbf{z}_i\right) \tag{6.23}$$

where

$$\nu'_{ij}\left(\mathbf{\Psi}\right) = \nabla_{\mathbf{\Psi}} \nu_{ij}\left(\mathbf{\Psi}, \mathbf{z}_i\right) \tag{6.24}$$

The components of $\nu'_{ij}\left(\mathbf{\Psi}\right)$ are

$$\nu'_{ij}\left(\mathbf{\Psi}\right) = -\begin{bmatrix} 1 & 0 & a_{13} & a_{14} & 0 & 0 \\ 0 & 1 & a_{23} & a_{24} & 0 & 0 \\ 0 & 0 & a_{33} & a_{34} & a_{35} & a_{36} \\ 0 & 0 & a_{34} & a_{44} & a_{45} & a_{46} \end{bmatrix} \tag{6.25}$$

where

$$\begin{bmatrix} a_{13} \\ a_{23} \\ a_{33} \\ a_{34} \end{bmatrix} = \begin{bmatrix} D(\psi)\,\mathbf{t}_j \\ -\dot{\psi}|\mathbf{t}_j|\sin(\psi+\theta_j) \\ \dot{\psi}|\mathbf{t}_j|\cos(\psi+\theta_j) \end{bmatrix} \tag{6.26}$$

$$\begin{bmatrix} a_{14} \\ a_{24} \\ a_{34} \\ a_{44} \end{bmatrix} = \begin{bmatrix} sD'(\psi)\,\mathbf{t}_j \\ -v\sin\psi - s\dot{\psi}|\mathbf{t}_j|\cos(\psi+\theta_j) \\ v\cos\psi - s\dot{\psi}|\mathbf{t}_j|\sin(\psi+\theta_j) \end{bmatrix} \tag{6.27}$$

$$\begin{bmatrix} a_{35} \\ a_{45} \end{bmatrix} = \begin{bmatrix} \cos\psi \\ \sin\psi \end{bmatrix} \tag{6.28}$$

$$\begin{bmatrix} a_{36} \\ a_{46} \end{bmatrix} = \begin{bmatrix} -s|\mathbf{t}_j|\sin(\psi+\theta_j) \\ s|\mathbf{t}_j|\cos(\psi+\theta_j) \end{bmatrix} \tag{6.29}$$

and

$$D'(\psi) = \begin{bmatrix} -\sin\psi & -\cos\psi \\ \cos\psi & -\sin\psi \end{bmatrix} \tag{6.30}$$

Since (6.20) cannot be solved directly, a first order Taylor expansion is used to find $\mathbf{\Psi}^{(l+1)}$, the maximizing $\mathbf{\Psi}$, given $\mathbf{\Psi}^{(l)}$, namely,

$$\begin{aligned} &\sum_{i=1}^{N}\sum_{j=1}^{M} w_{ij}\left(\mathbf{\Psi}^{(l)},\mathbf{z}_i\right)\nu'_{ij}\left(\mathbf{\Psi}\right)^{\mathrm{T}} R_{ij}^{-1} \\ &\cdot\left[\nu_{ij}\left(\mathbf{\Psi},\mathbf{z}_i\right)+\nu'_{ij}\left(\mathbf{\Psi}\right)\left(\mathbf{\Psi}^{(l+1)}-\mathbf{\Psi}^{(l)}\right)\right]=0 \end{aligned} \tag{6.31}$$

which leads to

$$\begin{aligned}\boldsymbol{\Psi}^{(l+1)} = \boldsymbol{\Psi}^{(l)} & \\ + \left(\sum_{i=1}^{N} \sum_{j=1}^{M} w_{ij} \left(\boldsymbol{\Psi}^{(l)}, \mathbf{z}_i \right) \nu'_{ij} \left(\boldsymbol{\Psi} \right)^{\mathrm{T}} R_{ij}^{-1} \nu'_{ij} \left(\boldsymbol{\Psi} \right) \right)^{-1} & \\ \cdot \left(\sum_{i=1}^{N} \sum_{j=1}^{M} w_{ij} \left(\boldsymbol{\Psi}^{(l)}, \mathbf{z}_i \right) \nu'_{ij} \left(\boldsymbol{\Psi} \right)^{\mathrm{T}} R_{ij}^{-1} \nu_{ij} \left(\boldsymbol{\Psi}, \mathbf{z}_i \right) \right) \Bigg|_{\boldsymbol{\Psi}^{(l)}} & \end{aligned} \tag{6.32}$$

The resulting EM algorithm is defined as follows:

1. Initialize $\boldsymbol{\Psi}^{(l)}$

2. Calculate w using (6.19)

3. Solve for $\boldsymbol{\Psi}^{(l+1)}$ using (6.32).

4. Iteratively repeat steps 2 and 3 until a convergence criterion is met (e.g. when the increase in the complete log-likelihood is below a threshold).

5. Set $\hat{\boldsymbol{\Psi}}(k) = \boldsymbol{\Psi}^{(L)}$ at the last iteration, $l = L$.

6.4.3 Observed Information Matrix

In order to provide a measure of uncertainty for the estimate $\hat{\boldsymbol{\Psi}}$, critical information for tracking, the observed information matrix is used as a surrogate for the inverse covariance matrix. Oakes' formula [46] for the observed information matrix is used (see Appendix H).

$$-\nabla_{\mathbf{\Psi}}\nabla_{\mathbf{\Psi}}^{\mathrm{T}}\ln\mathcal{L}\left(\mathbf{\Psi};\mathcal{Z}\right)=-\left[\nabla_{\mathbf{\Psi}}\nabla_{\mathbf{\Psi}}^{\mathrm{T}}\mathcal{Q}\left(\mathbf{\Psi};\mathbf{\Psi}^{(L)},\mathcal{Z}\right)\right.$$
$$\left.+\nabla_{\mathbf{\Psi}}\nabla_{\mathbf{\Psi}^{(L)}}^{\mathrm{T}}\mathcal{Q}\left(\mathbf{\Psi};\mathbf{\Psi}^{(L)},\mathcal{Z}\right)\right] \tag{6.33}$$

Evaluating (6.33) using $\mathbf{\Psi}=\mathbf{\Psi}^{(L)}$ results in the "observed information matrix", $I\left(\hat{\mathbf{\Psi}};\mathcal{Z}\right)$ [42].

The first term on the right hand side of (6.33) is the observed information if the associations were known, $I_{\mathbf{c}}\left(\hat{\mathbf{\Psi}};\mathcal{Z}\right)$:

$$I_{\mathbf{c}}\left(\hat{\mathbf{\Psi}};\mathcal{Z}\right)=-\nabla_{\mathbf{\Psi}}\nabla_{\mathbf{\Psi}}^{\mathrm{T}}\mathcal{Q}\left(\mathbf{\Psi};\mathbf{\Psi}^{(l)},\mathcal{Z}\right) \tag{6.34}$$
$$=-\sum_{i=1}^{N}\sum_{j=1}^{M}w_{ij}\left(\mathbf{\Psi}^{(l)},\mathbf{z}_i\right)$$
$$\cdot\left[\left(\nu_{ij}'\left(\mathbf{\Psi}\right)\right)^{\mathrm{T}}R_{ij}^{-1}\nu_{ij}'\left(\mathbf{\Psi}\right)+B_{ij}\left(\mathbf{\Psi},\mathbf{z}_i\right)\right] \tag{6.35}$$

where the B matrix is based on the second derivative of ν,

$$B_{ij}\left(\mathbf{\Psi},\mathbf{z}_i\right)=-\begin{bmatrix}0&0&0&0&0&0\\0&0&0&0&0&0\\0&0&0&b_{34}&0&b_{36}\\0&0&b_{34}&b_{44}&b_{45}&b_{46}\\0&0&0&b_{45}&0&0\\0&0&b_{36}&b_{46}&0&0\end{bmatrix} \tag{6.36}$$

with components:

$$b_{34} = \begin{bmatrix} D'(\psi)\,\mathbf{t}_j \\ -\dot{\psi}|\mathbf{t}_j|\cos(\psi+\theta_j) \\ -\dot{\psi}|\mathbf{t}_j|\sin(\psi+\theta_j) \end{bmatrix}^{\mathrm{T}} R_{ij}^{-1}\nu_{ij}(\mathbf{\Psi},\mathbf{z}_i) \tag{6.37}$$

$$b_{36} = \begin{bmatrix} 0 \\ 0 \\ -|\mathbf{t}_j|\sin(\psi+\theta_j) \\ |\mathbf{t}_j|\cos(\psi+\theta_j) \end{bmatrix}^{\mathrm{T}} R_{ij}^{-1}\nu_{ij}(\mathbf{\Psi},\mathbf{z}_i) \tag{6.38}$$

$$b_{44} = \begin{bmatrix} -sD(\psi)\,\mathbf{t}_j \\ -v\cos\psi + s\dot{\psi}|\mathbf{t}_j|\sin(\psi+\theta_j) \\ -v\sin\psi - s\dot{\psi}|\mathbf{t}_j|\cos(\psi+\theta_j) \end{bmatrix}^{\mathrm{T}} R_{ij}^{-1}\nu_{ij}(\mathbf{\Psi},\mathbf{z}_i) \tag{6.39}$$

$$b_{45} = \begin{bmatrix} 0 \\ 0 \\ -\sin\psi \\ \cos\psi \end{bmatrix}^{\mathrm{T}} R_{ij}^{-1}\nu_{ij}(\mathbf{\Psi},\mathbf{z}_i) \tag{6.40}$$

$$b_{46} = \begin{bmatrix} 0 \\ 0 \\ -s|\mathbf{t}_j|\cos(\psi+\theta_j) \\ -s|\mathbf{t}_j|\sin(\psi+\theta_j) \end{bmatrix}^{\mathrm{T}} R_{ij}^{-1}\nu_{ij}(\mathbf{\Psi},\mathbf{z}_i) \tag{6.41}$$

The second term on the right hand side of (6.33) accounts for the association

uncertainty, $I_{\mathbf{m}}\left(\hat{\mathbf{\Psi}};\mathcal{Z}\right)$. This is found by taking the derivative of $\mathcal{Q}$ with respect to $\mathbf{\Psi}$, and taking the derivative with respect to ${\mathbf{\Psi}^{(L)}}^{\mathrm{T}}$, i.e.

$$\begin{aligned} I_{\mathbf{m}}\left(\hat{\mathbf{\Psi}};\mathcal{Z}\right) &= -\nabla_{\mathbf{\Psi}}\nabla^{\mathrm{T}}_{\mathbf{\Psi}^{(L)}}\mathcal{Q}\left(\mathbf{\Psi};\mathbf{\Psi}^{(L)},\mathcal{Z}\right) \\ &= -\sum_{i=1}^{N}\sum_{j=1}^{M} w'_{ij}\left(\mathbf{\Psi}^{(L)},\mathbf{z}_i\right) \\ &\quad \cdot\left(\nu'_{ij}\left(\mathbf{\Psi}\right)\right)^{\mathrm{T}} R_{ij}^{-1}\nu_{ij}\left(\mathbf{\Psi},\mathbf{z}_i\right) \end{aligned} \tag{6.42}$$

where w' is the derivative of (6.19)

$$\begin{aligned} w'_{ij}\left(\mathbf{\Psi}^{(L)},\mathbf{z}_i\right) = \pi_j p_{ij}\left(\mathbf{z}_i|\mathbf{\Psi}^{(L)}\right) & \\ \left\{\left(\sum_{m=1}^{M}\pi_m p_{im}\left(\mathbf{z}_i|\mathbf{\Psi}^{(L)}\right)\right)^{-2}\right. & \\ \cdot\sum_{m=1}^{M}\left[\pi_m p_{im}\left(\mathbf{z}_i|\mathbf{\Psi}^{(L)}\right)\right. & \\ \left.\cdot\left(\nu'_{im}\left(\mathbf{\Psi}^{(L)}\right)\right)^{\mathrm{T}} R_{im}^{-1}\nu_{im}\left(\mathbf{\Psi}^{(L)},\mathbf{z}_i\right)\right] & \\ \left.-\frac{\left(\nu'_{ij}\left(\mathbf{\Psi}^{(L)}\right)\right)^{\mathrm{T}} R_{ij}^{-1}\nu_{ij}\left(\mathbf{\Psi}^{(L)},\mathbf{z}_i\right)}{\sum_{m=1}^{M}\pi_m p_{im}\left(\mathbf{z}_i|\mathbf{\Psi}^{(L)}\right)}\right\} & \end{aligned} \tag{6.43}$$

6.4.4 Extended Kalman Filter for Multi-Scan Estimation

The single scan estimate of the target state can be used in an EKF to provide multi-scan estimates. The EKF for a coordinated turn motion model is well known for the case of position only measurements (pp. 466-170 of [3]). The state vector for the CT-EKF is

$$\hat{\theta} = \left[x_{\hat{\theta}}\ \ \dot{x}_{\hat{\theta}}\ \ y_{\hat{\theta}}\ \ \dot{y}_{\hat{\theta}}\ \ \dot{\psi}_{\hat{\theta}}\right]^{\mathrm{T}} \tag{6.44}$$

Note that the subscript $\hat{\theta}$ is used to avoid confusion between the elements of $\hat{\theta}$ and $\mathbf{\Psi}$.

The dynamic equation is

$$\theta(k+1) = f[k, \theta(k)] + \Gamma(k)\upsilon(k) \tag{6.45}$$

and the state prediction is:

$$\hat{\theta}(k+1|k) = f\left[k, \hat{\theta}(k|k)\right] \tag{6.46}$$

where

$$f\left[k, \hat{\theta}(k|k)\right] = \begin{bmatrix} 1 & \frac{\sin\left(\dot{\psi}_{\hat{\theta}}(k)T\right)}{\dot{\psi}_{\hat{\theta}}(k)} & 0 & -\frac{1-\cos\left(\dot{\psi}_{\hat{\theta}}(k)T\right)}{\dot{\psi}_{\hat{\theta}}(k)} & 0 \\ 0 & \cos\left(\dot{\psi}_{\hat{\theta}}(k)T\right) & 0 & -\sin\left(\dot{\psi}_{\hat{\theta}}(k)T\right) & 0 \\ 0 & \frac{1-\cos\left(\dot{\psi}_{\hat{\theta}}(k)T\right)}{\dot{\psi}_{\hat{\theta}}(k)} & 1 & \frac{\sin\left(\dot{\psi}_{\hat{\theta}}(k)T\right)}{\dot{\psi}_{\hat{\theta}}(k)} & 0 \\ 0 & \sin\left(\dot{\psi}_{\hat{\theta}}(k)T\right) & 0 & \cos\left(\dot{\psi}_{\hat{\theta}}(k)T\right) & 0 \\ 0 & 0 & 0 & 0 & 1 \end{bmatrix} \hat{\theta}(k|k) \tag{6.47}$$

and

$$\Gamma(k) = \begin{bmatrix} \frac{1}{2}T^2 & 0 & 0 \\ T & 0 & 0 \\ 0 & \frac{1}{2}T^2 & 0 \\ 0 & T & 0 \\ 0 & 0 & T \end{bmatrix} \tag{6.48}$$

The state prediction covariance is:

$$P(k+1|k) = F(k)P(k|k)F(k)^{\mathrm{T}} + \Gamma(k)Q(k)\Gamma(k)^{\mathrm{T}} \tag{6.49}$$

where Q is the covariance of the process noise, υ, and

$$F(k) = \left.\frac{\partial f(k)}{\partial \theta}\right|_{\theta=\hat{\theta}(k+1|k)} \tag{6.50}$$

Two modifications to the CT-EKF in [3] are necessary for this application. This first is in the observation function. Using the single scan estimate, $\hat{\mathbf{\Psi}}$, as the observation, the full state vector can be observed, thus eliminating the need for an observation matrix (commonly referred to as the H matrix, i.e., here H is the identity matrix). The single scan observation, $\mathbf{z}_{\mathrm{C}}$ and the inverse observation error covariance, ${R_{\mathrm{C}}}^{-1}$, are:

$$\mathbf{z}_{\mathrm{C}}(k) = \begin{bmatrix} 1 & 0 & 0 & 0 & 0 & 0 \\ 0 & 0 & 0 & 0 & \cos\psi & 0 \\ 0 & 1 & 0 & 0 & 0 & 0 \\ 0 & 0 & 0 & 0 & \sin\psi & 0 \\ 0 & 0 & 0 & 0 & 0 & 1 \end{bmatrix} \mathbf{\Psi}(k) \tag{6.51}$$

$$R_{\mathrm{C}}(k)^{-1} = \left(A^{-1}\right)^{\mathrm{T}} I\left(\hat{\mathbf{\Psi}}; \mathcal{Z}\right) A^{-1} \tag{6.52}$$

where $I\left(\hat{\mathbf{\Psi}}; \mathcal{Z}\right)$ was defined following (6.33).

$$A = \begin{bmatrix} 1 & 0 & 0 & 0 & 0 & 0 \\ 0 & 0 & 0 & 0 & -\sin\psi & 0 \\ 0 & 1 & 0 & 0 & 0 & 0 \\ 0 & 0 & 0 & 0 & \cos\psi & 0 \\ 0 & 0 & 0 & 0 & 0 & 1 \end{bmatrix} \tag{6.53}$$

A second modification is required since ${R_{\mathrm{C}}}^{-1}$ is not necessarily invertible. The inverse error covariance matrices for the individual measurements, ${R_{ij}}^{-1}$, are not invertible due to the fact that the information related to cross range velocity is zero (it has a zero eigenvalue in the cross range rate direction). Although, ${R_{\mathrm{C}}}^{-1}$ will be invertible for most scans, it is not invertible if the target aspect is 90°, or if there is only one measurement in the scan. To allow for this possibility, the information form of the EKF is utilized. The EKF update is:

$$W(k+1) = \left[P(k+1|k)^{-1} + R_{\mathrm{C}}(k+1)^{-1}\right]^{-1} R_{\mathrm{C}}(k+1)^{-1} \quad (6.54)$$

$$P(k+1|k+1) = \left[P(k+1|k)^{-1} + R_{\mathrm{C}}(k+1|k)^{-1}\right]^{-1} \quad (6.55)$$

$$\hat{\theta}(k+1|k+1) = \hat{\theta}(k+1|k) + W(k+1)\left[\mathbf{z}_{\mathrm{C}}(k) - \hat{\theta}(k+1|k)\right] \quad (6.56)$$

6.5 Implementation and Results

6.5.1 Implementation

EM Initialization

As with any optimization approach, care must be taken when employing the algorithm during initialization to avoid convergence to a local maximum. The initialization approach chosen here is as follows.

The initial value for $\mathbf{x}^{(\mathbf{0})}$ is simply the mean of all the position measurements. The initial value for size, $s^{(0)}$, is set to the ratio of the average distance from the measurement to $\mathbf{x}^{(\mathbf{0})}$ and the average distance of the target highlight, $\mathbf{t}$, to the

target center. The initial value for heading, $\psi^{(0)}$, is calculated by finding the covariance of the position measurements and estimating the heading based on the largest eigenvector. The initial speed and turn rate are set to 0.

A particular concern for local maximums for many target models is one at a heading of 180 degrees from the true heading. To avoid maximizing at this incorrect heading, the algorithm is optimized using two initial headings, 180 degrees apart, and the result with the highest likelihood is used.

Even with proper initialization, converging to a local instead of global maximum is a concern. To help, the R matrix is artificially inflated for the first few iterations of the algorithm. This tends to smooth the likelihood surface. Optimization on the augmented surface first reduces the probability of converging to a local maximum. This approach is related to the deterministic annealing EM algorithm [51].

Limitations

It is important to note the limitations of the algorithm in its ability to estimate velocity and turn rate. Regardless of the target model, the ability to estimate velocity from range rate measurements will be limited when the target is traveling across the line of sight from the sensor. Turn rate estimation will also be limited for targets that do not have significant width when the target is traveling directly towards or away from the sensor. To analyze these effects the Cramer-Rao low

bound (CRLB) is examined for two target types. Evident in (6.33) is that the CRLB is a function of the measurements. A looser bound is used here that is calculated using the expected measurement:

$$J = -\sum_{i=1}^{N}\sum_{j=1}^{M} w_{ij}\left(\mathbf{\Psi}^{(L)}, \mathbf{z}_i\right)\left[\left(\nu'_{ij}\left(\mathbf{\Psi}\right)\right)^{\mathrm{T}} R_{ij}^{-1}\nu'_{ij}\left(\mathbf{\Psi}\right)\right] \tag{6.57}$$

The bound provides a lower bound on the average square error, but is looser than the CRLB due to the fact that is does not consider assignment uncertainty Nevertheless, this bound is sufficient to demonstrate the limitations in the algorithm at various aspect angles. For this test the heading was varied from -180 to 180 degrees, the probability of detection was set to 1, the size was set to 70 m, position set to $[10\ 0]'$ km, the speed set 120 m/s and the turn-rate set to 3 deg/sec. The measurement error covariance was set as follows:

1. $\sigma_r = 2$ m
2. $\sigma_{\dot{r}} = 1$ m/s
3. $\sigma_\alpha = 0.05$ deg
4. $\rho\sigma_r\sigma_{\dot{r}} = 0$

As seen from Figure 6.4, if the target has width then turn-rate and speed can be estimated at all aspects with the exception of +/-90 degrees. In the case of a line-like target, such as target 2 in Figure 6.4, speed can be estimated at all

aspects with the exception of aspects near +/-90 degrees, while turn-rate cannot be estimated at +/-90 degrees and near 0 or 180 degrees.

Implementation Details

There are three notable implementation details that are required for robust performance of the algorithm. The first is dealing with the inability to estimate velocity when the target aspect is near 90 deg. Since the true error covariance of the single scan estimate is unknown, the observed information matrix serves as a surrogate. When the true target aspect is 90 deg, while the observed aspect is near 90, the observed information matrix will be overconfident in the velocity estimate. To avoid this, when the estimated aspect, based on $\hat{\theta}(k+1|k)$, is near 90 degrees, the velocity estimate should not be used. This is achieved by setting the appropriate rows and columns of $R_{\mathrm{C}}(k)^{-1}$ to zero. (For targets with little or no width, a similar test is required for turn-rate estimation at aspects near 0 or 180 deg.)

Since the EM algorithm may converge on a local maximum, gating is used to validate the single scan estimate based on the innovation in the EKF update. If the innovation for either the velocity or turn-rate is too large, only the position portion of the single scan estimate is used. Again, this is achieved by setting the appropriate rows and columns of $R_{\mathrm{C}}(k)^{-1}$ to zero.

Finally, when the observed target aspect is near 90 deg, components of

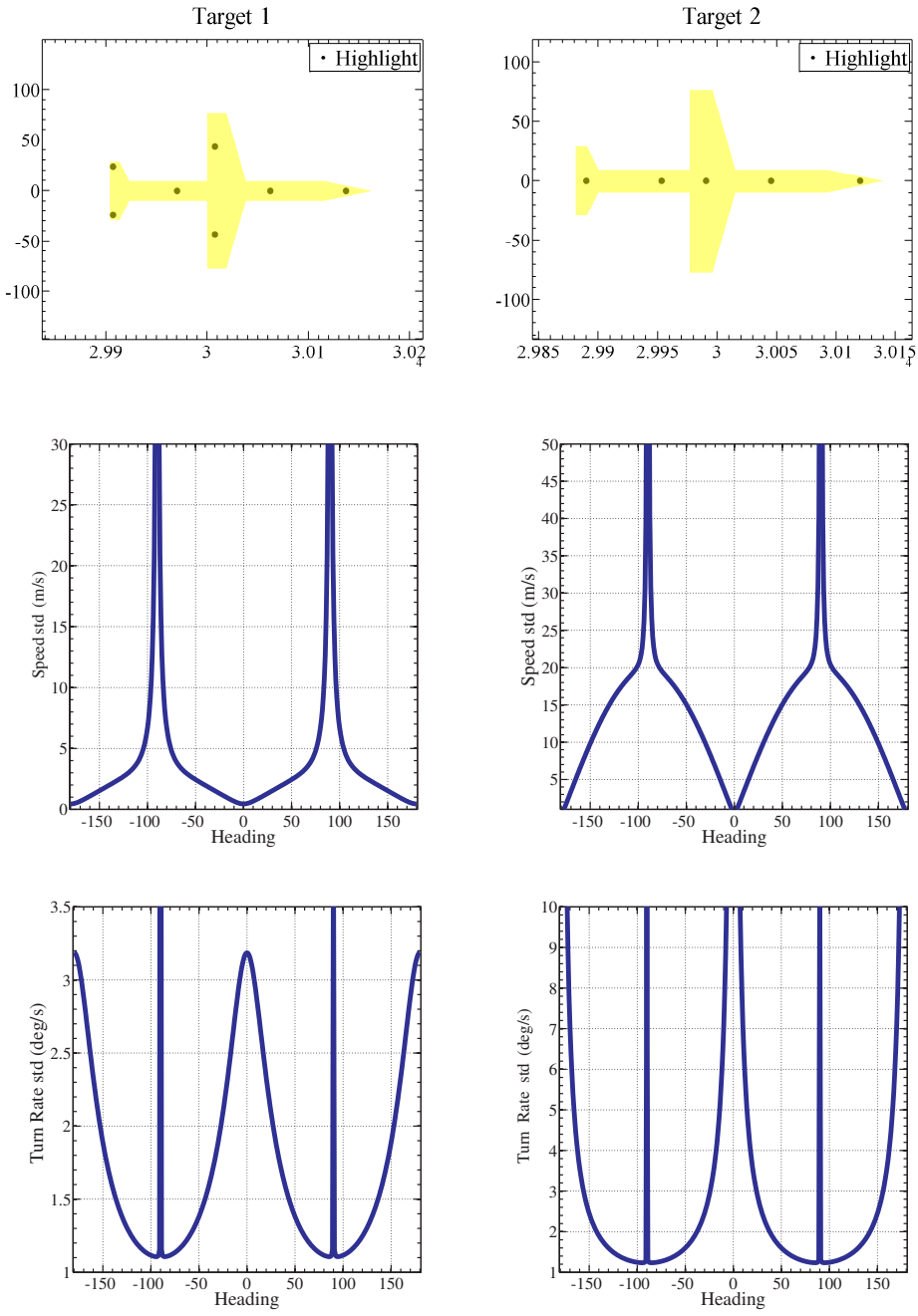

Fig. 6.4: CRLB analysis (using 6.57) for a target that has width (target 1) and one without width (target 2).

$R_{\mathrm{C}}(k)^{-1}$ may be close to zero, resulting in a badly conditioned matrix. In these cases, only the position portion of the single scan estimate is used.

6.5.2 Results

The new algorithm was tested in a aircraft tracking application. The target template is based on a commercial airliner (see Fig. 6.5), with probability of detections for the highlights at 0.8 and 0.9. The aircraft follows the path shown in Fig. 6.6. The measurement error covariance was set the same as Section 6.5.1. The EKF is implemented assuming the following process noise:

$$Q = \begin{bmatrix} (0.25)^2 & 0 & 0 \\ 0 & (0.25)^2 & 0 \\ 0 & 0 & (0.6\frac{\pi}{180})^2 \end{bmatrix} \tag{6.58}$$

Fig. 6.7 shows the average normalized estimation error squared (ANEES) [3] and mean square error for position, velocity and turn rate. Errors are shown for the state update ($\mathbf{x}(k|k)$) and the state prediction ($\mathbf{x}(k|k-1)$) for the algorithm (EXTGTEKF). For comparison, a simple position-only cluster tracker (CLUSTEREKF), using the same EKF with the appropriate observation matrix, is shown (see Appendix I). The proposed algorithm exhibits better consistency (ANEES closer to 1) and, in general, improved mean square error (MSE). Unlike the CLUSTEREKF algorithm, the EXTGTEKF does not lag in the turn-rate estimate since turn-rate is measured directly. The turn rate estimate for the

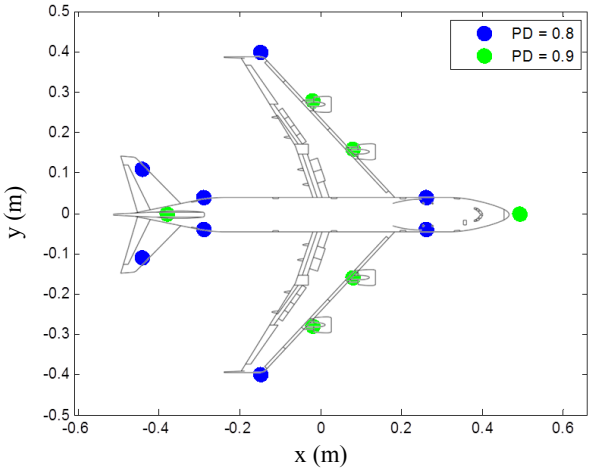

Fig. 6.5: Target template

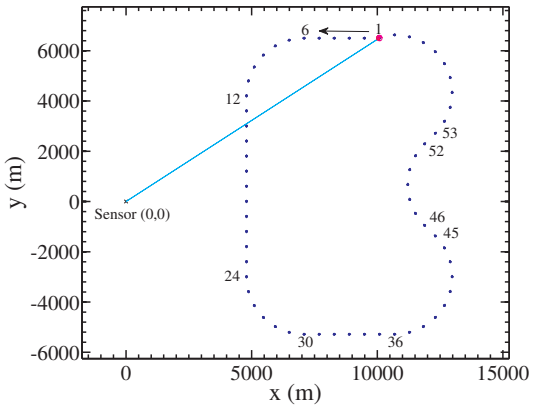

Fig. 6.6: Target path for the test case. The position of the target at each scan is shown. The first scan, as well as any scan that is starting a maneuver is labeled. The sensor position is at the origin. The line-of-sight for the first scan is also shown.

EXTGTEKF is significantly better when the turn initiates, but it worse in steady state. This is due to the fact that the turn rate estimate for the CLUSTEREKF requires three position measurements, resulting in a smoother estimate. It is a trade-off between lag and smoothing.

Since the measurements are quite accurate, the MSE of $\mathbf{x}(k|k)$ is very good for both trackers, while the EXTGTEKF demonstrates improved state prediction MSE performance (see Fig. 6.8). Performance of the EXTGTEKF is, as expected, degraded for target aspects near 90 deg., as the EXTGTEKF reverts to position only measurements during those periods.

6.6 Conclusion

A novel approach to extended object tracking has been presented. A target model has been developed for the target spatial characteristics that is appropriate for estimation, flexible enough to handle various target types, and loose enough such that detailed knowledge of the target characteristics is not required. By restricting the spatial characteristics to be fixed with respect to the line of motion, the resulting algorithm allows for single scan estimation of position, heading, size, velocity and turn rate by using measurements of position and range rate. These single scan measurements when used in a multi-scan tracking algorithm (i.e. extended Kalman filter) provide improved estimates of target position, velocity and turn rate compared to a traditional cluster tracker using only position measurements.

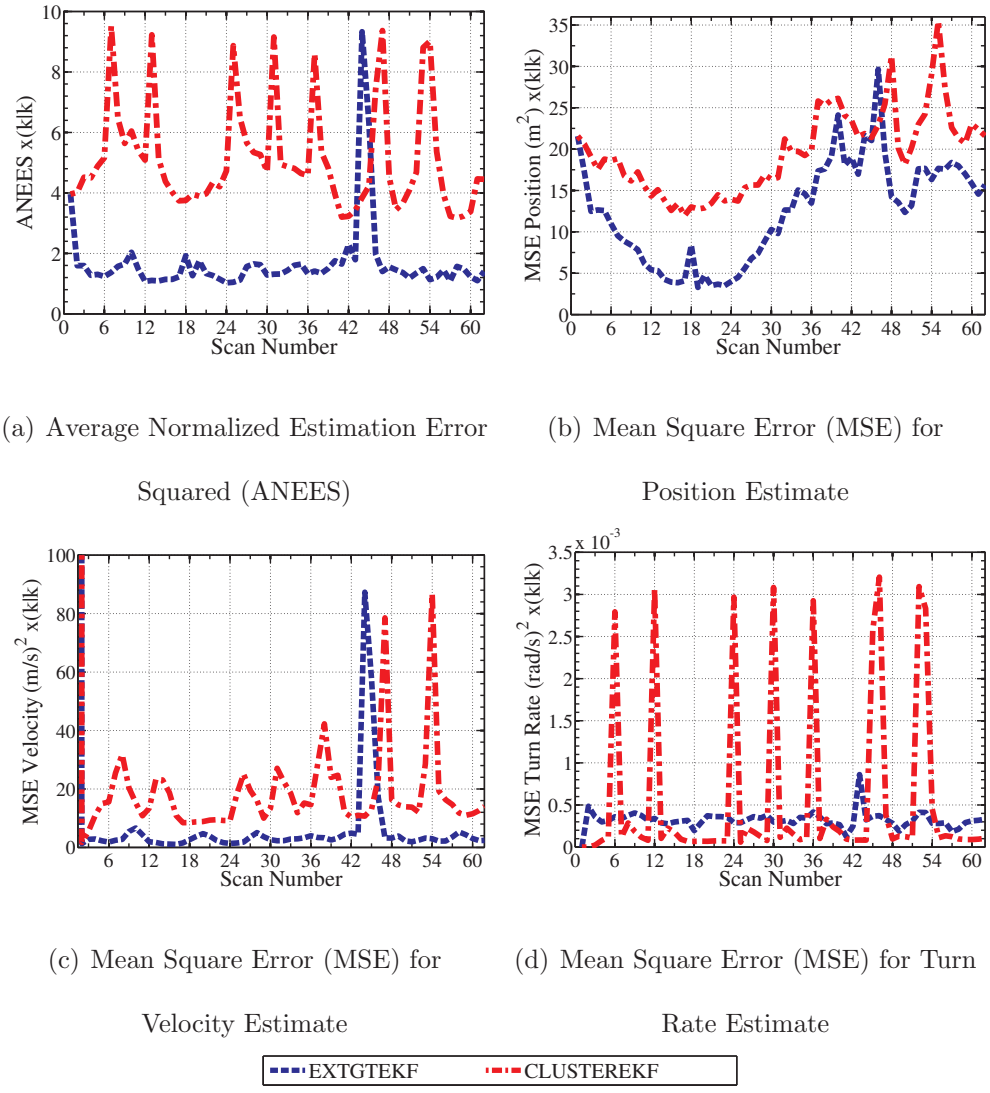

(a) Average Normalized Estimation Error Squared (ANEES)

(b) Mean Square Error (MSE) for Position Estimate

(c) Mean Square Error (MSE) for Velocity Estimate

(d) Mean Square Error (MSE) for Turn Rate Estimate

Fig. 6.7: Results of a 500 run Monte Carlo evaluation of the estimated state for the new EXTGTEKF and a position-only cluster tracker (CLUSTEREKF).

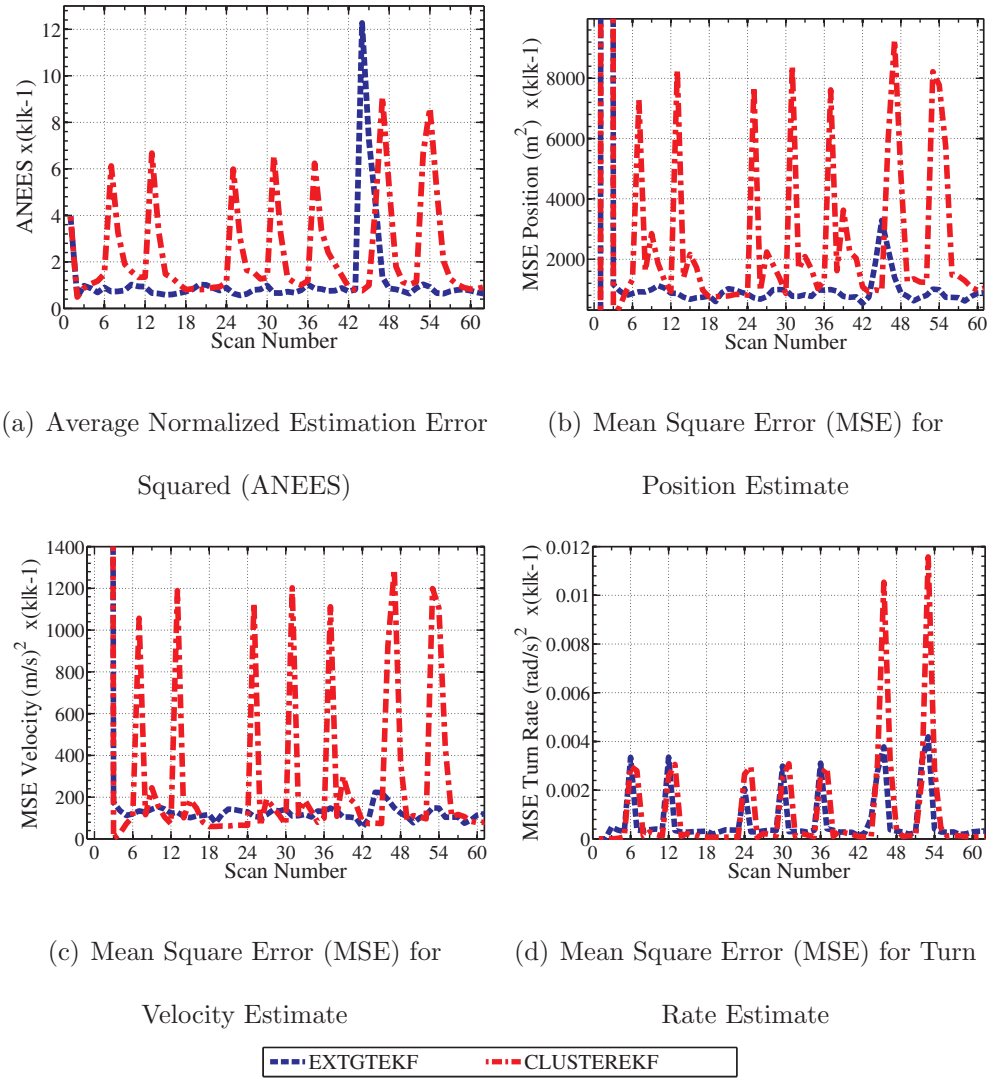

(a) Average Normalized Estimation Error Squared (ANEES)

(b) Mean Square Error (MSE) for Position Estimate

(c) Mean Square Error (MSE) for Velocity Estimate

(d) Mean Square Error (MSE) for Turn Rate Estimate

Fig. 6.8: Results of a 500 run Monte Carlo evaluation of the predicted state for the new EXTGTEKF and a position-only cluster tracker (CLUSTEREKF).

A primary advantage is that the new method, unlike methods using only position measurements, does not suffer from a lag in the estimation of turn rate and the resulting estimation errors.

Chapter 7

Conclusion

7.1 Conclusion

For tracking problems in which the measurements are a nonlinear function of the state, mixed coordinate filters have been a common solution. Popular implementations, such as the EKF, UKF and CKF, perform well in some situations, but may not be acceptable in terms of mean square error or tracker consistency in others. Converted measurement Kalman filters have shown improved performance over mixed coordinate filters in the specific cases of polar and spherical measurements, but have not been widely adopted in other scenarios. The primary contributions of this thesis are (1) the reformulation of the converted measurement Kalman filter to avoid estimation bias and conversion bias, and (2) the extension of the converted measurement Kalman filter to numerous tracking scenarios.

The initial work of [39] lead to numerous efforts related to the converted measurement Kalman filter for polar and spherical measurements. While [39] addressed the problem of conversion bias, this work and its successors did not ad-

dress the problem of estimation bias. Estimation bias, a term coined during this research, comes about due to the practical issue that the calculation of the converted measurement error covariance requires the true target position, that is not available in practice. Previously proposed practical resolutions to this problem evaluated the covariance at the measurement. This results in correlation between the measurement error covariance estimate and the measurement error itself, leading to an estimation bias when the converted measurement is used in tracking. This research resolves the estimation bias issue by evaluating the converted measurement error covariance at the one step prediction. The resulting filter exhibits improved mean square error and consistency performance when applied to tracking in Cartesian coordinates with polar (or spherical) measurements.

The resulting filter was then applied to various tracking scenarios, expanding the potential use of the filter well beyond polar measurements. The technique was examined for the problem of range rate estimation from a moving platform. As in the polar measurement case, the converted measurement formulation for this problem is natural and the bias and converted measurement error covariance can be derived. The method was then used to address the problem of tracking with polar (or spherical) measurements with the addition of a range rate measurement. In this case the conversion is less obvious and requires the inclusion of a non-informative measurement. The method was further extended to tracking with bi-static measurements. In this case the development of the conversion requires

numerical integration. The result is the development of a new converted measurement sigma point Kalman filter. The final extension of the method was for the case of extended target tracking. This explored the case where the measurement conversion process requires an iterative approach. The iterative approach used was the expectation-maximization (EM) algorithm using the probabilistic multi-hypothesis tracker (PMHT) association model.

The result of the research conducted in this thesis is an advancement in the state-of-the-art in nonlinear tracking by providing significant contributions in converted measurement tracking. By developing and evaluating new converted measurement tracking techniques for a wide range of tracking problems, the resulting research has the potential to provide a benefit to many commercial and military systems. By developing conversion techniques for cases where (1) the bias and converted measurement error covariance can be derived; (2) the bias and converted measurement error covariance can be derived with the addition of a non-informative measurement; (3) the bias and converted measurement error covariance must be evaluated using numerical integration and (4) the bias and converted measurement error covariance must be evaluated using iterative maximization, the flexibility and utility of the new converted measurement approach has been demonstrated.

Appendix A

Development of Measurement Error Covariance Evaluated at the Prediction

The R^{11}_{DUCM} term is derived below. The remaining terms can be derived in a similar manner.

$$R^{11}_{\text{DUCM}} = E\{[r_{true}cos\,(\alpha_{true}) - e^{\sigma_\alpha^2/2} r_m cos\,(\alpha_m)]^2\} \tag{A.1}$$

Since the true range and bearing are not available in practice, the estimated range, r_t and bearing, α_t are used. Assuming the estimate errors in range and bearing, w_{r_t} and w_{α_t}, as well as the measurement errors, w_r and w_α, are uncorrelated, zero mean, and Gaussian with standard deviations of σ_{r_t}, σ_{α_t}, σ_r and σ_α, the following assertions can be made

$$\begin{aligned} r_t &= r_{true} + w_{r_t} \qquad & r_m &= r_{true} + w_r \\ \alpha_t &= \alpha_{true} + w_{\alpha_t} \qquad & \alpha_m &= \alpha_{true} + w_\alpha \end{aligned} \tag{A.2}$$

Substituting (A.2) into (A.1),

$$R^{11}_{\text{DUCM}} = E\{[(r_t - w_{r_t})\, cos\,(\alpha_t - w_{\alpha_t}) \\ -e^{\sigma^2_\alpha/2}\,(r_t - w_{r_t} + w_r)\, cos\,(\alpha_t - w_{\alpha_t} + w_\alpha)]^2\} \tag{A.3}$$

Taking the expectation of (A.3) gives the expression in (2.22).

Appendix B

Sequential Processing of Position and Range Rate

In order to process position and range rate based measurements sequentially, the range rate based measurement, η_m^{pseudo} or η_m^{raw}, must first be decorrelated from the position components of the measurement. This is achieved as follows. The covariance matrix of the converted measurement error can be partitioned into the position and pseudo range rate blocks [21]

$$R_{\text{CONV}} = \begin{bmatrix} R^{pp} & R^{p\eta} \\ R^{\eta p} & R^{\eta\eta} \end{bmatrix} \tag{B.1}$$

where

$$R^{pp} = \begin{bmatrix} R^{xx} & R^{xy} \\ R^{yx} & R^{yy} \end{bmatrix} \tag{B.2}$$

and

$$R^{\eta p} = \begin{bmatrix} R^{x\eta} & R^{y\eta} \end{bmatrix} \tag{B.3}$$

Let

$$L = -R^{\eta p} \left(R^{pp}\right)^{-1} = \begin{bmatrix} L_1 & L_2 \end{bmatrix} \tag{B.4}$$

and

$$B = \begin{bmatrix} I_{2x2} & 0 \\ L & 1 \end{bmatrix} \tag{B.5}$$

By pre-multiplying B on both sides of the measurement conversion equation, a new measurement prediction function can be obtained in which the position measurement is unmodified, and the pseudo range rate is replaced with a decorrelated pseudo range rate, ε

$$\varepsilon \triangleq L_1 x_m + L_2 y_m + \eta_m \tag{B.6}$$

with the corresponding measurement prediction function

$$h_{\varepsilon}^{\text{pseudo}} = L_1 x + L_2 y + x\dot{x} + y\dot{y} \tag{B.7}$$

for the pseudo range rate approach, and

$$h_{\varepsilon}^{\text{raw}} = L_1 x + L_2 y + \frac{x\dot{x} + y\dot{y}}{\sqrt{x^2 + y^2}} \tag{B.8}$$

for the raw range rate approach.

Appendix C

Second Order EKF for Range Rate Measurements

$$S_{k+1} = R^{\varepsilon\varepsilon}_{k+1} + H^{\varepsilon\varepsilon}_{k+1} P^{\mathrm{p}}_{k+1|k+1} \left(H^{\varepsilon\varepsilon}_{k+1}\right)' + A_{k+1} \tag{C.1}$$

$$W_{k+1} = P^{\mathrm{p}}_{k+1|k+1} \left(H^{\varepsilon\varepsilon}_{k+1}\right)' S^{-1}_{k+1} \tag{C.2}$$

$$P_{k+1|k+1} = P^{\mathrm{p}}_{k+1|k+1} - W_{k+1} S_{k+1} W'_{k+1} \tag{C.3}$$

$$\hat{\mathbf{x}}_{\mathbf{k+1|k+1}} = \hat{\mathbf{x}}^{\mathrm{p}}_{\mathbf{k+1|k+1}} + W_{k+1}\left[\varepsilon_{k+1} - h^{\mathrm{pseudo}}_{\varepsilon}\left(\hat{\mathbf{x}}^{\mathrm{p}}_{\mathbf{k+1|k+1}}\right) - \frac{1}{2}\delta^2_{k+1}\right]$$

where

$$G_{k+1} = \begin{bmatrix} 0_{2x2} & I_{2x2} \\ I_{2x2} & 0_{2x2} \end{bmatrix} P^{\mathrm{p}}_{k+1|k+1} \tag{C.4}$$

$$A_{k+1} = \frac{1}{2}\mathrm{tr}\left(G_{k+1}G_{k+1}\right)$$

$$\delta^2_{k+1} = \mathrm{tr}\left(G_{k+1}\right)$$

$$H^{\varepsilon\varepsilon}_{k+1} = \begin{bmatrix} L_1 + \hat{\dot{x}} & L_2 + \hat{\dot{y}} & \hat{x} & \hat{y} \end{bmatrix}$$

and $R^{\varepsilon\varepsilon}_{k+1}$ is the variance of the debiased pseudo range rate measurement. $\hat{\dot{x}}$, $\hat{\dot{y}}$, $\hat{x}$, and $\hat{y}$ are components of $\hat{\mathbf{x}}^{\mathrm{p}}_{\mathbf{k+1|k+1}}$.

Appendix D

Converted Measurement Error Covariance

The converted measurement error covariance is defined as

$$R_{\mathrm{C}} = E\left[\tilde{x}'\tilde{x}\right] \tag{D.1}$$

where

$$\begin{aligned}
\tilde{x} &= e^{\sigma_\alpha^2/2} D\left(\alpha_m\right) \begin{bmatrix} r_m \\ 0 \\ \dot{r}_m \\ \dot{c}_m \end{bmatrix} - \begin{bmatrix} x_{\mathrm{TRUE}} \\ y_{\mathrm{TRUE}} \\ \dot{x}_{\mathrm{TRUE}} \\ \dot{y}_{\mathrm{TRUE}} \end{bmatrix} \\
\tilde{x} &= e^{\sigma_\alpha^2/2} D\left(\alpha_m\right) \begin{bmatrix} r_m \\ 0 \\ \dot{r}_m \\ \dot{c}_m \end{bmatrix} - D\left(\alpha_{\mathrm{TRUE}}\right) \begin{bmatrix} r_{\mathrm{TRUE}} \\ 0 \\ \dot{r}_{\mathrm{TRUE}} \\ \dot{c}_{\mathrm{TRUE}} \end{bmatrix}
\end{aligned} \tag{D.2}$$

All of the raw measurements are assumed to unbiased and corrupted by addition Gaussian noise

$$\alpha_m = \alpha_{\text{TRUE}} + w_\alpha \quad r_m = r_{\text{TRUE}} + w_r \quad \dot{r}_m = \dot{r}_{\text{TRUE}} + w_{\dot{r}} \tag{D.3}$$

Since the true state is not available in practice, an approximation from the tracker's one step prediction, $\hat{\mathbf{x}}_{\mathbf{k+1|k}}$, is used as a substitute (subscript $k+1|k$ omitted)

$$\begin{bmatrix} r_{\text{TRUE}} \\ 0 \\ \dot{r}_{\text{TRUE}} \\ \dot{c}_{\text{TRUE}} \end{bmatrix} \approx D(\alpha_t)' \begin{bmatrix} \hat{\mathbf{x}}^{\mathbf{1}} \\ \hat{\mathbf{x}}^{\mathbf{2}} \\ \hat{\mathbf{x}}^{\mathbf{3}} \\ \hat{\mathbf{x}}^{\mathbf{4}} \end{bmatrix} + \begin{bmatrix} w_{\mathbf{x}^1} \\ w_{\mathbf{x}^2} \\ w_{\mathbf{x}^3} \\ w_{\mathbf{x}^4} \end{bmatrix} \tag{D.4}$$

and

$$E\left\{ \begin{bmatrix} w_{\mathbf{x}^1} \\ w_{\mathbf{x}^2} \\ w_{\mathbf{x}^3} \\ w_{\mathbf{x}^4} \end{bmatrix}' \begin{bmatrix} w_{\mathbf{x}^1} \\ w_{\mathbf{x}^2} \\ w_{\mathbf{x}^3} \\ w_{\mathbf{x}^4} \end{bmatrix} \right\} = D(\alpha_t)' P_{k+1|k} D(\alpha_t) \tag{D.5}$$

Furthermore, the target bearing from the predicted estimate is assumed to be[1]

$$\alpha_t = \tan^{-1}\left(\frac{\hat{\mathbf{x}}^2}{\hat{\mathbf{x}}^1}\right) \approx \alpha_{\text{TRUE}} + w_{\alpha_t} \tag{D.6}$$

[1] The four quadrant inverse tangent can be used. Also, $\tan^{-1}\left(\frac{\hat{\mathbf{x}}^2}{\hat{\mathbf{x}}^1}\right) = \frac{\pi}{2} - \tan^{-1}\left(\frac{\hat{\mathbf{x}}^1}{\hat{\mathbf{x}}^2}\right)$ and should be used when $\left|\hat{\mathbf{x}}^1\right| < \left|\hat{\mathbf{x}}^2\right|$

where

$$E\left[w_{\alpha_t}\right] = 0 \quad E\left[{w_{\alpha_t}}^2\right] = \sigma_{\alpha_t}^2 \tag{D.7}$$

The approximate bearing variance is based on a linearization of the track's covariance,

$$\sigma_{\alpha_t}^2 = \left[\begin{array}{cccc} \frac{\partial \alpha_t}{\partial \hat{\mathbf{x}}^1} & \frac{\partial \alpha_t}{\partial \hat{\mathbf{x}}^2} & \frac{\partial \alpha_t}{\partial \hat{\mathbf{x}}^3} & \frac{\partial \alpha_t}{\partial \hat{\mathbf{x}}^4} \end{array} \right] P_{k+1|k} \left[\begin{array}{c} \frac{\partial \alpha_t}{\partial \hat{\mathbf{x}}^1} \\ \\ \frac{\partial \alpha_t}{\partial \hat{\mathbf{x}}^2} \\ \\ \frac{\partial \alpha_t}{\partial \hat{\mathbf{x}}^3} \\ \\ \frac{\partial \alpha_t}{\partial \hat{\mathbf{x}}^4} \end{array} \right] \tag{D.8}$$

which simplifies to:

$$\begin{aligned} \sigma_{\alpha_t}^2 = & \frac{1}{\left(\left(\hat{\mathbf{x}}^1\right)^2 + \left(\hat{\mathbf{x}}^2\right)^2\right)^2} \\ & \cdot \left[\begin{array}{cccc} -\hat{\mathbf{x}}^2 & \hat{\mathbf{x}}^1 & 0 & 0 \end{array} \right] P_{k+1|k} \left[\begin{array}{c} -\hat{\mathbf{x}}^2 \\ \\ \hat{\mathbf{x}}^1 \\ \\ 0 \\ \\ 0 \end{array} \right] \end{aligned} \tag{D.9}$$

Defining

$$R_{\mathrm{R}} = R_{\mathrm{C}}|_{\alpha_t = 0} \tag{D.10}$$

and acknowledging

$$R_{\mathrm{C}} = D\left(\alpha_t\right) R_{\mathrm{R}} D\left(\alpha_t\right)' \tag{D.11}$$

we can derive the components of R_{R}, using the following,

$$E\left\{\left[\cos\left(-w_{\alpha_t}+w_\alpha\right)\right]^2\right\}=\frac{1}{2}\left(1+e^{-2\sigma_\alpha^2}e^{-2\sigma_{\alpha_t}^2}\right)$$

$$E\left\{\left[\cos\left(-w_{\alpha_t}\right)\right]^2\right\}=\frac{1}{2}\left(1+e^{-2\sigma_{\alpha_t}^2}\right)$$

$$E\left[\cos\left(-w_{\alpha_t}+w_\alpha\right)\cos\left(-w_{\alpha_t}\right)\right]=\frac{1}{2}\left(1+e^{-2\sigma_{\alpha_t}^2}\right)e^{-\sigma_\alpha^2/2}$$

$$E\left\{\left[\sin\left(-w_{\alpha_t}+w_\alpha\right)\right]^2\right\}=\frac{1}{2}\left(1-e^{-2\sigma_\alpha^2}e^{-2\sigma_{\alpha_t}^2}\right)$$

$$E\left\{\left[\sin\left(-w_{\alpha_t}\right)\right]^2\right\}=\frac{1}{2}\left(1-e^{-2\sigma_{\alpha_t}^2}\right)$$

$$E\left[\sin\left(-w_{\alpha_t}+w_\alpha\right)\sin\left(-w_{\alpha_t}\right)\right]=\frac{1}{2}\left(1-e^{-2\sigma_{\alpha_t}^2}\right)e^{-\sigma_\alpha^2/2}$$

$$E\left[\sin\left(-w_{\alpha_t}+w_\alpha\right)\cos\left(-w_{\alpha_t}\right)\right]=0$$

$$E\left[\cos\left(-w_{\alpha_t}+w_\alpha\right)\sin\left(-w_{\alpha_t}\right)\right]=0$$

$$E\left[\sin\left(-w_{\alpha_t}+w_\alpha\right)\cos\left(-w_{\alpha_t}+w_\alpha\right)\right]=0$$

$$E\left[\sin\left(-w_{\alpha_t}\right)\cos\left(-w_{\alpha_t}\right)\right]=0$$

The components of R_{R} are:

$$R_{\mathrm{R}}^{11}=E\Big\{\Big[e^{\sigma_\alpha^2/2}\left(\hat{\mathbf{x}}_{\mathrm{R}}^1-w_{\mathbf{x}_{k+1|k}^1}+w_r\right)\cos\left(-w_{\alpha_t}+w_\alpha\right)$$
$$-\left(\hat{\mathbf{x}}_{\mathrm{R}}^1-w_{\mathbf{x}_{k+1|k}^1}\right)\cos\left(-w_{\alpha_t}\right)\Big]^2\Big\} \tag{D.12}$$

which equates to (4.23),

$$\begin{aligned} R_{\mathrm{R}}^{12}=&E\big\{\big[e^{\sigma_\alpha^2/2}\left(\hat{\mathbf{x}}_{\mathrm{R}}^1-w_{\mathbf{x}_{k+1|k}^1}+w_r\right)\cos\left(-w_{\alpha_t}+w_\alpha\right)\\ &-\left(\hat{\mathbf{x}}_{\mathrm{R}}^1-w_{\mathbf{x}_{k+1|k}^1}\right)\cos\left(-w_{\alpha_t}\right)\big]\\ &\big[e^{\sigma_\alpha^2/2}\left(\hat{\mathbf{x}}_{\mathrm{R}}^1-w_{\mathbf{x}_{k+1|k}^1}+w_r\right)\sin\left(-w_{\alpha_t}+w_\alpha\right)\\ &-\left(\hat{\mathbf{x}}_{\mathrm{R}}^1-w_{\mathbf{x}_{k+1|k}^1}\right)\sin\left(-w_{\alpha_t}\right)\big]\big\} \end{aligned} \tag{D.13}$$

which equates to 0, (4.24),

$$\begin{aligned} R_{\mathrm{R}}^{13}=&E\big\{\big[e^{\sigma_\alpha^2/2}\left(\hat{\mathbf{x}}_{\mathrm{R}}^1-w_{\mathbf{x}_{k+1|k}^1}+w_r\right)\cos\left(-w_{\alpha_t}+w_\alpha\right)\\ &-\left(\hat{\mathbf{x}}_{\mathrm{R}}^1-w_{\mathbf{x}_{k+1|k}^1}\right)\cos\left(-w_{\alpha_t}\right)\big]\\ &\big[e^{\sigma_\alpha^2/2}\left(\hat{\mathbf{x}}_{\mathrm{R}}^3-w_{\mathbf{x}_{k+1|k}^3}+w_{\dot{r}}\right)\cos\left(-w_{\alpha_t}+w_\alpha\right)\\ &-\left(\hat{\mathbf{x}}_{\mathrm{R}}^3-w_{\mathbf{x}_{k+1|k}^3}\right)\cos\left(-w_{\alpha_t}\right)\\ &+e^{\sigma_\alpha^2/2}\left(\hat{\mathbf{x}}_{\mathrm{R}}^4-w_{\mathbf{x}_{k+1|k}^4}+w_{\dot{c}}\right)\sin\left(-w_{\alpha_t}+w_\alpha\right)\\ &-\left(\hat{\mathbf{x}}_{\mathrm{R}}^4-w_{\mathbf{x}_{k+1|k}^4}\right)\sin\left(-w_{\alpha_t}\right)\big]\big\} \end{aligned} \tag{D.14}$$

which equates to (4.25),

$$\begin{aligned} R_{\mathrm{R}}^{22}=&E\big\{\big[e^{\sigma_\alpha^2/2}\left(\hat{\mathbf{x}}_{\mathrm{R}}^1-w_{\mathbf{x}_{k+1|k}^1}+w_r\right)\sin\left(-w_{\alpha_t}+w_\alpha\right)\\ &-\left(\hat{\mathbf{x}}_{\mathrm{R}}^1-w_{\mathbf{x}_{k+1|k}^1}\right)\sin\left(-w_{\alpha_t}\right)\big]^2\big\} \end{aligned} \tag{D.15}$$

which equates to (4.26),

$$\begin{aligned}
R_{\mathrm{R}}^{23}=&E\Big\{\Big[e^{\sigma_\alpha^2/2}\left(\hat{\mathbf{x}}_{\mathrm{R}}^1-w_{\mathbf{x}_{k+1|k}^1}+w_r\right)\sin\left(-w_{\alpha_t}+w_\alpha\right)\\
&-\left(\hat{\mathbf{x}}_{\mathrm{R}}^1-w_{\mathbf{x}_{k+1|k}^1}\right)\sin\left(-w_{\alpha_t}\right)\Big]\\
&\Big[e^{\sigma_\alpha^2/2}\left(\hat{\mathbf{x}}_{\mathrm{R}}^3-w_{\mathbf{x}_{k+1|k}^3}+w_{\dot{r}}\right)\cos\left(-w_{\alpha_t}+w_\alpha\right)\\
&-\left(\hat{\mathbf{x}}_{\mathrm{R}}^3-w_{\mathbf{x}_{k+1|k}^3}\right)\cos\left(-w_{\alpha_t}\right)\\
&+e^{\sigma_\alpha^2/2}\left(\hat{\mathbf{x}}_{\mathrm{R}}^4-w_{\mathbf{x}_{k+1|k}^4}+w_{\dot{c}}\right)\sin\left(-w_{\alpha_t}+w_\alpha\right)\\
&-\left(\hat{\mathbf{x}}_{\mathrm{R}}^4-w_{\mathbf{x}_{k+1|k}^4}\right)\sin\left(-w_{\alpha_t}\right)\Big]\Big\}
\end{aligned}\tag{D.16}$$

which equates to (4.27), and

$$\begin{aligned}
R_{\mathrm{R}}^{33}=&E\Big\{\Big[e^{\sigma_\alpha^2/2}\left(\hat{\mathbf{x}}_{\mathrm{R}}^3-w_{\mathbf{x}_{k+1|k}^3}+w_{\dot{r}}\right)\cos\left(-w_{\alpha_t}+w_\alpha\right)\\
&-\left(\hat{\mathbf{x}}_{\mathrm{R}}^3-w_{\mathbf{x}_{k+1|k}^3}\right)\cos\left(-w_{\alpha_t}\right)\\
&+e^{\sigma_\alpha^2/2}\left(\hat{\mathbf{x}}_{\mathrm{R}}^4-w_{\mathbf{x}_{k+1|k}^4}+w_{\dot{c}}\right)\sin\left(-w_{\alpha_t}+w_\alpha\right)\\
&-\left(\hat{\mathbf{x}}_{\mathrm{R}}^4-w_{\mathbf{x}_{k+1|k}^4}\right)\sin\left(-w_{\alpha_t}\right)\Big]^2\Big\}
\end{aligned}\tag{D.17}$$

which equates to (4.28), where $\hat{\mathbf{x}}_{\mathrm{R}}$ is defined in (4.20).

The convenience of deriving R_{R} (as opposed to R_{C} directly) comes from the elimination of terms involving the sine of α_t ($E\left\{\sin\left(\alpha_t-w_{\alpha_t}\right)|_{\alpha_t=0}\right\}=0$). The calculation of (D.9) is also simplified since in the line of sight coordinate system, $\hat{\mathbf{x}}_{\mathrm{R}}^2=0$, reducing (D.9) to (4.29).

Appendix E

Conversion of Bi-Static Range and Bearing to Cartesian

The law of cosines [53] can be used to derive (5.6). Using the nomenclature of fig. 5.1 the law of cosines is

$$\cos(\alpha) = \frac{L^2 + {r_1}^2 - {r_2}^2}{2r_1 L} \tag{E.1}$$

r_2 can be replaced using measured bi-static range $r_2 = b - r_1$,

$$\cos(\alpha) = \frac{L^2 + {r_1}^2 - (b - r_1)^2}{2r_1 L} \tag{E.2}$$

Now, solving for r_1

$$\cos(\alpha) = \frac{L^2 + {r_1}^2 - b^2 + 2br_1 - {r_1}^2}{2r_1 L} \tag{E.3}$$

The ${r_1}^2$ terms cancel,

$$\cos(\alpha) = \frac{L^2 - b^2 + 2br_1}{2r_1 L} \tag{E.4}$$

$$2r_1 L\cos(\alpha) - 2br_1 = L^2 - b^2 \tag{E.5}$$

$$r_1 = \frac{L^2 - b^2}{2\left(L\cos(\alpha) - b\right)} \tag{E.6}$$

Appendix F

Unscented and Cubature Sigma Points

For the case of the Unscented transform, the parameters of the SPT are defined as follows [34]:

1. Let $m = 2n + 1$ where n is the state dimension and $i = 0 \dots m - 1$

2. Let S_{xx} be a matrix square root of P_{xx}

$$P_{xx} = S_{xx} S_{xx}{}' \tag{F.1}$$

   and $S_{xx,j}$ represent the jth column of S_{xx}.

3. The point mass displacements $\mathbf{\Delta}_i$ (from the mean) are set to

$$\mathbf{\Delta}_i = 0 \qquad i = 0 \tag{F.2}$$

$$\mathbf{\Delta}_i = -\sqrt{(n+\kappa)} S_{xx,i} \qquad i = 1 \dots n \tag{F.3}$$

$$\mathbf{\Delta}_i = \sqrt{(n+\kappa)} S_{xx,(i-n)} \quad i = n+1 \dots m-1 \tag{F.4}$$

$$\tag{F.5}$$

4. The weights w_i are set as

$$\mathrm{w}_1 = 0 \qquad i = 0 \tag{F.6}$$

$$\mathrm{w}_i = \frac{1}{2\left(n+\kappa\right)} \quad i = 1 \ldots m-1 \tag{F.7}$$

$$\tag{F.8}$$

The value $\kappa = 2$ was used in the evaluation. Note that the above matches the first two moments of $\mathbf{x}$ and yields an approximation for the moments of a nonlinear transformation of $\mathbf{x}$ as in (5.19).

For the case of the Cubature transform (using a third-degree cubature rule, which computes the first two-order moments exactly [1]) the parameters of the SPT are defined as follows [1]:

1. Let m equal twice the state dimension n and $i = 0 \ldots m-1$

2. Let $\mathcal{X}$ be defined as follows

$$\mathcal{X} = \sqrt{\frac{m}{2}} \left[\begin{array}{cc} I_n & -I_n \end{array} \right] \tag{F.9}$$

   where I_n is an $n \times n$ identity matrix. Let ξ_i represent column i of $\mathcal{X}$.

3. Let S_{xx} be a matrix square root of P_{xx}

$$P_{xx} = S_{xx} {S_{xx}}' \tag{F.10}$$

4. The point mass displacements $\mathbf{\Delta}_i$ are set to

$$\mathbf{\Delta}_i = S_{xx} \xi_{i+1} \tag{F.11}$$

5. All weights, w_i, are set to $1/m$.

Appendix G

Converted Measurement Error Covariance

The converted measurement error covariance is approximated using a simplification of [13]. The calculation requires a prediction, which is based on the one step prediction, $\theta(k|k-1)$. Using this prediction, in combination with the target template and the previous estimate of the size, s, the state of an individual highlight can be calculated (which will be referred to as $\mathbf{x}_j$).

First the predicted highlight state is rotated into the estimate's LOS coordinate system:

$$\hat{\mathbf{x}}_{\mathrm{R}} \quad = \quad D(\alpha_t)' \hat{\mathbf{x}}_j \tag{G.1}$$

where the predicted bearing to the highlight is

$$\alpha_t = \tan^{-1}\left(\frac{\hat{\mathbf{x}}^2_{k+1|k}}{\hat{\mathbf{x}}^1_{k+1|k}}\right) \tag{G.2}$$

and $\hat{\mathbf{x}}^n$ is the nth component of $\hat{\mathbf{x}}$.

$$
\begin{aligned}
R_{\mathrm{R}}^{11} &= \frac{1}{2}\left[\left(\hat{\mathbf{x}}_{\mathrm{R}}^{1}\right)^{2}+\sigma_{r}^{2}\right]\left(1+e^{-2\sigma_{\alpha}^{2}}\right)e^{\sigma_{\alpha}^{2}} \\
&\quad -\left(\hat{\mathbf{x}}_{\mathrm{R}}^{1}\right)^{2} && \text{(G.3)} \\
R_{\mathrm{R}}^{12} &= 0 && \text{(G.4)} \\
R_{\mathrm{R}}^{13} &= \frac{1}{2}\left(\hat{\mathbf{x}}_{\mathrm{R}}^{1}\hat{\mathbf{x}}_{\mathrm{R}}^{3}+\rho\sigma_{r}\sigma_{\dot{r}}\right)\left(1+e^{-2\sigma_{\alpha}^{2}}\right)e^{\sigma_{\alpha}^{2}} \\
&\quad -\hat{\mathbf{x}}_{\mathrm{R}}^{1}\hat{\mathbf{x}}_{\mathrm{R}}^{3} && \text{(G.5)} \\
R_{\mathrm{R}}^{22} &= \frac{1}{2}\left[\left(\hat{\mathbf{x}}_{\mathrm{R}}^{1}\right)^{2}+\sigma_{r}^{2}\right]\left(1-e^{-2\sigma_{\alpha}^{2}}\right)e^{\sigma_{\alpha}^{2}} && \text{(G.6)} \\
R_{\mathrm{R}}^{23} &= \frac{1}{2}\left(\hat{\mathbf{x}}_{\mathrm{R}}^{1}\hat{\mathbf{x}}_{\mathrm{R}}^{4}\right)\left(1-e^{-2\sigma_{\alpha}^{2}}\right)e^{\sigma_{\alpha}^{2}} && \text{(G.7)} \\
R_{\mathrm{R}}^{33} &= \frac{1}{2}\left[\left(\hat{\mathbf{x}}_{\mathrm{R}}^{3}\right)^{2}+\sigma_{\dot{r}}^{2}\right]\left(1+e^{-2\sigma_{\alpha}^{2}}\right)e^{\sigma_{\alpha}^{2}}-\left(\hat{\mathbf{x}}_{\mathrm{R}}^{3}\right)^{2} \\
&\quad +\frac{1}{2}\left[\left(\hat{\mathbf{x}}_{\mathrm{R}}^{4}\right)^{2}+\sigma_{\dot{c}}^{2}\right]\left(1-e^{-2\sigma_{\alpha}^{2}}\right)e^{\sigma_{\alpha}^{2}} && \text{(G.8)}
\end{aligned}
$$

Since the cross range rate measurement, $\dot{c}_m$, is non-informative, its standard deviation, $\sigma_{\dot{c}}$, is infinite. One can, however, set the value of $\sigma_{\dot{c}}$ used in (G.8) based on an a priori estimate of the standard deviation of target cross range rate to capture the effect that the cross range rate has on the ability to measure the line of sight velocity. The remaining components of the measurement noise covariance in the LOS coordinate system, R_{R} (e.g. R_{R}^{44}, R_{R}^{34}), are are set to infinity to capture that $\dot{c}_m$ is non-informative. It is therefore useful to deal with the inverse of R_{R} and note that for a positive definite covariance matrix,

$$\left[\begin{array}{cc} \sigma_1^2 & \rho\sigma_1\sigma_2 \\ \rho\sigma_1\sigma_2 & \sigma_2^2 \end{array}\right]^{-1}\Bigg|_{\sigma_2\to\infty} = \left[\begin{array}{cc} (\sigma_1^2)^{-1} & 0 \\ 0 & 0 \end{array}\right] \tag{G.9}$$

therefore

$$R_{\mathrm{R}}{}^{-1} = \left[\begin{array}{cccc} & & & 0 \\ & \left(R_{\mathrm{R}}^{1:3,1:3}\right)^{-1} & & 0 \\ & & & 0 \\ 0 & 0 & 0 & 0 \end{array}\right] \tag{G.10}$$

Since the inverse of the direction cosine matrix, $D(\alpha_m)$, is its transpose, the measurement noise covariance for (6.5), R_{ij}, is

$$R_{ij}{}^{-1} = D(\alpha_t)\, R_{\mathrm{R}}{}^{-1} D(\alpha_t)' \tag{G.11}$$

Since $R_{\mathrm{C}}{}^{-1}$ is not invertible, R_{ij} is not available for use in the Kalman filter gain calculation; one has to use the information form of the Kalman filter. The determinant of R_{ij} (needed for (6.9) in the calculation of w_{ij} using (6.19)) is also not available, so the determinant of R_{R} is used as a surrogate.

This is a simplification of (35)-(38) in [13]. The simplification is warranted due to the more accurate measurement in the present manuscript when compared to the measurement accuracy of [13].

Appendix H

Oakes' Formula

In [46], a simple explicit formula is given for the observed information matrix. A summary of Oakes' work is provided below with the necessary background from [19].

$$\begin{aligned}\mathcal{L}\left(\boldsymbol{\Psi};\mathcal{Z}\right)&=p_{\mathcal{Z}}\left(\mathcal{Z}|\boldsymbol{\Psi}\right)\\&=\frac{p_{\mathrm{c}}\left(\mathcal{Z},\mathcal{Y}|\boldsymbol{\Psi}\right)p_{\mathcal{Z}}\left(\mathcal{Z}|\boldsymbol{\Psi}\right)}{p_{\mathrm{c}}\left(\mathcal{Z},\mathcal{Y}|\boldsymbol{\Psi}\right)}\end{aligned}\tag{H.1}$$

where $p_{\mathrm{c}}\left(\mathcal{Z},\mathcal{Y}|\boldsymbol{\Psi}\right)$ is defined after (6.16). Let $k\left(\mathcal{X}|\mathcal{Z},\boldsymbol{\Psi}\right)$ be the conditional probability of the complete data, $\mathcal{X}$, given the observed data, $\mathcal{Z}$, namely

$$k\left(\mathcal{X}|\mathcal{Z},\boldsymbol{\Psi}\right)=\frac{p_{\mathrm{c}}\left(\mathcal{Z},\mathcal{Y}|\boldsymbol{\Psi}\right)}{p_{\mathcal{Z}}\left(\mathcal{Z}|\boldsymbol{\Psi}\right)}\tag{H.2}$$

Therefore

$$\mathcal{L}\left(\boldsymbol{\Psi};\mathcal{Z}\right)=\frac{p_{\mathrm{c}}\left(\mathcal{Z},\mathcal{Y}|\boldsymbol{\Psi}\right)}{k\left(\mathcal{X}|\mathcal{Z},\boldsymbol{\Psi}\right)}\tag{H.3}$$

and

$$\ln\mathcal{L}\left(\boldsymbol{\Psi};\mathcal{Z}\right)=\ln p_{\mathrm{c}}\left(\mathcal{Z},\mathcal{Y}|\boldsymbol{\Psi}\right)-\ln k\left(\mathcal{X}|\mathcal{Z},\boldsymbol{\Psi}\right)\tag{H.4}$$

Taking the expectation of both sides with respect to the conditional distribution of $\mathcal{X}$ given $\mathcal{Z}$, using the previous estimate $\mathbf{\Psi}^{(l)}$ for $\mathbf{\Psi}$ gives

$$\begin{aligned}\ln \mathcal{L}\left(\mathbf{\Psi};\mathcal{Z}\right)=&E\left\{\ln \mathcal{L}_{\mathrm{c}}\left(\mathbf{\Psi};\mathcal{Z},\mathcal{Y}\right)|\mathcal{Z},\mathbf{\Psi}^{(l)}\right\}-E\left\{\ln k\left(\mathcal{X}|\mathcal{Z},\mathbf{\Psi}\right)|\mathcal{Z},\mathbf{\Psi}^{(l)}\right\}\\ =&\mathcal{Q}\left(\mathbf{\Psi};\mathbf{\Psi}^{(l)},\mathcal{Z}\right)-H\left(\mathbf{\Psi};\mathbf{\Psi}^{(l)},\mathcal{Z}\right)\end{aligned} \tag{H.5}$$

using (6.17) and where

$$H\left(\mathbf{\Psi};\mathbf{\Psi}^{(l)},\mathcal{Z}\right)=E\left\{\ln k\left(\mathcal{X}|\mathcal{Z},\mathbf{\Psi}\right)|\mathcal{Z},\mathbf{\Psi}^{(l)}\right\} \tag{H.6}$$

In [19] the following is shown using Jensen's inequality,

$$H\left(\mathbf{\Psi};\mathbf{\Psi}^{(l)},\mathcal{Z}\right)\leq H\left(\mathbf{\Psi}^{(l)};\mathbf{\Psi}^{(l)},\mathcal{Z}\right) \tag{H.7}$$

for all $\mathbf{\Psi}$ in the parameter space. This is fundamental in the proof for EM convergence, and leads to

$$\nabla_{\mathbf{\Psi}}\, H\left(\mathbf{\Psi};\mathbf{\Psi}^{(l)},\mathcal{Z}\right)\big|_{\mathbf{\Psi}=\mathbf{\Psi}^{(l)}}=0 \tag{H.8}$$

Assuming that the expectation with respect to $\mathcal{X}$ and differentiation with respect to $\mathbf{\Psi}$ are interchangeable,

$$E\left\{\nabla_{\mathbf{\Psi}}\ln k\left(\mathcal{X}|\mathcal{Z},\mathbf{\Psi}\right)|\mathcal{Z},\mathbf{\Psi}^{(l)}\right\}=0 \tag{H.9}$$

Also, from equivalent statements of Fisher's information,

$$-E\left\{\nabla_{\mathbf{\Psi}}\nabla_{\mathbf{\Psi}}^{\mathrm{T}}\ln k\left(\mathcal{X}|\mathcal{Z},\mathbf{\Psi}\right)|\mathcal{Z},\mathbf{\Psi}^{(l)}\right\}=E\left\{\nabla_{\mathbf{\Psi}}k\left(\mathcal{X}|\mathcal{Z},\mathbf{\Psi}\right)\nabla_{\mathbf{\Psi}}k\left(\mathcal{X}|\mathcal{Z},\mathbf{\Psi}\right)^{\mathrm{T}}|\mathcal{Z},\mathbf{\Psi}^{(l)}\right\} \tag{H.10}$$

Differentiation of (H.5) with respect to $\mathbf{\Psi}$ gives

$$\nabla_{\mathbf{\Psi}} \ln \mathcal{L}\left(\mathbf{\Psi}; \mathcal{Z}\right) = \nabla_{\mathbf{\Psi}} \mathcal{Q}\left(\mathbf{\Psi}; \mathbf{\Psi}^{(l)}, \mathcal{Z}\right) - E\left\{\nabla_{\mathbf{\Psi}} \ln k\left(\mathcal{X}|\mathcal{Z}, \mathbf{\Psi}\right)|\mathcal{Z}, \mathbf{\Psi}^{(l)}\right\} \quad \text{(H.11)}$$

By evaluating (H.11) using $\mathbf{\Psi}^{(l)} = \mathbf{\Psi}$ and noting (H.9), we obtain

$$\nabla_{\mathbf{\Psi}} \ln \mathcal{L}\left(\mathbf{\Psi}; \mathcal{Z}\right) = \nabla_{\mathbf{\Psi}} \mathcal{Q}\left(\mathbf{\Psi}; \mathbf{\Psi}^{(l)}, \mathcal{Z}\right)\Big|_{\mathbf{\Psi}^{(l)}=\mathbf{\Psi}} \quad \text{(H.12)}$$

Differentiation of (H.11) with respect to $\mathbf{\Psi}$ gives,

$$\begin{aligned}\nabla_{\mathbf{\Psi}} \nabla_{\mathbf{\Psi}}^{\mathrm{T}} \ln \mathcal{L}\left(\mathbf{\Psi}; \mathcal{Z}\right) = {} & \nabla_{\mathbf{\Psi}} \nabla_{\mathbf{\Psi}}^{\mathrm{T}} \mathcal{Q}\left(\mathbf{\Psi}; \mathbf{\Psi}^{(l)}, \mathcal{Z}\right) \\ & - E\left\{\nabla_{\mathbf{\Psi}} \nabla_{\mathbf{\Psi}}^{\mathrm{T}} \ln k\left(\mathcal{X}|\mathcal{Z}, \mathbf{\Psi}\right)|\mathcal{Z}, \mathbf{\Psi}^{(l)}\right\} \quad \text{(H.13)}\end{aligned}$$

Differentiation of (H.11) with respect to $\mathbf{\Psi}^{(l)}$ gives,

$$\mathbf{0} = \nabla_{\mathbf{\Psi}} \nabla_{\mathbf{\Psi}^{(l)}}^{\mathrm{T}} \mathcal{Q}\left(\mathbf{\Psi}; \mathbf{\Psi}^{(l)}, \mathcal{Z}\right) - E\left\{\nabla_{\mathbf{\Psi}} \ln k\left(\mathcal{X}|\mathcal{Z}, \mathbf{\Psi}\right) \nabla_{\mathbf{\Psi}^{(l)}} \ln k\left(\mathcal{X}|\mathcal{Z}, \mathbf{\Psi}\right)^{\mathrm{T}}|\mathcal{Z}, \mathbf{\Psi}^{(l)}\right\} \quad \text{(H.14)}$$

where $\mathbf{0}$ is the appropriately sized null matrix.

Substitution $\mathbf{\Psi} = \mathbf{\Psi}^{(l)}$ and adding (H.13) and (H.13) results in

$$\nabla_{\mathbf{\Psi}} \nabla_{\mathbf{\Psi}}^{\mathrm{T}} \ln \mathcal{L}\left(\mathbf{\Psi}; \mathcal{Z}\right) = \nabla_{\mathbf{\Psi}} \nabla_{\mathbf{\Psi}}^{\mathrm{T}} \mathcal{Q}\left(\mathbf{\Psi}; \mathbf{\Psi}^{(l)}, \mathcal{Z}\right) + \nabla_{\mathbf{\Psi}} \nabla_{\mathbf{\Psi}^{(l)}}^{\mathrm{T}} \mathcal{Q}\left(\mathbf{\Psi}; \mathbf{\Psi}^{(l)}, \mathcal{Z}\right) \quad \text{(H.15)}$$

This result is used in (6.33), using the $\mathbf{\Psi}^{(l)}$ from the last EM iteration for a scan (i.e. $\mathbf{\Psi}^{(L)}$).

Appendix I

Position Only Cluster Tracker

A simple way to deal the extended nature of the target and the accompanying issue of multiple measurements per target is to perform centroid group tracking [9]. The CLUSTEREKF used in Section 6.5 uses the centroid of the measurements after being converted to Cartesian. For the measurement noise covariance matrix, the upper two-by-two components of converted measurement error covariance is used, reduced to account for the number of elements, namely R/N. These measurements are used in the EKF described in 6.4.4, with the addition of an H matrix to account for position only measurements.

Bibliography

[1] I. Arasaratnam and S. Haykin, *Cubature Kalman filters*, IEEE Transactions on Automatic Control **54** (2009), no. 6, 1254–1269.

[2] Y. Bar-Shalom, *Negative correlation and optimal tracking with doppler measurements*, IEEE Transactions on Aerospace and Electronic Systems **37** (2001), no. 3, 1117 –1120.

[3] Y. Bar-Shalom, X. R. Li, and T. Kirubarajan, *Estimation with applications to tracking and navigation*, John Wiley and Sons, New York & Boston, 2001.

[4] Y. Bar-Shalom, P. Willett, and X. Tian, *Tracking and data fusion: A handbook of algorithms*, YBS Publishing, 2011.

[5] M. Baum and U. Hanebeck, *Shape tracking of extended objects and group targets with star-convex RHMs*, Proceedings of the 14th International Conference on Information Fusion (FUSION), IEEE, 2011, pp. 1–8.

[6] M. Baum, B. Noack, and U. Hanebeck, *Extended object and group tracking with elliptic random hypersurface models*, Proceedings of the 13th Conference on Information Fusion (FUSION), IEEE, 2010, pp. 1–8.

[7] Jeff A Bilmes et al., *A gentle tutorial of the EM algorithm and its application to parameter estimation for gaussian mixture and hidden markov models*, International Computer Science Institute **4** (1998), no. 510, 126.

[8] D. F. Bizup and D. E. Brown, *The over-extended Kalman filter - don't use it!*, Proceedings of the Sixth International Conference of Information Fusion, vol. 1, 2003, pp. 40 – 46.

[9] Samuel S Blackman, *Multiple-target tracking with radar applications*, Dedham, MA, Artech House, Inc., 1986, 463 p. **1** (1986).

[10] Yvo Boers and Johannes N Driessen, *A track before detect approach for extended objects*, 2006 9th International Conference on Information Fusion, IEEE, 2006, pp. 1–7.

[11] S. Bordonaro, P. Willett, and Y. Bar-Shalom, *Tracking with converted position and Doppler measurements*, Proceedings of SPIE Conference on Signal and Data Processing of Small Targets (O. E. Drummond, ed.), Proc. SPIE, vol. 8137, 2011, pp. 8137–12.

[12] ———, *Bias elimination in tracking with converted position and Doppler measurements*, IEEE Conference on Decision and Control (Maui, HI, USA), Proc. IEEE, Dec. 2012, pp. 4089 – 4094.

[13] S. Bordonaro, P. Willett, and Y. Bar-Shalom, *Consistent linear tracker with position and range rate measurements*, Conference Record of the Forty Sixth Asilomar Conference on Signals, Systems and Computers (ASILOMAR), 2012, pp. 880–884.

[14] ———, *Performance analysis of the converted range rate and position linear kalman filter*, Signals, Systems and Computers (ASILOMAR), 2013 Conference Record of the Forty Seventh Asilomar Conference on, 2013.

[15] ———, *Decorrelated, unbiased converted measurement kalman filter*, IEEE Transactions on Aerospace and Electronic Systems. (Accepted).

[16] Steven Bordonaro, Peter Willett, Yaakov Bar-Shalom, Marcus Baum, and Tod Luginbuhl, *Extracting speed, heading and turn-rate measurements from extended objects using the EM algorithm*, Aerospace Conference, 2015 IEEE, IEEE, 2015, pp. 1–12.

[17] S. Coraluppi, *Multistatic sonar localization*, IEEE Journal of Oceanic Engineering **31** (2006), no. 4, 964–974.

[18] D. Crouse, *One can do better than the unscented kalman filter for multistatic tracking*, Aerospace Conference, 2013 IEEE, IEEE, 2013, pp. 1–20.

[19] Arthur P Dempster, Nan M Laird, and Donald B Rubin, *Maximum likelihood from incomplete data via the EM algorithm*, Journal of the royal statistical society. Series B (methodological) (1977), 1–38.

[20] Z. Duan, C. Han, and X. R. Li, *Comments on unbiased converted measurements for tracking*, IEEE Transactions on Aerospace and Electronic Systems. **40(4)** (2004), 1374–1377.

[21] Z. Duan, C. Han, and X. R. Li, *Sequential nonlinear tracking filter with range-rate measurements in spherical coordinates*, Proceedings of the 7th International Conference on Information Fusion, vol. 1, Citeseer, 2004, pp. 599–605.

[22] Z. Duan, X. R. Li, C. Han, and H. Zhu, *Sequential Unscented Kalman filter for radar target tracking with range rate measurements*, Proceedings of the 8th International Conference on Information Fusion, vol. 1, IEEE, 2005, pp. 8–pp.

[23] A. Farina and F. Studer, *Radar data processing, vol. I: Introduction and tracking, vol. II: Advanced topics and applications*, (1985).

[24] RJ Fitzgerald, *Effects of range-doppler coupling on chirp radar tracking accuracy*, Aerospace and Electronic Systems, IEEE Transactions on (1974), no. 4, 528–532.

[25] D. Fränken, *Some results on linear unbiased filtering with polar measurements*, IEEE International Conference on Multisensor Fusion and Integration for Intelligent Systems (Heidelberg, Germany), IEEE, 2006, pp. 297–302.

[26] ———, *Consistent unbiased linear filtering with polar measurements*, Proceedings of the 10th International Conference on Information Fusion, 2007, pp. 1–8.

[27] L. Gao, J. Lan, J. Jiang, and X. Fan, *Performance analysis of sequential filter based on unbiased converted measurements with doppler*, Proceedings of the International Conference on Electronics and Optoelectronics (ICEOE), vol. 1, IEEE, 2011, pp. V1–9.

[28] K. Gilholm, S. Godsill, S. Maskell, and D. Salmond, *Poisson models for extended target and group tracking*, SPIE, Signal and Data Processing of Small Targets, San Diego, CA, USA **5913** (2005), 59130R.

[29] K. Gilholm and D. Salmond, *Spatial distribution model for tracking extended objects*, Radar, Sonar and Navigation, IEE Proceedings, vol. 152, IET, 2005, pp. 364–371.

[30] S. Godsill, J. Li, and W. Ng, *Multiple and extended object tracking with Poisson spatial processes and variable rate filters*, 1st IEEE International Workshop on Computational Advances in Multi-Sensor Adaptive Processing, IEEE, 2005, pp. 93–96.

[31] Sébastien Granger and Xavier Pennec, *Multi-scale EM-ICP: A fast and robust approach for surface registration*, Computer VisionECCV 2002, Springer, 2002, pp. 418–432.

[32] L. Jiao, Q. Pan, Y. Liang, and F. Yang, *A nonlinear tracking algorithm with range-rate measurements based on unbiased measurement conversion*, Proceedings of the 15th International Conference on Information Fusion (FUSION), IEEE, 2012, pp. 1400–1405.

[33] T. Jorgensen and R. Rothrock, *Removal of bias due to propagation of estimates through nonlinear mappings*, Proceedings of SPIE Conference on Signal and Data Processing of Small Targets (O. E. Drummond, ed.), vol. 6969, Proc. SPIE, no. 1, 2008.

[34] S. Julier and J. Uhlmann, *A consistent, debiased method for converting between polar and cartesian coordinate systems*, SPIE Proceedings of AeroSense: Acquisition, Tracking and Pointing XI (Orlando, FL, USA), vol. 34, Oct 1997, pp. 110–121.

[35] S.M. Kay, *Fundamentals of statistical signal processing – estimation theory*, Prentice Hall PRT, New Jersey, 1993.

[36] W. Koch, *Bayesian approach to extended object and cluster tracking using random matrices*, IEEE Transactions on Aerospace and Electronic Systems **44** (2008), no. 3, 1042–1059.

[37] J. Lan and X. R. Li, *Tracking of extended object or target group using random matrix - part II: Irregular object*, Proceedings of the 15th International Conference on Information Fusion (FUSION), IEEE, 2012, pp. 2185–2192.

[38] M. Lei and C. Han, *Sequential nonlinear tracking using UKF and raw range-rate measurements*, IEEE Transactions on Aerospace and Electronic Systems **43** (2007), no. 1, 239 –250.

[39] D. Lerro and Y. Bar-Shalom, *Tracking with debiased consistent converted measurements versus EKF*, IEEE Transactions on Aerospace and Electronic Systems. **29(3)** (1993), 1015–1022.

[40] T. Luginbuhl and C. Hempel, *Converting bearings-only measurements to cartesian coordinates*, IEEE Transactions on Aerospace and Electronic Systems. **45(1)** (2009), 393–404.

[41] D. Martina and E. Frank, *Tracking algorithms for multistatic sonar systems*, EURASIP Journal on Advances in Signal Processing **2010** (2010).

[42] Geoffrey McLachlan and Thriyambakam Krishnan, *The EM algorithm and extensions*, John Wiley & Sons, 2007.

[43] W. Mei and Y. Bar-Shalom, *Unbiased Kalman Filter using converted measurements: Revisit*, Proceedings of SPIE Conference on Signal and Data Processing of Small Targets (O. E. Drummond and R. D. Teichgraeber, eds.), Proc. SPIE, vol. 7445, 2009, p. 731.

[44] M. D. Miller and O. E. Drummond, *Comparison of methodologies for mitigating coordinate transformation bias in target tracking*, Proceedings of SPIE Conference on Signal and Data Processing of Small Targets, vol. 4048, 2000, pp. 414–427.

[45] L. Mo, X. Song, Y. Zhou, Z. Sun, and Y. Bar-Shalom, *Unbiased converted measurements for tracking*, IEEE Transactions on Aerospace and Electronic Systems. **34(3)** (1998), 1023–1027.

[46] David Oakes, *Direct calculation of the information matrix via the EM*, Journal of the Royal Statistical Society: Series B (Statistical Methodology) **61** (1999), no. 2, 479–482.

[47] F. Spitzmiller and R. Adhami, *Tracking with estimate-conditioned debiased 3-D converted measurement*, IEEE Aerospace Conference, Proc. IEEE, vol. 1066, 2010, pp. 1–16.

[48] R. Streit and T. Luginbuhl, *Probabilistic multi-hypothesis tracking*, Tech. report, Technical Report 10428, Naval Undersea Warfare Center, Newport, RI February 1995 (available from DTIC), 1995.

[49] P. Suchomski, *Explicit expressions for debiased statistics of 3D converted measurements*, Aerospace and Electronic Systems, IEEE Transactions on **35** (1999), no. 1, 368–370.

[50] P. Tichavsky, C.H. Muravchik, and A. Nehorai, *Posterior Cramer-Rao bounds for discrete-time nonlinear filtering*, IEEE Transactions on Signal Processing **46** (1998), no. 5, 1386 –1396.

[51] Naonori Ueda and Ryohei Nakano, *Deterministic annealing EM algorithm*, Neural Networks **11** (1998), no. 2, 271–282.

[52] R. Van Der Merwe, *Sigma-point kalman filters for probabilistic inference in dynamic state-space models*, Ph.D. thesis, University of Stellenbosch, 2004.

[53] E. W. Weisstein, *"Law of Cosines"*.

[54] M. Wieneke and W. Koch, *Probabilistic tracking of multiple extended targets using random matrices*, SPIE Defense, Security, and Sensing, International Society for Optics and Photonics, 2010, pp. 769812–769812.

[55] ———, *A PMHT approach for extended objects and object groups*, IEEE Transactions on Aerospace and Electronic Systems **48** (2012), no. 3, 2349–2370.

[56] P. Willett, Y. Ruan, and R. Streit, *PMHT: Problems and some solutions*, Aerospace and Electronic Systems, IEEE Transactions on **38** (2002), no. 3, 738–754.

[57] X Xuezhi, D. Musicki, R. Ellem, and F. Fletcher, *Enhanced multi-target tracking with doppler measurements*, Information, Decision and Control, 2007. IDC '07, 2007, pp. 53–58.

[58] Z. Zhang, *Iterative point matching for registration of free-form surfaces*, Int. Journal of Computer Vision, **13** (1994), no. 2, 119–152.

[59] Z. Zhao, X. R. Li, and V.P. Jilkov, *Best linear unbiased filtering with nonlinear measurements for target tracking*, IEEE Transactions on Aerospace and Electronic Systems **40** (2004), no. 4, 1324 – 1336.

[60] Z. Zhao, X. R. Li, V.P. Jilkov, and Y. Zhu, *Optimal linear unbiased filtering with polar measurements for target tracking*, Proceedings of the Fifth International Conference on Information Fusion, vol. 2, IEEE, 2002, pp. 1527–1534.

[61] G. Zhou, T. Quan, and T. Kirubarajan, *Pseudo states estimation for maneuvering target tracking in doppler radar systems*, Radar Conference (RADAR), 2012 IEEE, 2012, pp. 0735–0740.

[62] G. Zhou, N. Zhao, T. Fu, T. Quan, and T. Kirubarajan, *Enhanced sequential nonlinear tracking filter with denoised pseudo measurements*, Proceedings of the 14th International Conference on Information Fusion (FUSION), 2011, pp. 1–7.